DOE/NV/0003590-56

Evaluation of Timber Mountain Recharge and Groundwater Flow in Relation to Pahute Mesa-Oasis Valley Flow System

Prepared by

Ronald L. Hershey, Rishi Parashar, Clay A. Cooper, Kevin M. Heintz,
Hai V. Pham, and Bradley F. Lyles

Submitted to

U.S. Department of Energy
Environmental Management Nevada Program
Las Vegas, Nevada

December 2020

Publication No. 45294

Nevada System of Higher Education

Available for sale to the public from:

U.S. Department of Commerce
National Technical Information Service
5301 Shawnee Rd.
Alexandria, VA 22312
Phone: 800.363.2068
Fax: 703.605.6880
Email: info@ntis.gov
Online ordering: https://ntrl.ntis.gov/NTRL/

Available electronically at https://www.osti.gov/

DOE/NV/0003590-56

Evaluation of Timber Mountain Recharge and Groundwater Flow in Relation to Pahute Mesa-Oasis Valley Flow System

Prepared by

Ronald L. Hershey, Rishi Parashar, Clay A. Cooper, Kevin M. Heintz,
Hai V. Pham, and Bradley F. Lyles

Division of Hydrologic Sciences
Desert Research Institute
Nevada System of Higher Education

Publication No. 45294

Submitted to

U.S. Department of Energy
Environmental Management Nevada Program
Las Vegas, Nevada

December 2020

The work upon which this report is based was supported by the U.S. Department of Energy under Contracts #DE-AC52-06NA26383, #DE-NA0000939, and #DE-NA0003590. Approved for public release; further dissemination unlimited.

THIS PAGE INTENTIONALLY LEFT BLANK

ABSTRACT

The purpose of this study was to evaluate the effect of Timber Mountain recharge on groundwater flow in the surrounding Pahute Mesa-Oasis Valley groundwater basin using several different methodologies. These methodologies included examining climatic and soil moisture data, estimating groundwater recharge by chloride mass balance, interpreting water chemical and isotopic data, and modeling groundwater flow along faults.

Climatic and soil moisture data from the Timber Mountain weather monitoring site showed that shallow soil at the site became fully saturated six times during nine winters between 2010 and 2019. At full saturation, drainage was suggested immediately following significant winter/spring rainfall events and during snowmelt. Recharge at Timber Mountain was estimated to be 1.48 ± 0.96 cm/yr (0.58 ± 0.38 in/yr), or 5.5 percent of annual precipitation using the chloride mass-balance method. Water chemical and isotopic interpretations and water-rock chemical and isotopic reaction modeling suggested that Timber Mountain recharge was approximately 10 percent to 45 percent of the groundwater in ER-18-2, which is thought to be upgradient of Timber Mountain relative to the general southwest groundwater flow in the Pahute Mesa-Oasis Valley groundwater basin. Interpretations and modeling also suggested that Timber Mountain recharge is approximately 15 percent to 40 percent of the groundwater at UE-18r_o1, which is northwest of Timber Mountain; approximately 5 percent to 20 percent of the groundwater at ER_EC-5_m1-3, which is west of Timber Mountain; 30 percent to 50 percent of the groundwater at ER-OV-3c, which is southwest of Timber Mountain; and 100 percent of the groundwater at ER-EC-7, which is southwest of Timber Mountain.

Two-dimensional models were created in MODFLOW and MODPATH to examine the patterns of groundwater pathlines under different recharge scenarios. The model domain was parametrized by accounting for the influence of regional stress on the enhancement of fault permeability. For the scenario of uniformly distributed recharge for low, medium, and high amounts of recharge based on the chloride mass-balance method and the release of particles only at the highest elevations, the pattern of the pathlines was only mildly influenced by the amount of recharge. The pathlines in these cases eventually aligned with the general direction of groundwater flow and left the model domain at the southern boundary. However, when the particles were released over a much larger area of Timber Mountain, they produced pathlines with significant variability with increasing recharge. As the recharge values increased, a small portion of the pathlines trended northeastward. These simulations indicated some hydraulic connection between Timber Mountain recharge and the northeast area around ER-18-2, which is consistent with the results from the water-rock geochemical reaction modeling. When the net infiltration models were used to apply the recharge values, the simulated pathlines were similar to those obtained using the low recharge values of the chloride mass-balance method.

Based on the methods applied here, the results indicate that Timber Mountain produces enough groundwater recharge to form a groundwater mound and that recharge flows radially outward from Timber Mountain. Water chemistry and isotopic interpretations and water-rock geochemical reaction modeling results are consistent with groundwater flow modeling scenarios, which suggests that groundwater recharge from Timber Mountain flows northeastward toward ER-18-2 against the general southwestward groundwater flow of the Pahute Mesa-Oasis Valley groundwater basin.

ACKNOWLEDGEMENTS

The authors thank the U.S. Department of Energy and the Underground Test Area Activity Leads, Bill Wilborn and John Myers, for providing funding to accomplish the work described herein. We also thank Monica Arienzo, Susan Rybarski, and Karl Pohlmann for their reviews and for providing comments, suggestions, and recommendations that helped improve this report.

CONTENTS

LIST OF FIGURES

LIST OF TABLES

LIST OF ACRONYMS AND ABBREVIATIONS

amsl	above mean sea level
cm	centimeters
cm/hr	centimeters per hour
cm/yr	centimeters per year
Cl	chloride
DFN	discrete fracture network
FC	fracture continuum
ft	feet
GMWL	global meteoric water line
hrs	hours
HSU	hydrostratigraphic unit
in	inches
in/yr	inches per year
km^2	square kilometers
L	length
LMWL	local meteoric water line
LPF	layer property flow
M	mass
m	meters
Ma	million years ago
m/s	meters per second
mi^2	square miles
mg/L	milligrams per liter
mmol/Kg	millimoles per kilogram
n	number of samples
NE	northeast
NNSS	Nevada National Security Site
NW	northwest
NTMMSZ	northern Timber Mountain moat structural zone
PM	Pahute Mesa
RM	Rainier Mesa
SATSI	spatial and temporal stress inversion

SD	standard deviation
SE	southeast
SW	southwest
TDR	time-domain reflectometry
TM	Timber Mountain
TMCC	Timber Mountain caldera complex
TMCCSM	Timber Mountain caldera complex structural margin
TMVA	Timber Mountain volcanic aquifer
T	time
Td	dilation tendency
Ts	slip tendency
UCDB	UGTA Chemical Database
UGTA	Underground Test Area
VWC	volumetric water content
WY	water year
WFS	wet-fall sampler
yr	year

INTRODUCTION

Timber Mountain is located on the western boundary of the Nevada National Security Site (NNSS) in southern Nevada (Figure 1). It is a resurgent volcanic dome within the Timber Mountain caldera complex and it is bisected by the southeastern boundary of the Pahute Mesa-Oasis Valley groundwater basin (Figure 2). Precipitation falling on Timber Mountain contributes groundwater recharge to the Pahute Mesa-Oasis Valley groundwater basin (Fenelon *et al.*, 2016). According to Fenelon *et al.* (2016), Timber Mountain may influence groundwater flow because of confining units in the mountain that restrict flow or groundwater mounding of recharge. However, there are no wells within the mountain block and water levels in the wells surrounding Timber Mountain do not indicate that Timber Mountain recharge has a major influence on flow within the Pahute Mesa-Oasis Valley groundwater basin, as interpreted by Fenelon *et al.* (2016).

The purpose of this study was to evaluate the effect of Timber Mountain recharge on groundwater flow in the surrounding Pahute Mesa-Oasis Valley groundwater basin using several different methodologies. The methodologies used to evaluate Timber Mountain recharge and its effects on groundwater flow included:

1) Installing a monitoring station on Timber Mountain to monitor weather and assess the infiltration of precipitation.
2) Estimating the amount of groundwater recharge using the chloride mass-balance method.
3) Evaluating potential groundwater flow paths that include Timber Mountain recharge by modeling water-rock chemical and isotopic reactions from Timber Mountain to the Pahute Mesa-Oasis Valley groundwater basin.
4) Modeling the effects of the regional stress field on the hydraulic properties of faults in Timber Mountain and the adjacent Pahute Mesa-Oasis Valley groundwater basin and its influence on the configuration of groundwater pathlines originating from the Timber Mountain area under different groundwater recharge regimes.

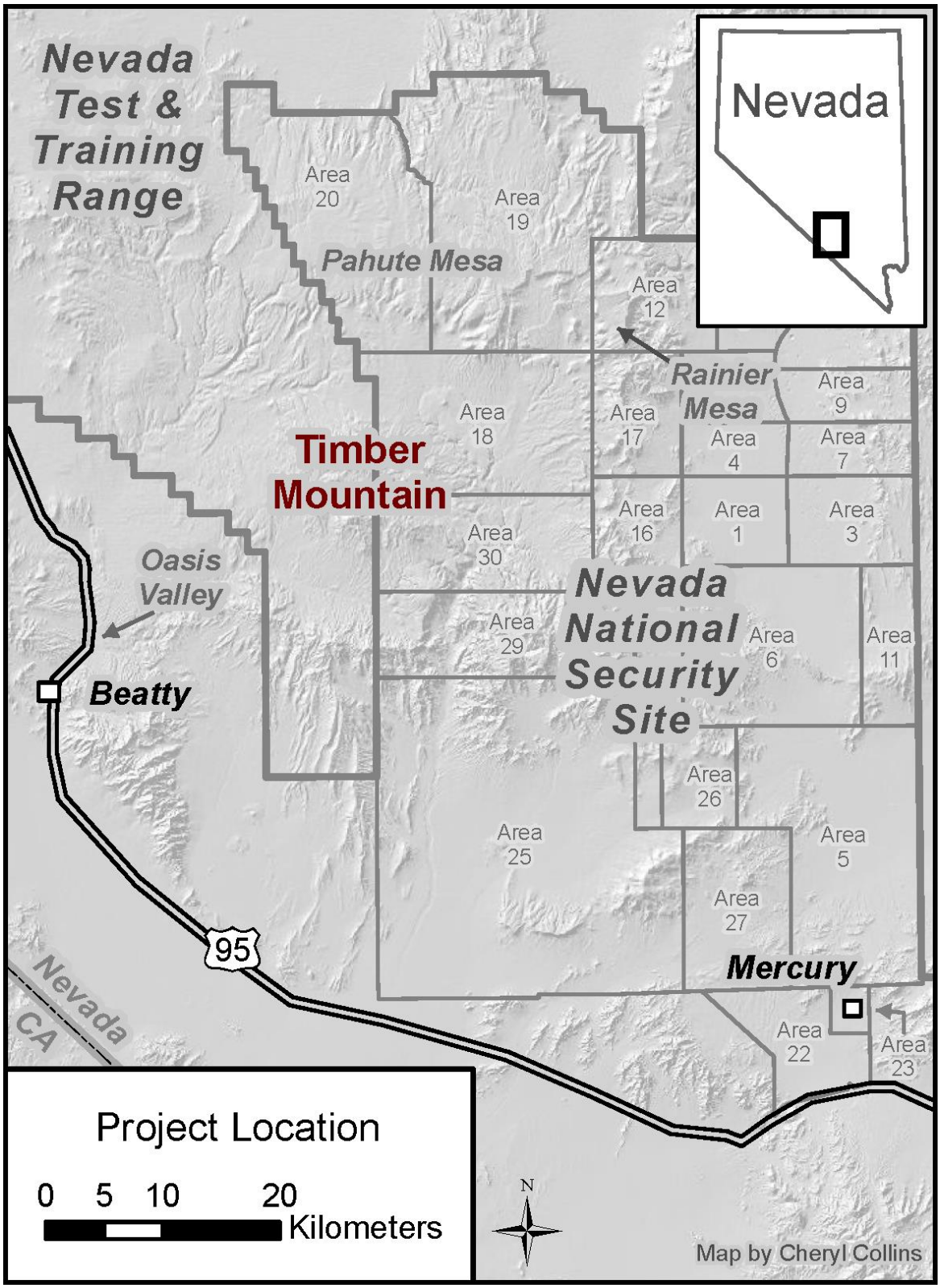

Figure 1. Location of Timber Mountain.

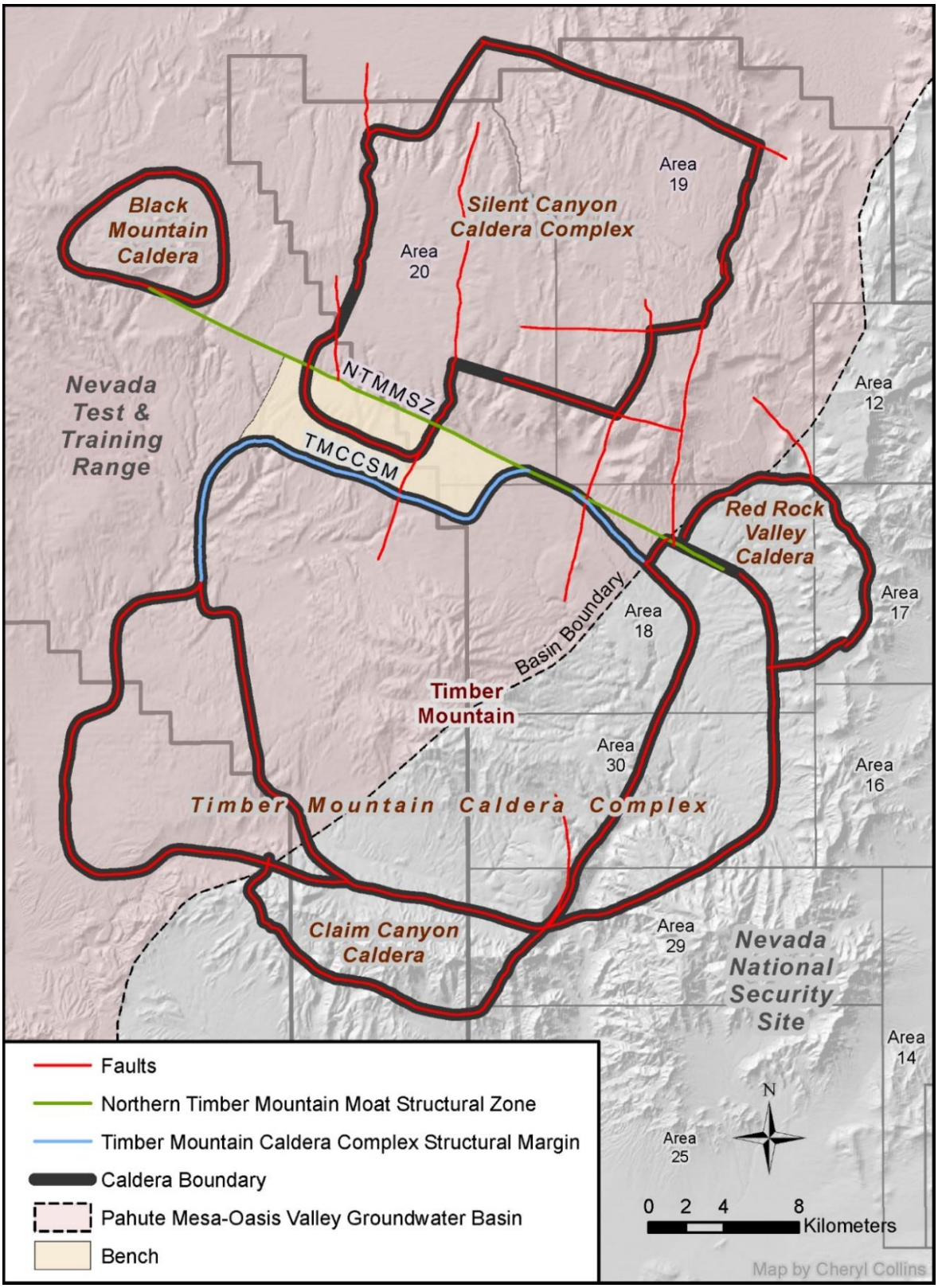

Figure 2. Timber Mountain caldera complex and southeastern boundary of the Pahute Mesa-Oasis Valley groundwater basin boundary (from Fenelon *et al.* [2016]), which bisects Timber Mountain.

BACKGROUND

Geology

Geologic mapping of the Timber Mountain area was initiated in the early 1960s for the U.S. Atomic Energy Commission and later for the U.S. Department of Energy (Carr and Quinlivan, 1964; Byers *et al.*, 1976a; Christiansen *et al.*, 1977). Timber Mountain geology is described most recently in the Pahute Mesa-Oasis Valley hydrostratigraphic framework model (U.S. Department of Energy, 2020). Timber Mountain is a resurgent volcanic dome near the center of a volcanic complex, commonly referred to as the Timber Mountain caldera complex (TMCC). Several overlapping calderas exist within this complex (Figure 2).

Calderas form when large volcanic eruptions deplete the underlying magma chambers, which then subside and form large basins. These basins are then filled by continued volcanic eruptions. Often, the underlying magma will push upward and form domes at the center of the calderas. This doming results in the formation of a topographic moat, which is a low-lying area around the dome within the rim of the caldera (Figure 3) (U.S. Department of Energy, 2020).

The TMCC covers nearly 11,000 square kilometers (km^2) (6,800 square miles [mi^2]) and it is the source of nine voluminous rhyolitic ash-flow sheets and numerous smaller rhyolitic tuffs and lava flows (Christiansen *et al.*, 1977). The TMCC is made up of two nested calderas, the Rainier Mesa and Ammonia Tanks calderas, and it has a central resurgent dome and partially exposed topographic margin (U.S. Department of Energy, 2020). The Rainier Mesa caldera first erupted 11.6 million years ago (Ma) and the rocks of this caldera are mostly buried by the later Ammonia Tanks caldera that formed 11.45 Ma, whose tuffs are exposed on Timber Mountain (Sawyer *et al.*, 1994; U.S. Department of Energy, 2020).

Basin-and-range extension and volcanism were synchronous within the southwestern Nevada volcanic field (Sawyer *et al.*, 1994). Numerous high-angle normal faults are common within the Timber Mountain resurgent dome, which was predominantly formed by extension and caldera collapse. These normal faults may extend several kilometers deep, but the openness of these fractures is thought be low at depths greater than 1 km (0.6 mi) (Zablocki, 1979).

Most of the volcanic hydrogeologic units in the area have very low rock-matrix permeability relative to bulk-rock permeability because of faulting and fractures. Faults and fractures are important geologic and hydrologic features because groundwater flow is dominated by fracture flow (U.S. Department of Energy, 2020). Fracture flow is examined in more detail by modeling the effects of the regional stress field on the hydraulic properties of faults in Timber Mountain and parts of the Pahute Mesa-Oasis Valley groundwater basin adjacent to Timber Mountain (Figure 2).

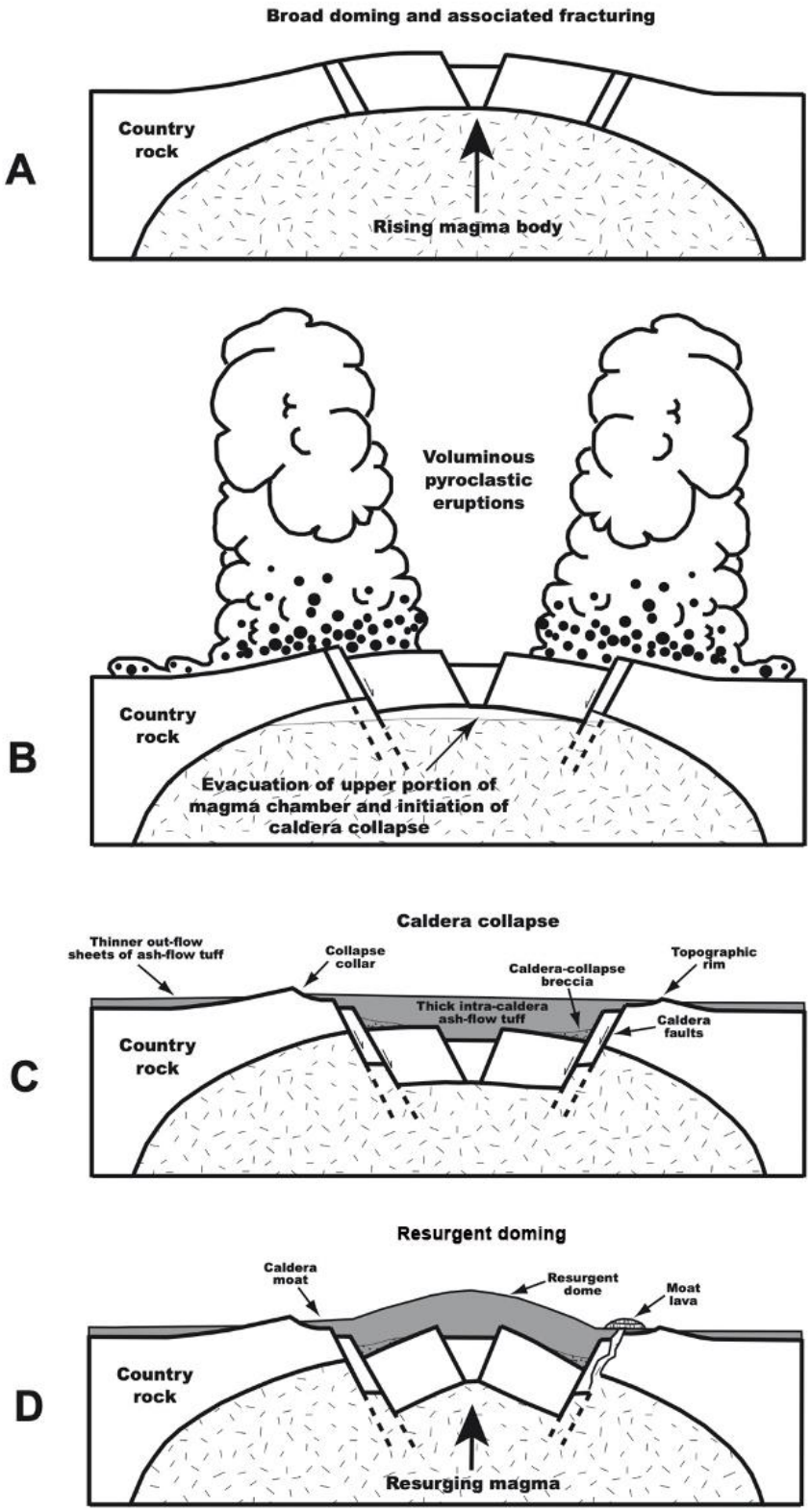

Figure 3. Conceptual model of a typical resurgent caldera (from U.S. Department of Energy [2020]).

An area on the northern edge of the TMCC, designated the northwestern Timber Mountain Bench (Warren *et al.*, 2000), or more commonly referred to as "the Bench," is important because it is downgradient of underground tests in western Pahute Mesa. The Bench is defined by the northern Timber Mountain moat structural zone (NTMMSZ) on the north and by the TMCC structural margin (TMCCSM) on the south (Figure 2). The NTMMSZ is a west-northwest-trending buried structural zone related to the formation of the TMCC (U.S. Department of Energy, 2020). More detail on Timber Mountain geology can be found in Carr and Quinlivan (1964), Byers *et al.* (1976a,b), Christiansen *et al.* (1977), Zablocki (1979), Grauch *et al.*, (1999), Sawyer *et al.* (1994), and U.S. Department of Energy (2020).

Hydrology

Timber Mountain is located on the hydrographic boundary of the Pahute Mesa-Oasis Valley and Alkali Flat-Furnace Creek Ranch groundwater basins (Fenelon *et al.*, 2016). Groundwater flow within the Pahute Mesa-Oasis Valley groundwater basin is generally from the north to the south—discharging in Oasis Valley near Beatty, Nevada—and approximately 7.3×10^6 m^3 (5,900 acre-ft) of water discharges annually to Oasis Valley (Fenelon *et al.*, 2016). Figure 4 shows the Pahute Mesa-Oasis Valley groundwater basin boundary, hydrologic characterization wells, water-level contours from Fenelon *et al.* (2016), structural features, and caldera boundaries in the vicinity of Timber Mountain.

No wells exist on the resurgent dome of Timber Mountain proper and only a few wells are located in the Timber Mountain moat, which include UE-18r, ER-18-2, ER-EC-2A, ER-EC-5, ER-EC-7, ER-EC-8, ER-EC-13, and ER-EC-14 (Figure 4). Many of the hydrostratigraphic units (HSU) within the Pahute Mesa area shown in Figure 5 are also present within the Timber Mountain caldera complex, except for the HSUs below the Crater Flat Group. Figure 5 lists aquifers in green, confining units in orange, and composite units in pink. Hydrostratigraphic unit thicknesses range from 250 m to 1,451 m (820 ft to 4,760 ft) and in many cases the units are laterally discontinuous, as shown in the geologic cross section B-B' (Figures 4 and 6). The B-B' cross section (Figure 6) shows the hydrostratigraphic unit relationships from western Pahute Mesa, across the Bench, and into the TMCC moat.

Groundwater recharge in the Pahute Mesa-Oasis Valley groundwater basin occurs on the volcanic highlands of Pahute Mesa and Timber Mountain (Fenelon *et al.*, 2016). However, recharge on Timber Mountain is thought to be small (1-2 mm/yr) because of the presence of clay-rich soils and steep slopes (Middleton *et al.*, 2019). Fenelon *et al.* (2016) hypothesized that Timber Mountain may influence groundwater flow because of the presence of confining-unit rocks in the mountain that may restrict flow or groundwater mounding from recharge. The limited number of wells around the mountain and the water levels in those wells do not provide direct evidence that Timber Mountain has a major influence on flow in the Pahute Mesa-Oasis Valley groundwater basin. Fenelon *et al.* (2016) interpreted water-level contours in the vicinity of Timber Mountain such that groundwater flow diverges away from the mountain because of some small amount of local recharge, but on significant groundwater mounding (Figure 4). Groundwater chemistry and isotopic data agree with the groundwater flow directions of Fenelon *et al.* (2016) and the groundwater basin boundary passing through Timber Mountain (Navarro 2020).

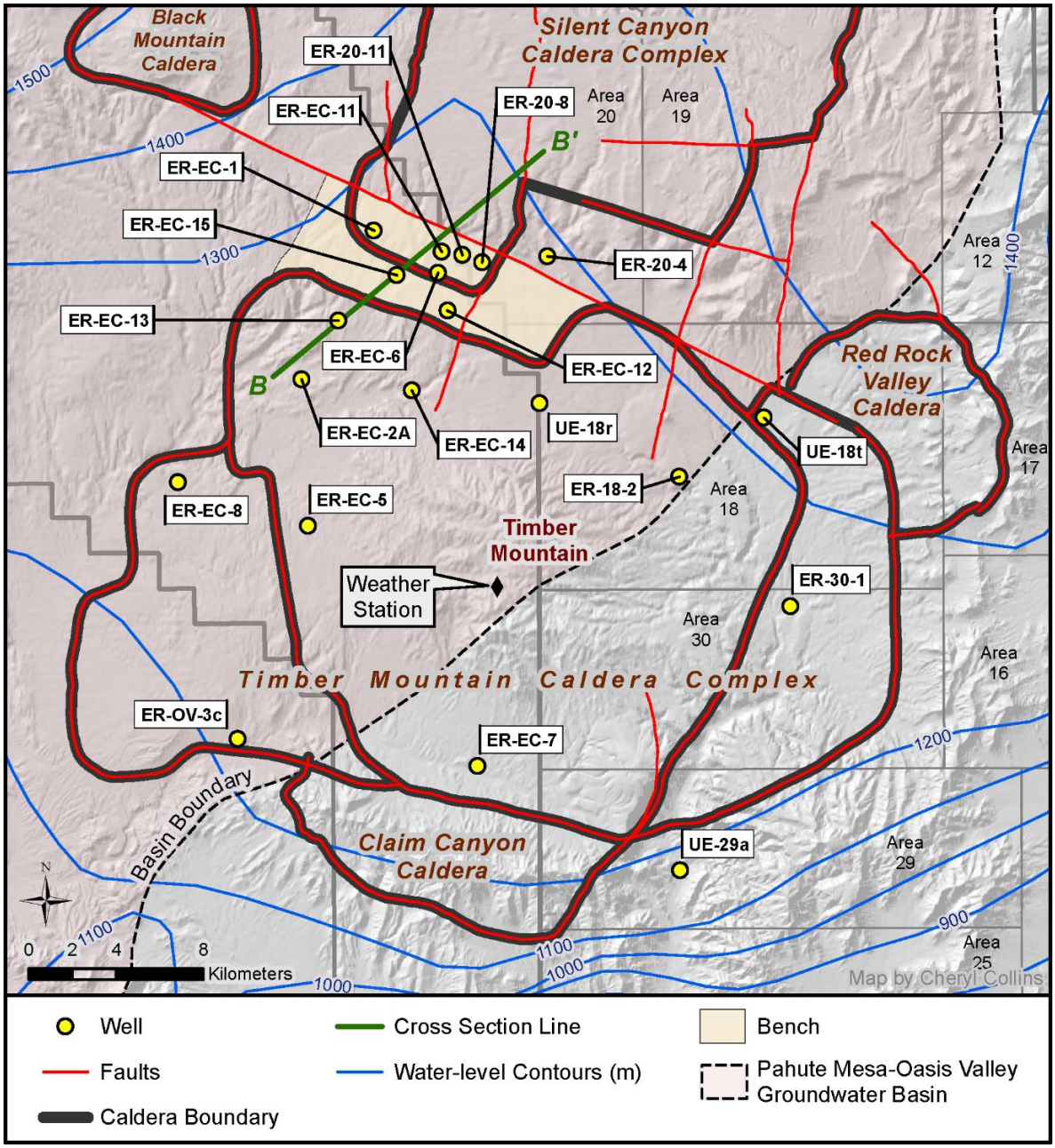

Figure 4. Hydrologic characterization wells near Timber Mountain. Water-level contours from Fenelon *et al.* (2016).

Group[1]	Age[1] (millions of years)	Volcanic center[1]	HSU[2]	HSU thickness[3] (feet)	Hydrostratigraphic unit (HSU) name[2]
			AA	328	Alluvial aquifer
			YVCU	984	Younger volcanic confining unit
Thirsty Canyon Group	9.4–9.15	Black Mountain caldera	TCVA	6,890	Thirsty Canyon volcanic aquifer
			FCCM	4,757	Fortymile Canyon composite unit
			FCULFA 1–7	820–1,640	Fortymile Canyon upper lava-flow aquifers 1–7
Volcanics of Fortymile Wash	11.45–10.3	Diverse vent areas	FCWTA	1,148	Fortymile Canyon welded-tuff aquifer
			FCLLFA	164	Fortymile Canyon lower lava-flow aquifer
			BWWTA	492	Beatty Wash welded-tuff aquifer
			BWCU	984	Beatty Wash confining unit
			ATWTA	820	Ammonia Tanks welded-tuff aquifer
			ATCCU	1,312	Ammonia Tanks caldera confining unit
			TMUWTA	4,757	Timber Mountain upper welded-tuff aquifer
			THLFA	1,476	Tannenbaum Hill lava-flow aquifer
			THCM	1,312	Tannenbaum Hill composite unit
Timber Mountain Group	11.6–11.45	Timber Mountain caldera complex	THCU	1,312	Tannenbaum Hill confining unit
			TMWTA	1,312	Timber Mountain welded-tuff aquifer
			TMLVTA	1,148	Timber Mountain lower vitric-tuff aquifer
			RMWTA	5,249	Rainier Mesa welded-tuff aquifer
			FCCU	984	Fluorspar Canyon confining unit
			WWA	820	Windy Wash aquifer
			CPA	656	Comb Peak aquifer
			PBPCU	656	Post-Benham Paintbrush confining unit
			BA	1,312	Benham aquifer
			UPCU	820	Upper Paintbrush confining unit
			SPA	492	Scrugham Peak aquifer
Paintbrush Group	12.7	Claim Canyon caldera and local vents	MPCU	328	Middle Paintbrush confining unit
			TCA	820	Tiva Canyon aquifer
			PVTA	492	Paintbrush vitric-tuff aquifer
			LPCU	984	Lower Paintbrush confining unit
			PLFA	1,640	Paintbrush lava-flow aquifer
	12.8		TSA	656	Topopah Spring aquifer
			CHVTA	1,969	Calico Hills vitric-tuff aquifer
Calico Hills Formation	12.9	Local vents	CHZCM	3,937	Calico Hills zeolitic composite unit
			CHLFA 1–5	164–2,297	Calico Hills lava-flow aquifers 1–5
			IA	1,640	Inlet aquifer
Crater Flat Group	13.5–13.1	Area 20 caldera	CFCM	1,476	Crater Flat composite unit
			CFCU	1,312	Crater Flat confining unit
			BFCU	2,789	Bullfrog confining unit
Belted Range Group	13.85–13.5	Grouse Canyon caldera	BRA	3,445	Belted Range aquifer
Pre-Belted Range Group volcanic rocks			PBRCM	5,906	Pre-Belted Range composite unit
			SCVCU	2,625	Silent Canyon volcanic confining unit
			LCCU1	656	Lower clastic confining unit, thrusted
Pre-volcanic rocks			UCCU	2,461	Upper clastic confining unit
			LCA	4,265	Lower carbonate aquifer
			BMICU	164	Black Mountain intrusive confining unit
Caldera-related intrusive rocks			RMICU	2,297	Rainier Mesa intrusive confining unit
			ATICU	2,953	Ammonia Tanks intrusive confining unit

[1] Stratigraphic assignment, age, and inferred volcanic source area after Sawyer and others (1994).
[2] Hydrostratigraphic unit names and abbreviations after Prothro and others (2009).
[3] Thickness based on HSUs vertically sampled at a 164-feet (50-meter) interval.

Figure 5. Hydrographic units (HSUs) (from Garcia *et al.* [2017]).

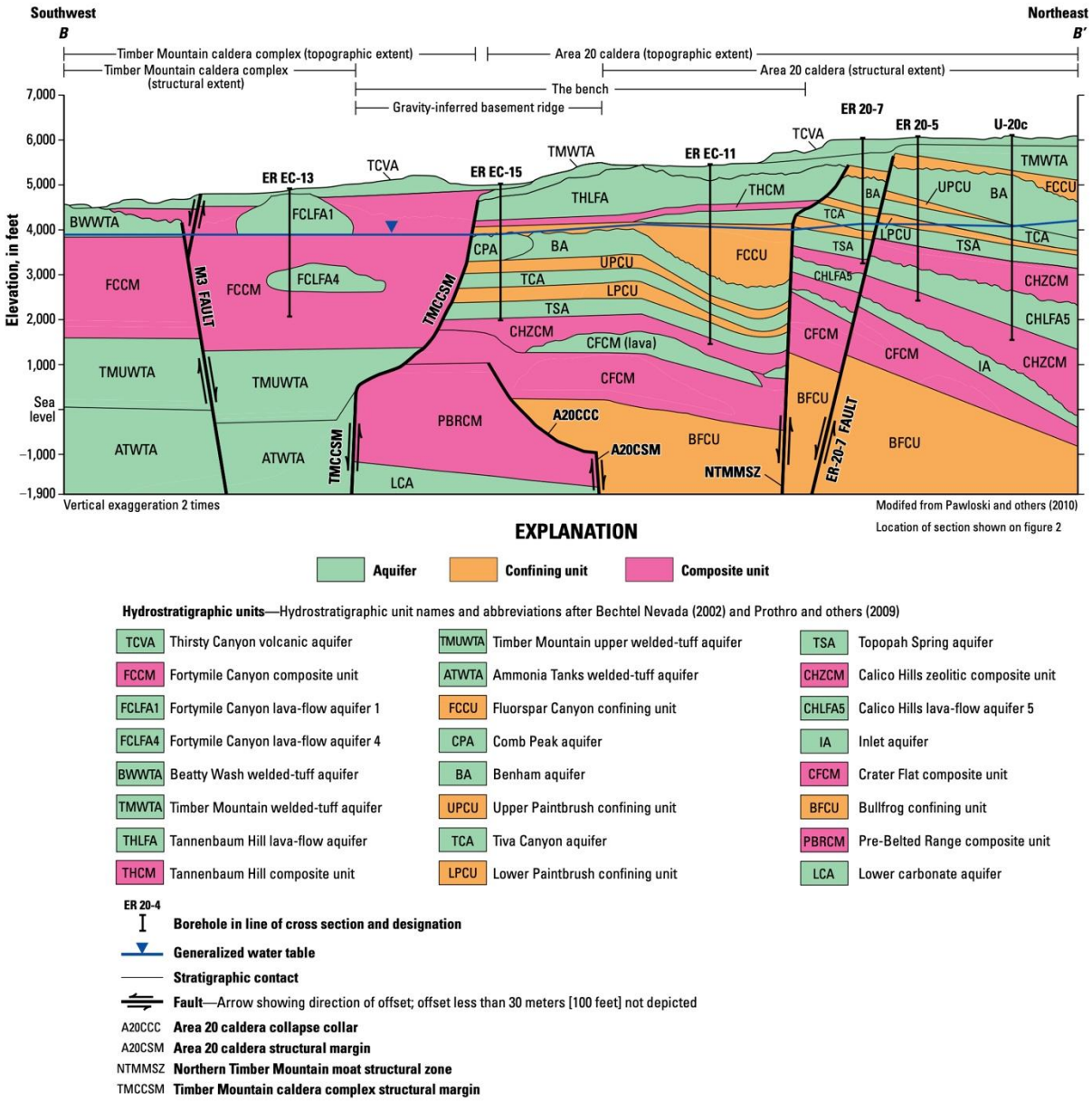

Figure 6. Hydrologic cross section from the Timber Mountain caldera complex, across the Bench, and into the Silent Canyon caldera complex (from Garcia *et al.* [2017]).

METHODS

Weather and Infiltration

A weather monitoring station was installed on Timber Mountain along Cat Canyon Road on the west side of the Timber Mountain summit (Figure 4) on June 4, 2010. This station is equipped to measure basic weather conditions (i.e., air temperature, relative humidity, wind speed, wind direction, barometric pressure, shortwave solar radiation, precipitation, and snow depth), as well as soil moisture and soil temperature. Precipitation is measured by a tipping bucket or "tipper" (Texas Instruments, Dallas, TX), a Geonor weighing-bucket gauge (Geonor, Inc., Branchville, NJ), and an SR50A (Campbell Scientific Inc., Logan, UT) sonic distance sensor to measure snow depth. A thin veneer of soil exists at the site, approximately 25 cm (10 in) thick, which is underlain by fractured volcanic bedrock. Soil moisture and temperature sensors were installed at three depths (5 cm [2 in], 10 cm [4 in], and 20 cm [8 in]). A detailed discussion of this installation can be found in Lyles *et al.* (2019). Soil-moisture conditions (volumetric water content [VWC] and soil temperature) were examined from 2010 through 2019 and compared with precipitation timing and amount, air temperature, and snow depth to determine the timing and extent of soil saturation and drainage. Precipitation was also measured in a bulk precipitation gauge and precipitation samples were collected for major-ion chemistry and stable isotopes of hydrogen and oxygen analysis.

Chloride Mass Balance

Recharge was estimated by applying a chloride mass-balance approach using the precipitation amount and chloride (Cl) concentration in precipitation collected from the Timber Mountain weather monitoring station, as well as the Cl concentration from wells near Timber Mountain (Cooper *et al*., 2013). A chloride mass balance equates Cl input from precipitation and inflowing groundwater with Cl output from runoff and recharge; that is:

$$\boldsymbol{PC_p + \sum_{i=0}^{n} q_{gw_i} C_{gw_i} = NC_r + Q_{ro} C_{ro}} \quad (1)$$

where P, q_{gw}, N, and Q_{ro} are precipitation, groundwater flow from upgradient basins, groundwater recharge, and surface runoff, respectively (all [LT^{-1}]) [1]; C_p, C_{gw}, C_r, and C_{ro} are Cl concentrations in precipitation, flowing groundwater within the study area, groundwater recharge, and runoff, respectively (all [ML^{-3}]); and n is the number of adjacent subbasins from which groundwater may be derived. If there is no runoff or inflow of groundwater from subbasins, then recharge can be estimated as:

$$\boldsymbol{N = \frac{PC_p}{C_r}} \quad (2)$$

The important assumptions when implementing the chloride mass-balance method are that: (1) the only source of Cl is from precipitation, (2) Cl is inert and undergoes no chemical reactions in the rocks and/or soil, (3) the deposition rate of Cl has been constant over the

[1] These are dimensions: L (length), M (mass), and T (time).

period of time equal to the residence time of the groundwater being sampled, and (4) the Cl concentration in groundwater accurately reflects the Cl concentration in groundwater from recharge. The last assumption merely states that Cl concentration in space is uniform and if recharge is primarily through fractures in one location and through soil in another location, the integrated sample may not reflect mean Cl conditions in groundwater. It is also important to note that the recharge model assumes no runoff or mixing of flowing groundwater.

Groundwater Water-rock Chemical and Isotopic Reaction Modeling

Groundwater chemical and isotopic data from wells surrounding Timber Mountain were compiled and evaluated to identify end-member mixing components and potential groundwater flow paths radiating outward from Timber Mountain. A chemical and isotopic groundwater recharge end-member from Timber Mountain was estimated based on data collected from the Timber Mountain weather monitoring station, NNSS springs, and Rainier Mesa (RM) tunnels. The recharge end-member was used with chemical and isotopic end-member mixing components to construct water-rock chemical and isotopic reaction models to test the potential flow paths identified. The percentage of recharge relative to other end-member mixing components was quantified.

A comprehensive groundwater chemical and isotopic dataset was generated from the UGTA Chemical Database (UCDB). These data were reviewed and reduced to means with standard deviations for further geochemical and isotopic analysis. Appendix A lists the mean groundwater chemical constituent concentrations and isotopic signatures with standard deviations for each well or piezometer considered. The results of duplicate analyses conducted on samples from the same completion interval on the same day were used to determine an average sample value for that sampling event. When samples were collected from the same interval of a main well completion or piezometer by pumping on different days, means and standard deviations were calculated for each interval or piezometer.

Groundwater water-rock chemical and isotopic reaction models were developed based on the well and piezometer completion zone in specific HSUs and the associated mineral phases used in previous studies (Thomas *et al.*, 2002; Kwicklis *et al.*, 2005; Rose *et al.*, 2006; Kwicklis *et al.*, 2020). The computer program NETPATH (Plummer *et al.*, 1994; Parkhurst and Charlton, 2008) was used to model the water-rock chemical and isotopic reactions and physical processes (e.g., ion and isotopic exchange with aquifer materials) for proposed groundwater flow paths and groundwater mixing. The NETPATH program can also correct carbon-14 groundwater ages from the initial isotopic composition of dissolved inorganic carbon sources, the amount of carbon moving in and out of the groundwater, and the isotopic fractionation between phase changes.

The water-rock reaction chemical and isotopic models used the same water chemical and isotopic parameters and mineralogical data as the previously cited studies. The observed groundwater chemical and isotopic changes along a proposed flow direction (i.e., flow path) should be the result of reasonable chemical and isotopic reactions between groundwater and the aquifers the groundwater is flowing through, or other physical processes (such as mixing or ion exchange between dissolved ions in the groundwater and aquifer or fracture lining materials). The chemical and isotopic compositions of the downgradient groundwater(s) should result primarily from the mixing and dissolution of phases (primarily minerals and volcanic glass) that are undersaturated in the water and the precipitation or formation of

phases that are saturated in the groundwater. For example, if groundwater is below saturation with respect to calcite, then calcite will dissolve as the water flows downgradient. Conversely, if the upgradient groundwater is above saturation with respect to calcite, then calcite will precipitate from the groundwater as it flows through the aquifer. Similarly, a volcanic glass will undergo incongruent dissolution as groundwater flows through it, adding dissolved ions to the groundwater while forming clays.

When running simulations, NETPATH will produce all possible combinations regardless of whether or not they are thermodynamically or physically valid. It is up to the modeler to evaluate whether the NETPATH simulation results are geochemically reasonable. The following criteria were applied to evaluate whether a geochemical model result was geochemically reasonable. First, a phase needs to be below saturation to dissolve in groundwater or above saturation to precipitate from a groundwater or form by incongruent dissolution (i.e., dissolution of volcanic glass or feldspars to form clays or zeolites) along a flow path. Model results with mineral phase changes from upgradient to downgradient that were not consistent with the change in the mineral saturation state between upgradient and downgradient sample locations were not considered valid representations of the chemical and isotopic reaction between the sample locations. Second, the amount of any phase precipitating or dissolving along the flow path had to be less than 10.0 mmol per liter.

Influence of Regional Stress on Fault Permeability and Flow Paths

It is widely known that regional stress exerts considerable influence on the permeability of faults. Fracture transmissivity and velocity are extremely sensitive to the hydraulic aperture, which in turn critically depends on the effective normal stress acting on the fracture planes. This stress is defined as the difference between the total stress applied on the fracture and the pore fluid pressure within the fracture. Stress interactions within a fracture can result in simultaneous aperture dilation and permeability enhancement for fractures oriented favorably within the stress field, and decreased permeability and fluid flow caused by reduction in aperture in fractures oriented perpendicular to the maximum normal stress. Traditional approaches to parameterizing fractured rock models according to physical fracture attributes typically disregard the potential influence of in-situ stress and mechanical fluid stress interactions within interconnected networks of fractures. These hydromechanical factors may impart directionality and anisotropy to fluid pathways that are not sufficiently resolved in traditional simulations.

Dilation and slip tendency analysis is a technique that allows for a simple assessment of stress states and the related potential fault activity. The hydraulic function of fractures can be inferred from the normal and shear stresses using dilation (Morris *et al.*, 1996) and slip tendency (Ferrill *et al.*, 1999) metrics. A method described in a recent study by Reeves *et al.* (2017) to characterize the stress field at Pahute Mesa based on an inversion of stress field data from short-period earthquake focal mechanisms, stress magnitudes, orientations, and horizontal stress anisotropy estimates was implemented to infer the hydraulic function of faults and fractures. A computer code, RStress (Reeves *et al.*, 2017), designed to compute dilation and slip tendencies in faults and structural features contained in the Phase II Pahute Mesa hydrogeologic framework model (U.S. Department of Energy, 2020), uses the traction vector method to resolve normal and shear stresses delineated from short-period earthquake focal mechanisms. The stress field in the northwest NNSS region—represented in terms of *Shmin*, *Shmax*, and *Sv* stress components—was estimated from 699

short-period focal mechanism data using the spatial and temporal stress inversion (SATSI) software of Hardebeck and Michael (2006). The SATSI algorithm allowed for the direction of horizontal principal stresses, *Shmin* and *Shmax*, to be determined. The dip angles were undifferentiated for the faults and were set at a constant value of 80 degrees. The short-period focal mechanisms were compiled from a number of reports on NNSS seismicity developed by the U.S. Geological Survey and the Nevada Seismological Laboratory (Reeves *et al.*, 2017). Normal and shear stresses for each fault segment were then computed, followed by the computation of dilation and slip tendency values.

Although a direct relationship between dilation tendency, slip tendency, and fault permeability does not exist, a fault will be more likely to function as a strong conduit if the configuration of normal and shear stresses acting on its surfaces result in enhanced dilation and/or slip tendency values. The major faults are likely to differ in their hydraulic properties, mainly guided by their orientation vis-à-vis the regional stress field directions. Parashar *et al.* (2018) examined the configuration of flow pathlines in Western Pahute Mesa with an emphasis on the specific locations of detonations. This study incorporated the stress-influenced hydraulic function of large-scale Pahute Mesa faults into simple two-dimensional flow and transport models to understand how regional stress influences pathlines in the Timber Mountain region under different recharge scenarios.

Simple two-dimensional groundwater flow models of the Timber Mountain area were created using MODFLOW and the recharge estimates and hydraulic head values used to model the boundary conditions were extracted from the Death Valley Regional Flow System model (Belcher and Sweetkind, 2010) outputs. The rock properties were parametrized to depict scenarios of the low, medium, and high conditions that favor the migration of contaminants. The faults in the area were assigned varying degrees of conductivity based on their relationship with the horizontal stress field directions. The layer property flow (LPF) package in MODFLOW was used to specify properties controlling flow between cells. The cells intersected by faults were parametrized using the fracture continuum (FC) methodology (Botros *et al.*, 2008; Reeves *et al.*, 2008; Parashar and Reeves, 2011), which combines the approaches of discrete fracture network (DFN) and continuum models by mapping the geometry of fracture networks on a finite-difference grid to compute the cell conductivities so that the total flow across the domain simulated through the DFN is preserved. The 100-meter segments of faults in the RStress code were conceptualized as high aperture, medium aperture, or low aperture according to the computed values of the dilation tendencies. After solving for flow in the model domain, particles were released in model cells covering the Timber Mountain area. Particle pathlines were computed using MODPATH simulations to investigate their configuration and their sensitivity to primary model variables. The model runs were conducted for the simple case of movement through only the fracture continuum.

RESULTS AND DISCUSSION

Weather and Infiltration on Timber Mountain

Soil moisture conditions at the Timber Mountain monitoring station change throughout the year in response to local weather and are sensitive to precipitation events, most noticeably at shallow depths. Generally, wetting fronts reach deeper into the soil profile during periods of high precipitation and during snowmelt. Soil temperature typically exhibits

diurnal fluctuations, but variations in soil temperature lag ambient air temperature fluctuations and that lag increases with soil depth. The amplitude of soil temperature change is also dampened increasingly with depth. Soil temperature is less likely to vary as surface snow depth increases because of insulation from the snow layer.

As an example of typical behavior during a precipitation event at the monitoring station, Figure 7a shows the volumetric water content at three depths as a function of time during water year (WY) 2011 (October 1, 2010, to September 30, 2011). A winter precipitation event started as rain on December 16, 2010, and then turned to snow by December 20th, which was followed by several small snowstorms. Soil temperature during this same period no longer exhibited diurnal variability of soil exposed to the atmosphere, but instead exhibited trends of soil insulated by snow (Figure 7b). On January 14, 2011, soil temperature trends returned to the typical pattern of soil exposed to the atmosphere after melting and sublimation. The tipping-bucket rain gauge only measures liquid precipitation and the funnel does not normally capture significantly large snow events. However, when compared with the measurements from the weighing-bucket gauge (which can accurately measure frozen precipitation quantity and timing), there do not appear to be large discrepancies between the two measurements (Figure 7c). The precipitation events in late February 2011 (Figure 7c) show a deviation in accumulated precipitation where the weighing-bucket gauge recorded approximately 2 cm (1 in) more than the tipping bucket. The snow-depth sensor confirms that snow was present, and therefore the tipping bucket likely underestimated accumulated precipitation because it did not capture snowfall. During the spring and summer, the weighing-bucket gauge continued to accumulate mass as the tipping-bucket gauge did not record any rain, which is most likely the result of accumulated insects and other debris in the weighing-bucket gauge (Figure 7c).

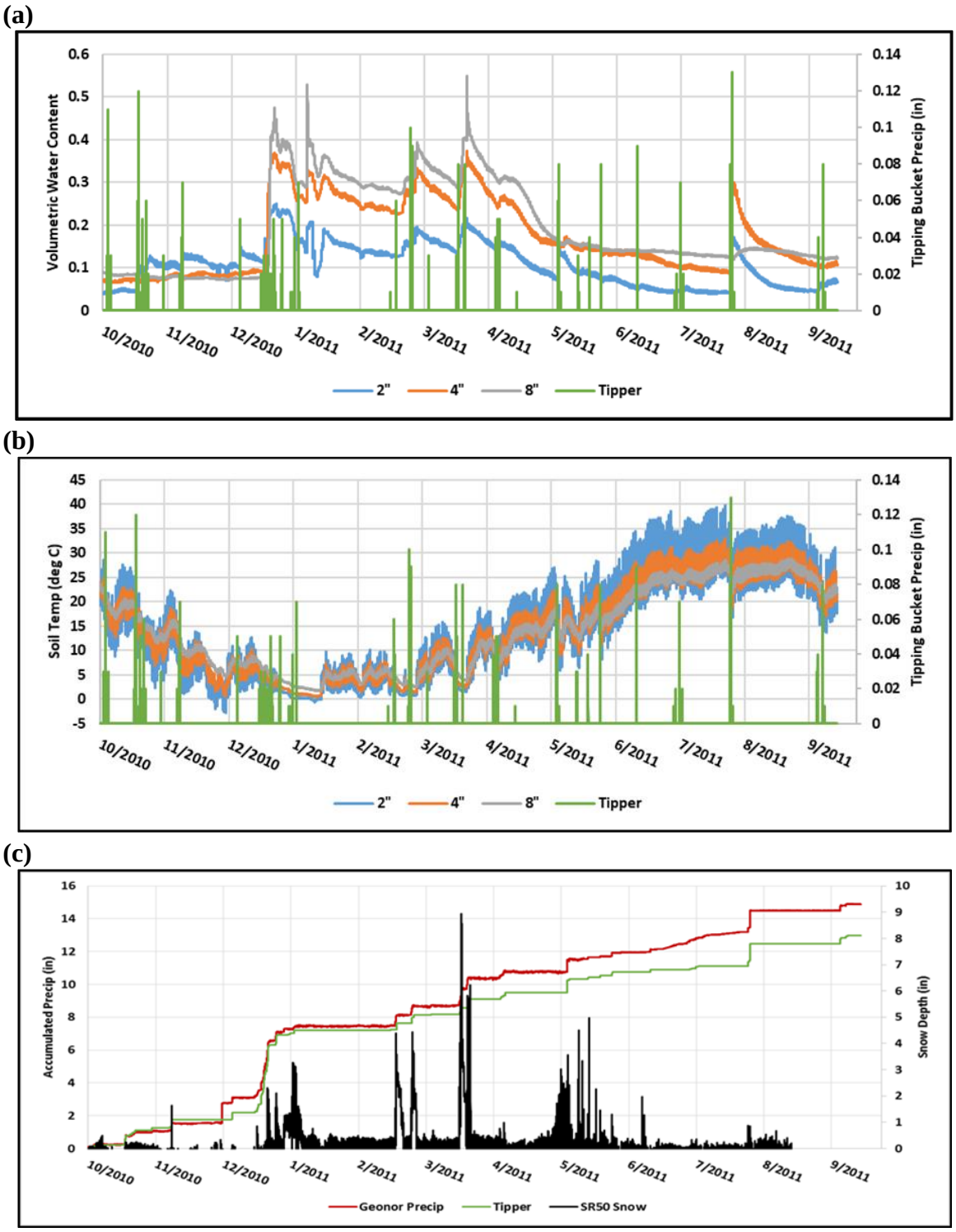

Figure 7. Timber Mountain weather monitoring station WY 2011 (October 1, 2010, to September 30, 2011). (a) Precipitation and VWC versus time. Higher VWC at the 20 cm (8 in) sensor indicates potential recharge in response to precipitation events. (b) Precipitation and soil temperature versus time, showing the soil is not frozen during the winter. (c) Snow depth and accumulated precipitation recorded by the weighing-bucket gauge (Geonor Precip), the tipping-bucket gauge versus time.

Rapid drainage can occur immediately after precipitation—sometimes in as short a time as one to two days—and subsequently, the soil returns to field capacity, which is the predicted water storage of the soil (Hillel, 1980). This suggests that soil-water drainage into the underlying fractured volcanic aquifer possibly contributed to mountain block recharge following significant precipitation events that saturated the soil at 20 cm (8 in) (Table 1 and Figure 8). From June 2010 to May 2019, six cases of deep drainage occurred. The drainage was usually identified immediately following significant winter/spring rainfall events, but in two cases, snowmelt was identified to induce saturation and cause drainage. Table 1 characterizes the identified drainage events at Timber Mountain. It shows that all events occurred in February or March and had pre-wetted soils, and that rainfall events had sufficient rainfall intensity for multiple hours to induce drainage. The Atlas 14 Precipitation Frequency Data Server (NOAA, 2014) provides context for the magnitude of observed rainfall during the drainage events with respect to estimated precipitation frequency intervals. According to the Atlas 14 (NOAA, 2014), the predicted rainfall depth of a 24-hour storm with a 100-year return interval (i.e., the probability that a storm will occur once in 100 years) is 12.67 cm (4.99 in), assuming the exact location of the Timber Mountain monitoring station. Over the course of this study, the greatest 24-hour storm occurred on February 2, 2019, and contributed 6.48 cm (2.55 in) of precipitation (Table 1), which corresponds to a return interval of five years.

Drainage events caused by snowmelt on March 25, 2011, and February 7, 2016, are shaded in yellow in Figures 8 and 9, respectively. There are two explanations for the water content profile. First, drainage is determined by the tabletop shape of the deepest (20 cm [8 in]) soil moisture measurements (Figures 8a and 9a). Soil moisture increased to the maximum soil porosity and the pore space was entirely saturated, and then soil water was continuously lost to deep drainage. Once the soil had drained—indicated by the sharp

Table 1. Characteristics of identified drainage events at the Timber Mountain monitoring station between 2010 and 2019.

Date	Saturation Process	Rainfall or Snowmelt Duration (hrs)	Total Precipitation (cm)	Average Intensity (cm/hr)	Drainage Duration (hrs)	Antecedent Soil Moisture (at 20 cm depth)
3/25/11	snowmelt	101.3	4.27 (22.6 cm maximum snow depth)	0.04	7.0	0.29
2/7/16	snowmelt	14.6	3.45 (18.3 cm maximum snow depth)	0.24	5.1	0.31
2/17/17	rainfall	53.3	7.11	0.13	80.5	0.33
2/2/19	rainfall	16.5	6.48	0.39	11.5	0.28
2/14/19	rainfall	9.3	2.08	0.22	16.7	0.35
3/6/19	rainfall	17.5	3.94	0.23	31.1	0.36

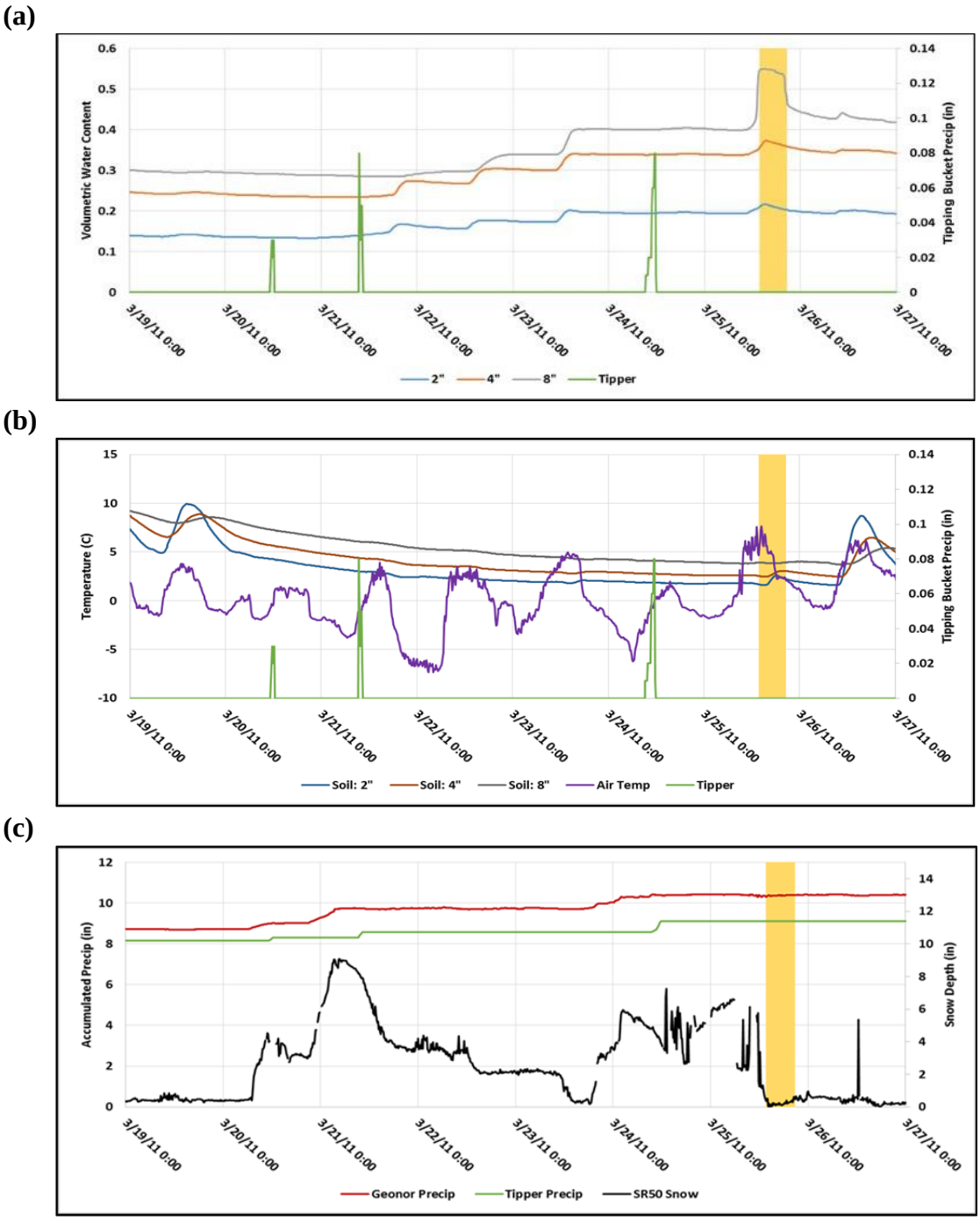

Figure 8. Timber Mountain station data between March 19, 2011, and March 27, 2011. Drainage timing on March 25th is highlighted in yellow. (a) Precipitation and soil VWC versus time. The maximum VWC at the 20 cm (8 in) sensor indicates drainage occurred, but saturation did not immediately follow precipitation. (b) Precipitation as well as soil and air temperature versus time. The soil temperature was invariant and insulated by a layer of snow until snowmelt occurred. (c) Snow depth and accumulated precipitation recorded by the weighing-bucket gauge (Geonor Precip) and the tipping-bucket gauge, showing that most of the precipitation preceding the drainage event was snow and the drainage event was timed with a decrease in snow depth.

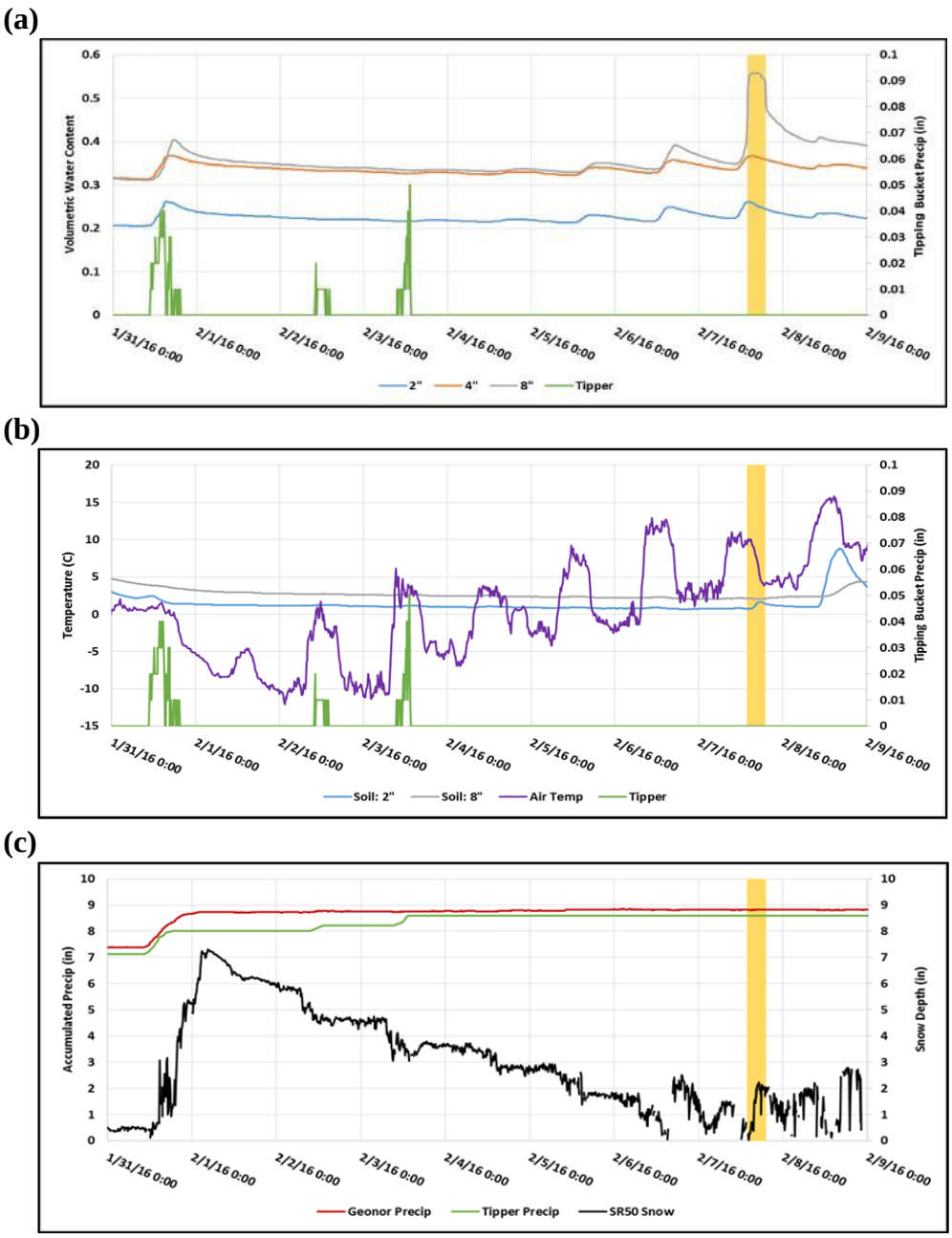

Figure 9. Timber Mountain station data between January 31, 2016, and February 9, 2016. Drainage timing on February 7th is highlighted in yellow. (a) Precipitation and soil VWC versus time. The maximum VWC at the 20 cm (8 in) sensor indicates drainage occurred, but saturation did not immediately follow precipitation. (b) Precipitation and soil and air temperatures versus time (the 10 cm [4 in] soil temperature sensor was nonfunctional at that time). The soil temperature was invariant and insulated by a layer of snow until snowmelt occurred. (c) Snow depth and accumulated precipitation recorded by the weighing-bucket gauge (Geonor Precip) and the tipping-bucket gauge, which shows that most of the precipitation preceding the drainage event was snow and the drainage event was timed with a general decrease in snow depth. The snow-depth signal shows substantial noise beginning on February 6th. Actual snow depth was expected to reduce to zero on the afternoon of February 7th.

decrease of soil moisture—the soil reached field capacity and evapotranspiration then became the primary mechanism of decreased soil moisture. Both drainage events exhibited a peak soil moisture of approximately 55 percent at 20 cm (8 in) that was delayed many hours after peak precipitation occurred, indicating soil moisture increased because of snowmelt. Figures 8b and 9b show that the temperature measurements of the soil prior to the drainage event were invariable, which suggests a dampened temperature change because of snow on the surface. Figures 8b and 9b also demonstrate that drainage occurred following warmer air temperatures, which melted the surface snow. Figures 8c and 9c confirm that snow depth decreased from a few centimeters to zero prior to drainage. Generally, soil moisture increased with warmer temperatures and lower snow depth, and soil moisture did not increase immediately with precipitation during these two events.

Second, the soil is hydraulically disconnected at the three measurement depths. Instead of the hydraulic conductivity being very high, allowing for rapid infiltration, it could be that the hydraulic conductivity among the three time-domain reflectometry (TDR) probes is essentially zero and that the three independent and separate flow paths became conductive nearly simultaneously. Figure 9a shows volumetric water content increasing at the same time for the three TDR probes. Although often considered highly unlikely, the second explanation suggests that three separate preferential flow paths are being monitored for soil moisture.

Drainage events caused by rainfall on February 17, 2017; February 2, 2019; February 14, 2019; and March 6, 2019, are shaded in yellow in Figures 10 through 13, respectively. Snowmelt can be ruled out as a mechanism for drainage because of the variability of soil temperature, the consistency between precipitation measurements made by the tipping-bucket and weighing-bucket gauges, and the absence of snow measured by the SR50A depth sensor. Drainage timing is determined based on the tabletop shape of the 20 cm (8 in) deep soil moisture measurements, where soil moisture increased to maximum saturation (approximately 50 percent to 55 percent) concurrent with rainfall events. Drainage into the underlying rock did not occur as fast as infiltration from precipitation. Therefore, soil moisture reached saturation in the increasingly shallower depth horizons as water filled the soil profile. Maximum saturation is found to be 45 percent to 50 percent at the 10 cm (4 in) depth and 40 percent to 45 percent at the 5 cm (2 in) depth. Soil water was eventually drained enough to reduce the water content at the shallower depths first and deeper depths later as the soil returned to field capacity, at which point evapotranspiration became the primary mechanism of decreased soil moisture. Figure 13 is a representative example of the filling and draining process of the soil profile in response to precipitation.

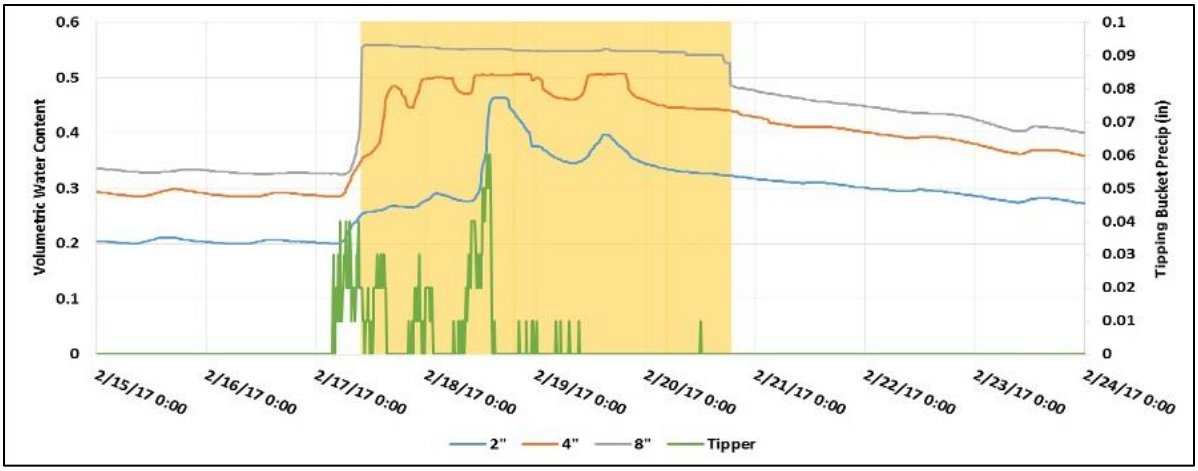

Figure 10. Precipitation and volumetric water content of the Timber Mountain soil profile between February 15, 2017, and February 24, 2017. Drainage timing on February 17th is highlighted in yellow. Soil moisture at the 10 cm (4 in) depth appears to have surged between saturated and unsaturated conditions in response to precipitation.

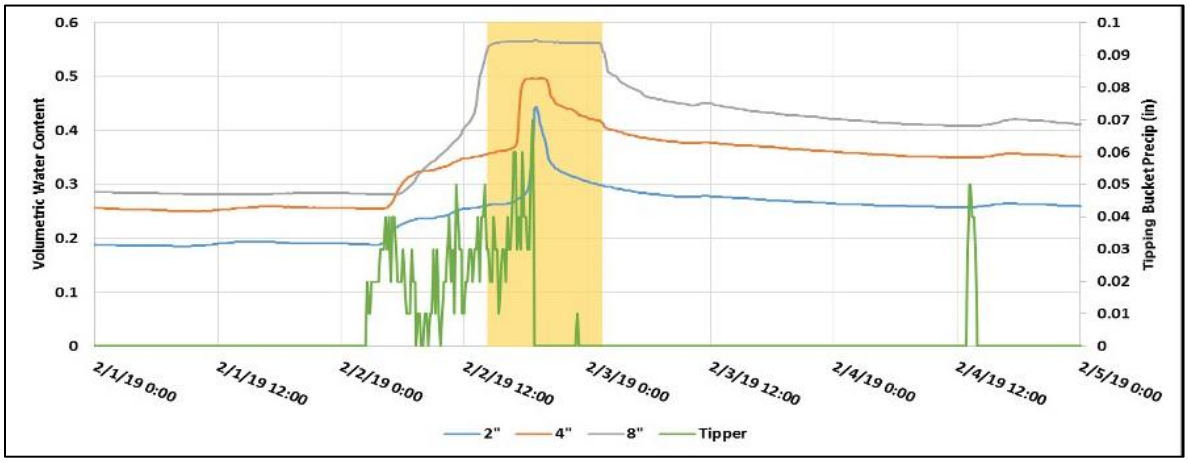

Figure 11. Precipitation and volumetric water content of the Timber Mountain soil profile between February 1, 2019, and February 5, 2019. Drainage timing on February 2nd is highlighted in yellow.

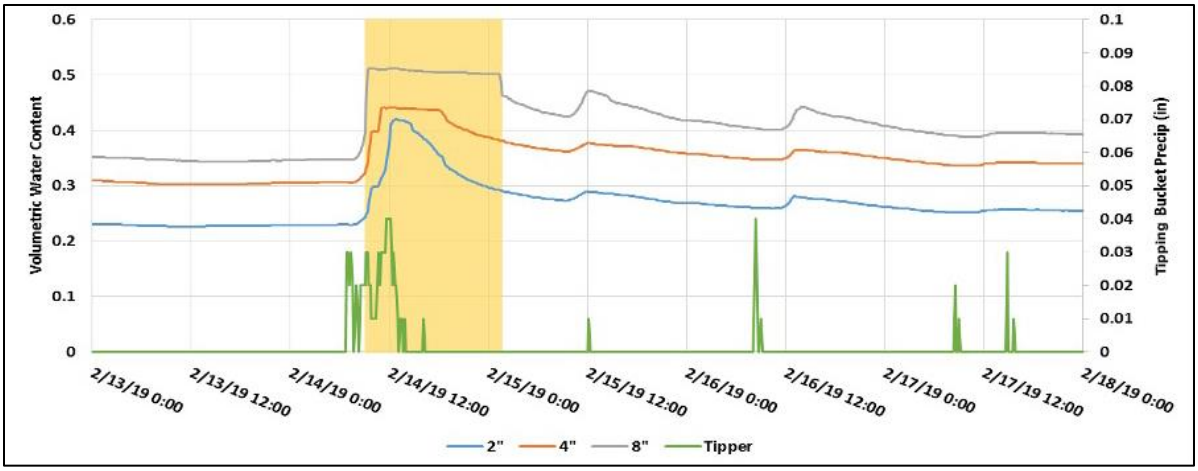

Figure 12. Precipitation and volumetric water content of the Timber Mountain soil profile between February 13, 2019, and February 18, 2019. Drainage timing on February 14th is highlighted in yellow.

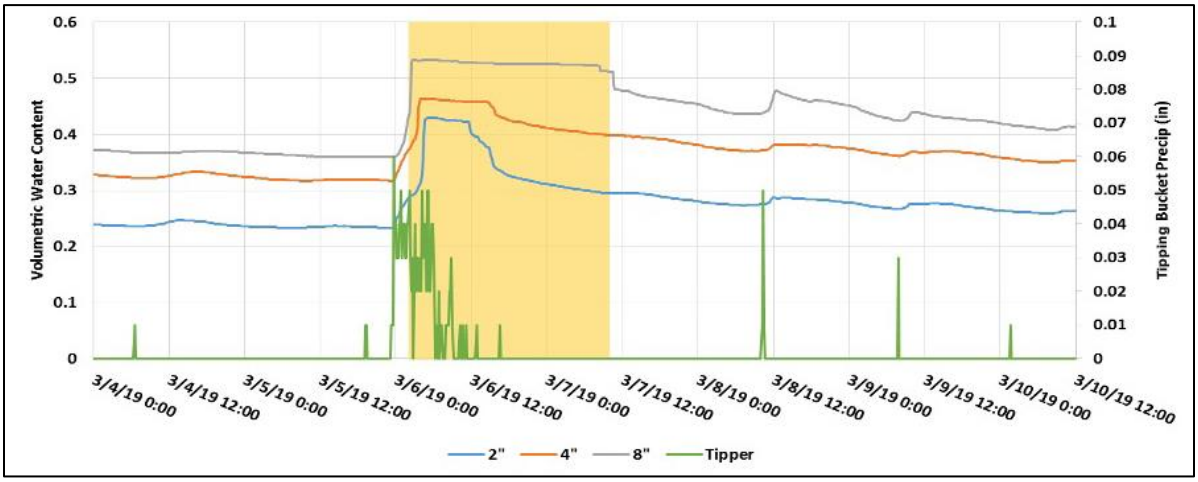

Figure 13. Precipitation and volumetric water content of the Timber Mountain soil profile between March 4, 2019, and March 10, 2019. Drainage timing on March 6th is highlighted in yellow. Soil moisture increased to saturation first at 20 cm (8 in) depth, and then saturated the entire soil profile. Soil water was eventually drained enough to reduce the water content at the shallower depths first, and then deeper depths later.

A nine-year recharge analysis of the Timber Mountain monitoring station has identified six events in which the deepest horizon of a soil profile exhibited saturation and soil-water drainage. It is possible that drainage occurred during other winter/spring precipitation events, but it is difficult to make a definitive statement pertaining to drainage below 20 cm (8 in) because of a lack of data. A drainage gauge (G3, METER Group, or similar) could be installed to directly measure the drainage of soil in the vicinity of the existing Timber Mountain monitoring station. In addition, data collected from the existing soil probes could be input into HYDRUS—the one-dimensional, variably saturated porous

media model—which is capable of modeling soil infiltration and drainage during rainfall events. Soil characterization, including porosity and bulk density, is recommended to accurately model results.

Recharge Estimate by Chloride Mass Balance

Precipitation Amount

Three precipitation gauges installed at the Timber Mountain monitoring station were monitored for nine years. A weighing Geonor gauge and a Hydrologic Services model TB4 tipping-bucket gauge were sampled at 10-minute intervals throughout the monitoring period, and a 20 cm (8 in) diameter bulk gauge was sampled periodically (roughly twice per year). Table 2 shows the precipitation measured from the three gauges (Lyles *et al.*, 2016, 2018a,b,c). The data are presented to compare the weighing gauges with the bulk gauge, which was sampled semiannually. Because the bulk gauge was not sampled on a schedule, the total amount of rainfall for each gauge is summed over the entire period of 7.4 years of data collection. Table 2 shows that mean precipitation from all three gauges at the station was 26.95 cm/yr (10.61 in/yr). Over the entire period, the error associated with the Geonor gauge

Table 2. Sample dates, precipitation values (cm) from the three gauges, and Cl concentration of precipitation from the bulk gauge. "Elapsed time" is the time between successive sample dates. The gauges were made operational on December 1, 2010.

Date	**Elapsed time, year(s)**	**Precipitation, cm**			**Cl, mg/L**
		Bulk Gauge	**Geonor (weighing)**	**TB4 Gauge (tipping)**	
12/1/2010					
5/16/2011	0.4545	22.56	22.58	26.52	0.99
9/20/2011	0.3477	5.41	8.48	6.76	2.37
8/2/2012	0.8679	12.70	11.84	9.14	1.5
12/4/2012	0.3395	11.76	11.28	10.97	0.7
5/16/2013	0.4463	11.76	11.99	11.38	0.4
11/19/2013	0.5120	10.49	10.87	10.90	0.61
1/8/2014	0.1369	4.78	4.34	2.57	NA
5/5/2014	0.3203	7.32	6.88	5.36	0.39
9/25/2014	0.3915	7.14	7.42	9.80	0.87
7/1/2015	0.7639	17.78	17.02	17.88	0.86
11/4/2015	0.3450	16.51	15.98	16.87	0.86
7/28/2016	0.7310	24.13	23.04	25.22	<0.46
11/18/2016	0.3094	NA[1]	2.13	2.41	NA
2/9/2017	0.2272	10.49	11.84	12.47	0.71
6/28/2017	0.38057	11.43	22.07	22.83	0.53
9/19/2017	0.2272	NA	1.55	2.01	NA
5/3/2018	0.6188	10.16	9.91	8.97	NA
TOTAL	**7.4196**	**184.42**	**199.21**	**202.06**	
Mean, cm/year		**26.8**	**26.9**	**27. 3**	
Mean of 3 gauges, cm/year			**27.0**		
Time-weighted Mean Cl, mg/L					**0.73**

[1]NA = not available because of malfunction of the wet-fall sampler mechanism. The elapsed time between NA and the previous sample date was subtracted from the total time for the bulk gauge.

compared with the bulk gauge was <0.1 percent, whereas the error associated with the TB4 gauge was 2.1 percent. This is surprisingly much less than the errors calculated for the semiannual comparisons that are presented in Lyles *et al.* (2016, 2018a,b,c).

Chloride Concentration in Precipitation

Chloride concentration in precipitation was determined from the bulk precipitation gauge located at the Timber Mountain station. These data include both wet-fall and dry-fall values for the years up to July 28, 2016. At this time, a mechanism was installed to allow Cl to enter the bulk gauge only during precipitation events. The mechanism turned out to be unreliable, so the measurements made during 2016 and 2017 are suspect but informative, as described below. The time-weighted mean value of all the Cl samples collected from the bulk sampler is 0.73 mg/L. The time-weighted mean value of Cl is determined by multiplying the elapsed time (yrs) for each time period by the amount of Cl in precipitation (mg/L) for each time period, summing the elapsed time, summing the amount of Cl multiplied by the elapsed time, and then dividing the total amount of Cl multiplied by the elapsed time by the total elapsed time. As discussed in Cooper *et al.* (2013), this is likely highly overestimated. For this reason, as well as others discussed in Cooper *et al.* (2013), Cl concentration in precipitation was calculated from the fewer but more reliable data from the wet-fall sampler (WFS).

The WFS mechanism became operational on July 28, 2016. Table 3 presents the dates, Cl concentrations, and remarks pertaining to wet-fall Cl deposition in the sampler. From Lyles *et al.* (2018b), the bulk gauge underestimated precipitation since the installation of the WFS because of intermittent failures of the WFS. For this reason, the WFS was deactivated on September 19, 2017, resulting in the collection of a combination of dry- and wet-fall chemistry samples after that time. Nonetheless, Cl data collected during the period of malfunction may be used to constrain the measurement of wet-fall Cl deposition. As long as the WFS mechanism is functioning properly, the only Cl in the bulk gauge is wet-fall Cl, so the Cl concentration of the precipitation in the bulk gauge will be the average for all precipitation events collected. If the WFS mechanism fails open, then any dry-fall Cl entering the bulk gauge will increase the Cl concentration of precipitation in the bulk gauge. If the WFS mechanism fails closed, then no dry-fall or wet-fall Cl will be added to the bulk gauge and the Cl concentration in the gauge will be the average Cl concentration for all precipitation events collected prior to the WFS mechanism failure. The degree of overestimation of Cl in precipitation is a function of the period of time in which the WFS mechanism was open during periods of no precipitation. Therefore, measured Cl concentrations are either representative of Cl in precipitation or are an overestimate because of accurate wet-fall deposition plus the inclusion of dry-fall contamination. Using this reasoning, it seems likely that for the period of deposition between February 9, 2017, and June 28, 2017, the best estimate of Cl concentration in precipitation is less than or equal to the time-weighted average of 0.60 mg/L (Table 3). The value used in Cooper *et al.* (2013) is 0.47 ± 0.17 mg/L, so the estimate of wet-fall at the site (C_p = 0.60 mg/L) is at the border of the uncertainty of the value used in Cooper *et al.* (2013).

Table 3. Chloride concentration in precipitation, from wet-fall sampler.

Date	Cl Concentration, mg/L	Remarks
11/18/2016[1]	NA	No water in bulk gauge because of malfunction
02/09/2017[2]	0.71	--
06/28/2017	0.53	--
09/19/2017	NA	WFS left in open position
Time-weighted Average	0.60	--

[1]From Lyles *et al.* (2018a).
[2]From Lyles *et al.* (2018b).
NA = no data available.

Chloride Concentration in Groundwater

There are no wells or springs on Timber Mountain in the location of the recharge zone (Fenelon *et al.*, 2010). Therefore, the nearest three wells that were either downgradient or cross gradient were used to estimate Cl concentration of recharge because the groundwater flow direction is thought to be toward the southwest (Fenelon *et al.*, 2010; Fenelon *et al.*, 2016). UE-18r is north, ER-EC-5 is west, and ER-EC-7 is south of Timber Mountain. Chemistry data from the UCDB (Navarro, 2019) were evaluated and included in the analysis based on the following constraints: (1) Cl values from open zones prior to well completion were not used because it was presumed that these may have been contaminated by drilling mud; (2) values flagged as suspect were not used, including values in which a bias was noted; (3) if duplicate samples were collected on the same day, they were averaged for the day; and (4) vertical mixing within the well was assumed, so data from all piezometer levels were used to compute an average for a given well. The remaining values were then averaged for each well and the average Cl concentration of groundwater was taken to be the average value of the three wells (Table 4), or C_r = 10.9 mg/L.

Table 4. Well identification, number of samples, mean Cl concentration from each well, and mean of the three wells (from Navarro [2019]).

Well	Number of Samples[1]	Mean Cl Concentration, mg/L
UE-18r	16	8.3
ER-EC-5	2	15.9
ER-EC-7	5	4.5
Mean of three wells	**23**	**9.6**

[1]Does not include duplicates.

Estimate of Recharge

For a mean precipitation value of 26.95 cm/yr (10.61 in/yr), the Cl concentration in precipitation is C_p , = 0.60 mg/L, the Cl concentration in recharge is C_r = 9.6 mg/L, and an estimate of recharge (N) from Equation (2) is 1.48 cm/yr (0.58 in/yr) for Timber Mountain. The recharge estimate for Pahute Mesa by the chloride mass-balance method by Cooper *et al.* (2013) used similar values that were approximately ±20 percent for P for Timber Mountain, ±35 percent for C_p, and ±10 percent for C_r. Using these values and error propagation through

Equation (1) results in an uncertainty range of ±0.96 cm/yr (±0.38 in/yr) around the recharge estimate of 1.48 cm/yr (0.58 in/yr). There are not enough data to accurately determine uncertainty in the recharge calculation.

Other estimates of recharge for Timber Mountain include 0.1-0.2 cm/yr (0.04-0.08 in/yr) (Middleton *et al.* 2019) using the INFIL 3.0 model, 0.2-1.0 cm/yr (0.08-0.39 in/yr) (Russell and Minor, 2002) using the chloride mass-balance method, 0.6-6.0 cm/yr (0.24-2.36 in/yr) (Fenelon *et al.*, 2016) by water-balance modeling, and 0.5-0.75 cm/yr (0.24-0.30 in/yr) (Middleton *et al.,* 2019) using the Maxey-Eakin method. The estimate here of 1.48 cm/yr ±0.96 cm/yr (0.58 in/yr ±0.38 in/yr) falls within the different reported ranges for recharge for Timber Mountain.

Two-dimensional Radial Flow of Groundwater with Recharge

Using this recharge value, a simple unconfined flow model can be developed to predict hydraulic head. Two-dimensional (horizontal), steady-state radial flow with constant vertical recharge can be expressed using Cartesian coordinates as:

$$\frac{\partial^2 h^2}{\partial x^2} + \frac{\partial^2 h^2}{\partial y^2} + \frac{N}{2K} = 0 \tag{3}$$

where $K = K(z)$ [LT^{-1}] is the hydraulic conductivity as a function of the vertical direction, Z, and the dependent variable is the square of the hydraulic head, h^2 [L^2] (or water table height above an arbitrary datum). For axisymmetric flow away from the center of a mountain, it is more appropriate to model flow in radial coordinates. In this case, the above equation for $h^2(r)$ becomes:

$$\frac{1}{r}\frac{d}{dr}\left(r\frac{dh^2}{dr}\right) + \frac{N}{2K} = 0 \tag{4}$$

The recharge area is assumed to extend to a distance, R_R, where $0 \le R_R \le R$, R is the extent of the domain of the flow problem. Recharge rate is assumed to be spatially uniform within the recharge area and there is no recharge outside of it, as expressed by:

$$N(r) = \begin{cases} N & \text{for} \quad 0 \le r \le R_R \\ 0 & \text{for} \quad R_R \le r \le R \end{cases} \tag{5}$$

The differential Equation (4) is solved as two separate equations: one within the recharge area, where $h = h_1$, and the other outside of the recharge area, where $h = h_2$. The two solutions are merged together at $r = R_R$. The boundary conditions are:

$$\begin{aligned} \frac{dh_1{}^2}{dr} &= 0 \quad \text{at} \quad r = 0 \\ h_2{}^2 &= 0 \quad \text{at} \quad r = R \\ h_1 &= h_2 \quad \text{at} \quad r = R_R \\ \frac{dh_1}{dr} &= \frac{dh_2}{dr} \quad \text{at} \quad r = R_R \end{aligned} \tag{6a–d}$$

The last two boundary conditions are applied at the distance R_R, where the hydraulic heads and the flow rates must match. The solutions to Equations (6a) through (6d) for h_1 and h_2 are:

$$h_1^2(r) = \frac{N}{8K}\left(R_R^2 - r^2\right) + \frac{N}{4K} R_R^2 \, ln\frac{R}{R_R}$$
$$h_2^2(r) = \frac{N}{4K} R_R^2 \, ln\frac{R}{r} \qquad (7a,b)$$

There are no wells or hydraulic conductivity data in the recharge area of Timber Mountain, so values of K are obtained from ranges reported for similar hydrogeologic units in the Death Valley regional groundwater flow system. The upper hydrogeologic unit has been mapped as the Thirsty Canyon-Timber Mountain volcanic aquifer (TMVA) (Garcia *et al.*, 2017), which consists of Pliocene to Miocene non-welded to densely welded ash-flow tuff, depositional and fault-related tuff breccia, ash-fall tuff, and rhyolite and trachyte lava flows (Belcher *et al.*, 2001). The hydraulic conductivity of the TMVA has been estimated by Belcher *et al.* (2001) to have a geometric mean of 0.01 m/d (0.03 ft/d) with a 95 percent confidence interval between 0.001 m/d (0.003 ft/d) (1.16 x 10^{-8} m/s [3.81 x 10^{-8} ft/s]) and 0.01 m/d (0.03 ft/d) (1.16 x 10^{-7} m/s [3.81 x 10^{-7} ft/s]) based on 11 analyses. For recharge occurring within a radius of 4 km (2.5 mi) (Fenelon *et al.*, 2010, plate 3), recharge (N) of 1.48 cm/yr (0.58 in/yr) (for $0 \leq r \leq R_R$; otherwise N=0), hydraulic conductivity of 1.16 x 10^{-7} m/s (3.81 x 10^{-7} ft/s), and radial flow occurring to 10 km (6.2 mi), the approximate distance from the center of Timber Mountain to the main flow path in the Pahute Mesa-Oasis Valley groundwater basin, the equation predicts a groundwater mound of 152 m (499 ft) at the center of Timber Mountain (Figure 14). For the same K ± 1 standard deviation of N, the results show maximum mound heights of 195 m (640 ft) and 122 m (400 ft), respectively, at the center.

Figure 14 also shows the results of the lower (95 percent confidence interval) K and mean N (1.48 cm/yr), where the maximum mound height is 479 m (1,572 ft) at the center. A one-order-of-magnitude change in K clearly has a more significant impact on the results than ± 1 standard deviation of the recharge rate.

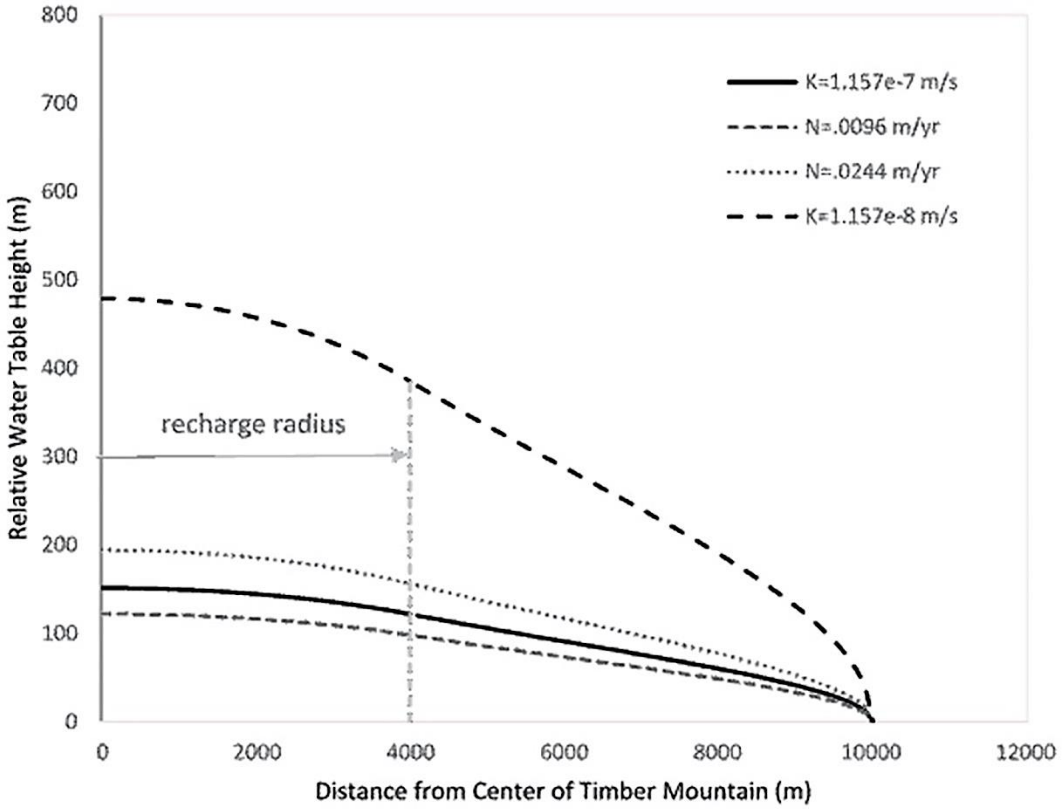

Figure 14. Cross section of theoretical groundwater mound from center to 10,000 m (6.2 mi) radius. The solid black line is for the higher estimate of *K* (1.157 x 10^{-7} m/s [3.796 x 10^{-7} ft/s]) from Belcher *et al.* (2001) and mean recharge estimate of 1.48 cm/yr (0.58 in/yr). This is enveloped by curves for the same hydraulic conductivity and the lower (0.96 cm/yr [0.38 in/yr], dashed gray line) and higher (2.44 cm/yr [0.96 in/yr], dotted gray line) recharge estimates that are plus or minus one standard deviation from the mean, respectively. A mound calculated for the lower estimate of *K* from Belcher *et al.* (2001) and mean recharge (dark dashed line) is also shown.

Movement of Recharge using Water-rock Reaction Chemical and Isotopic Modeling

Isotopic and Chemical Signatures of Timber Mountain Recharge

The Timber Mountain weather monitoring station was visited biannually to retrieve precipitation samples from the bulk gauge, download monitoring data, and service the equipment. Site visits were scheduled to correspond with the two principal precipitation periods of summer and winter. The summer precipitation period is June through September, which is characterized by monsoons and the moist, southerly winds that affect much of the southwestern United States. The monsoonal winds often develop into desert thunderstorms that cause flash floods. The winter period comprises the remaining months during which snow is more likely to occur and includes the "shoulder season" months of May and October.

Figure 15 presents the isotopic samples collected from the bulk precipitation gauge from June 2010 through May 2019. Precipitation samples show typical isotopic differences between summer and winter seasons (e.g., Ingraham *et al.* [1991]), with winter bulk

precipitation samples ranging from -16.7 to -13.6 ‰ $\delta^{18}O$ and from -125 to -101 ‰ $\delta^{2}H$, and summer samples ranging from -11.0 to -8.1 ‰ $\delta^{18}O$ and from -80 to -64 ‰ $\delta^{2}H$. Because of issues with site visitation scheduling, four samples (shown in yellow) had overlapping summer and winter precipitation collection periods. Most samples fell along the global meteoric water line (GMWL) developed by Craig (1961). Ingraham *et al.* (1991) developed a local meteoric water line (LMWL, $\delta^{2}H = 6.87\ \delta^{18}O - 6.5$) for the NNSS from bulk precipitation samples collected from 14 sites from 1982 to 1986. Ingraham *et al.* (1991) included three sites on Timber Mountain at elevations of 1,400 m (4,593 ft), 1,630 m (5,348 ft), and 1,840 m (6,037 ft). A total of 41 $\delta^{2}H$-$\delta^{18}O$ sample pairs from the three sites had a similar range in isotopic values (not shown on Figure 15) as those from this study. The LMWL for the bulk precipitation samples from the Timber Mountain monitoring station is remarkably similar (Figure 15, $\delta^{2}H = 6.8\ \delta^{18}O$ -7.89) to the Ingraham *et al.* (1991) line. Weighting the summer and winter isotopic values by the precipitation amount produces precipitation amount-weighted averages of -15.3 ‰ $\delta^{18}O$ and -115 ‰ $\delta^{2}H$ for winter and -9.7 ‰ $\delta^{18}O$ and -74 ‰ $\delta^{2}H$ for summer (Figure 15).

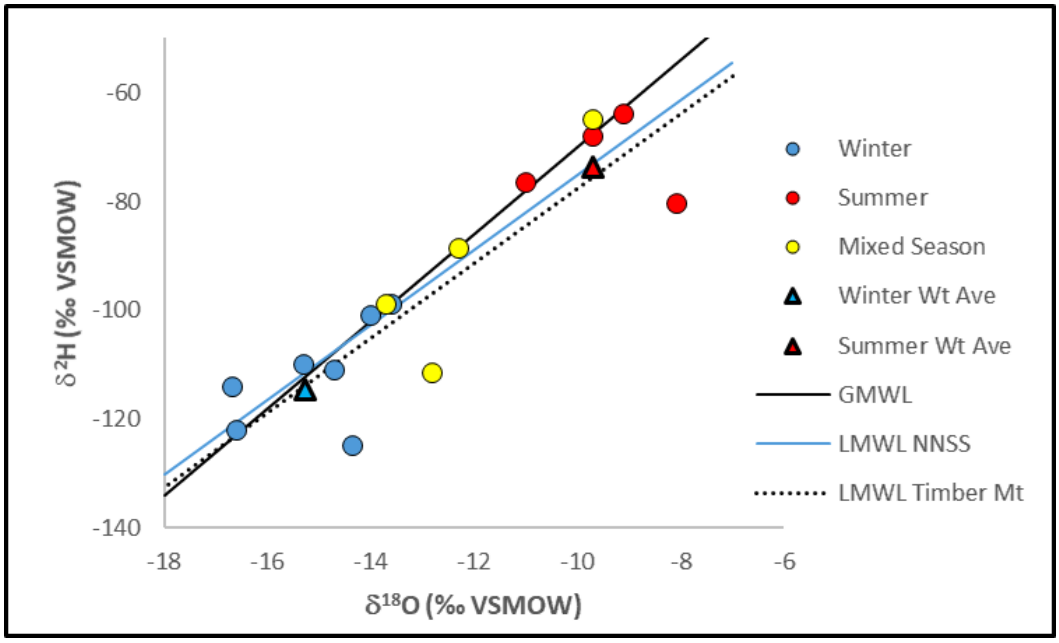

Figure 15. Isotopic signatures of precipitation samples from the bulk precipitation gauge at the Timber Mountain monitoring station from June 2010 through May 2019. The precipitation amount-weighted, isotopic average for winter and summer precipitation are presented as triangles. The global meteoric water line (GMWL, $\delta^{2}H = 8\ \delta^{18}O + 10$ [Craig, 1961]), an NNSS local meteoric water line (LMWL, $\delta^{2}H = 6.87\ \delta^{18}O$ -6.5 [Ingraham *et al.*, 1991]), and the Timber Mountain LMWL ($\delta^{2}H = 6.8\ \delta^{18}O$ -7.89) are also shown.

In the absence of springs or shallow water-table wells on Timber Mountain, a representative isotopic signature for local recharge from Timber Mountain can be developed by comparing the isotopic signature of the bulk precipitation samples to the isotopic signatures of perched groundwater emanating from volcanic rocks in the vicinity of Timber Mountain. Seven springs on the NNSS were identified for comparison, as were five recent sample locations from the Rainier Mesa tunnels (Figure 16).

Using the UCDB (Navarro, 2019), water samples that were collected on the same day but analyzed by different laboratories and duplicate analyses of the same spring sample were averaged for that sample date. Locations with multiple samples from different sample dates were averaged to develop an average isotopic composition for the location.

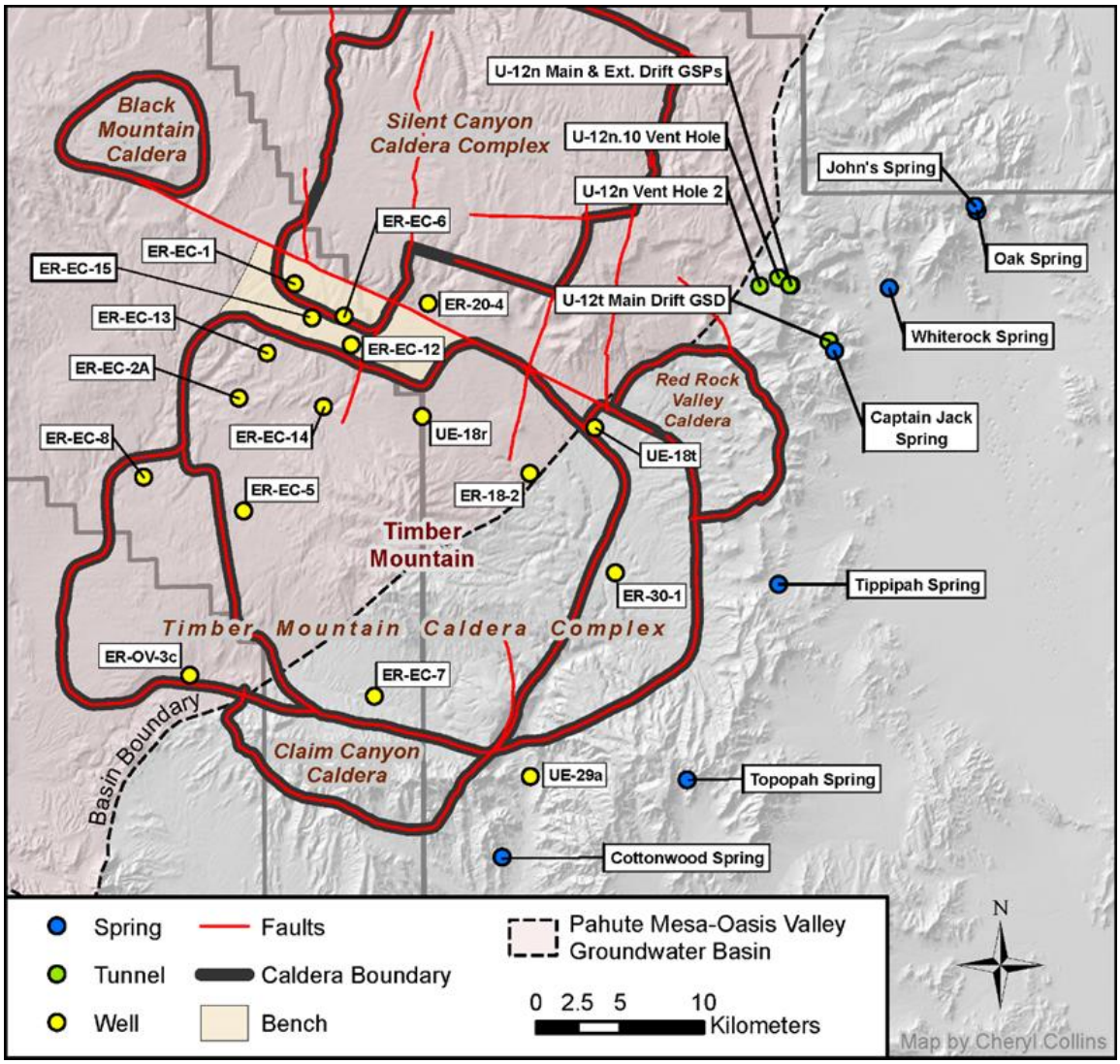

Figure 16. Wells and springs in the vicinity of Timber Mountain and Pahute Mesa and the Pahute Mesa-Oasis Valley groundwater basin boundary from Fenelon *et al.* (2016). The southern basin boundary bisects Timber Mountain. Rainier Mesa tunnel sample locations (U-12n and U-12t) are also shown.

The average isotopic signature for springs ranged from isotopically light Captain Jack Spring (-13.1 ‰ $\delta^{18}O$ and -107 ‰ $\delta^{2}H$) to isotopically heavy Cottonwood Spring (-11.7 ‰ $\delta^{18}O$ and -89 ‰ $\delta^{2}H$), whereas tunnel samples were in general isotopically light (-14.2 to -13.4 ‰ $\delta^{18}O$ and -107 to -101 ‰ $\delta^{2}H$) (Figures 17 and 18). Table A-4 in Appendix A provides the elevation of the spring and tunnel sample locations; the elevation of the highest point of the likely recharge catchment; and the mean, standard deviation, and number of isotopic samples. The isotopic signature of the springs and tunnel samples ($R^2 = 0.4$) is correlated with elevation (spring and/or peak elevation). Ingraham *et al.* (1990) showed that the average isotopic signature of precipitation sites at the NNSS were similarly correlated with elevation and that the higher elevation sites had an isotopically lighter average precipitation.

The isotopic signature of the NNSS springs plot between the winter and summer precipitation samples from Timber Mountain (Figure 17). Table A-5 in Appendix A presents the percent of summer verses winter precipitation amount-weighted isotopic averages to match the average isotopic value of the springs and Rainier Mesa tunnels. For the springs, the winter precipitation amount-weighted isotopic averages ranged from 36.7 percent to 68.4 percent. These winter percentages are substantially less than previous estimates of groundwater recharge in the southwestern United States whereby groundwater recharge is mostly attributed to winter precipitation (e.g., Simpson *et al.* [1972], Winograd and Riggs [1984], Ingraham *et al.* [1991], Winograd *et al.* [1998], and Earman *et al.* [2006]).

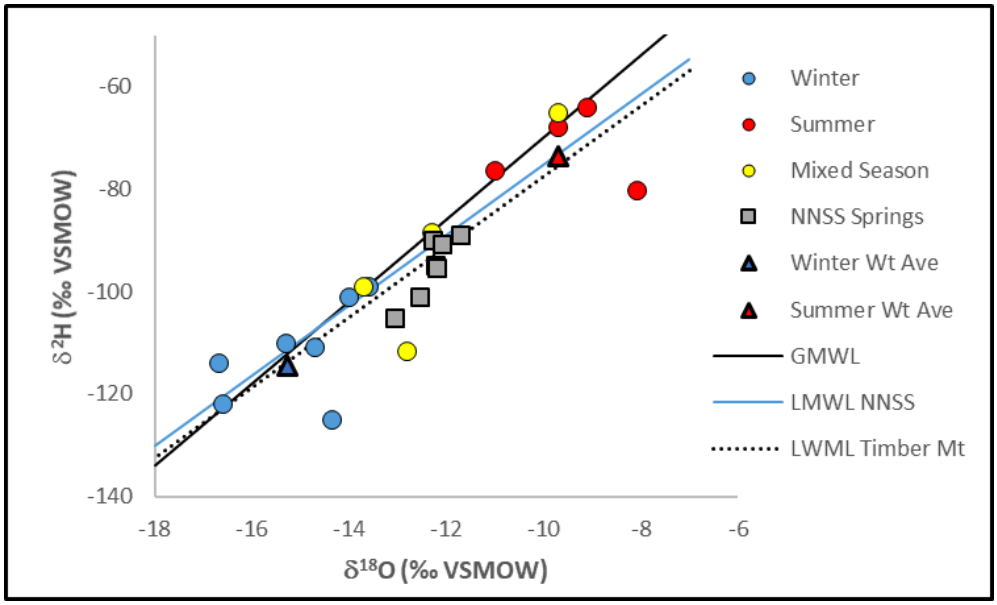

Figure 17. Isotopic signatures of precipitation samples from the bulk precipitation gauge at the Timber Mountain precipitation monitoring station from June 2010 through May 2019 and the isotopic signature of NNSS springs. The NNSS springs plot between the winter and summer isotopic signatures. The precipitation amount-weighted isotopic average for winter and summer precipitation are presented as triangles. The global meteoric water line (GMWL, $\delta^{2}H = 8\ \delta^{18}O + 10$ [Craig, 1961]), an NNSS local meteoric water line (LMWL, $\delta^{2}H = 6.87\ \delta^{18}O - 6.5$ [Ingraham *et al.*, 1991]), and Timber Mountain LMWL ($\delta^{2}H = 6.8\ \delta^{18}O$ -7.89) are also shown.

As discussed in the "Weather and Infiltration on Timber Mountain" section, during the eight full years of data collection at the Timber Mountain monitoring site, there were six infiltration events during which precipitation completely saturated the 20 cm depth of the soil profile at the site. These six events all occurred during the spring snowmelt period. Although the infiltration events at the monitoring site do not confirm that groundwater recharge occurred, the timing of infiltration events is consistent with previous research that most groundwater recharge is derived from winter precipitation (for a summary of studies see Beria *et al.* [2018]). Assuming that winter precipitation makes up most of the groundwater recharge at Timber Mountain, it is expected that the isotopic signature of groundwater recharge would be more similar to the isotopic signature of winter precipitation. Because most recharge occurs during the winter/spring snowmelt and because the isotopic signature of precipitation is lighter with increasing elevation at the NNSS, it is probable that groundwater recharge would be isotopically lighter than most of the NNSS springs.

Isotopic data are also available from the Rainier Mesa tunnels because they filled with water after plugging in 1993. The isotopic signature of water from N- and T-tunnels, collected behind the gas-sealed doors and plugs and from the U-12n vent holes, is isotopically lighter than the isotopic signature of most of the NNSS springs (Figure 18), except for Captain Jack Spring (Rainier Mesa) and Oak Spring (Oak Spring Butte, east of Rainier Mesa).

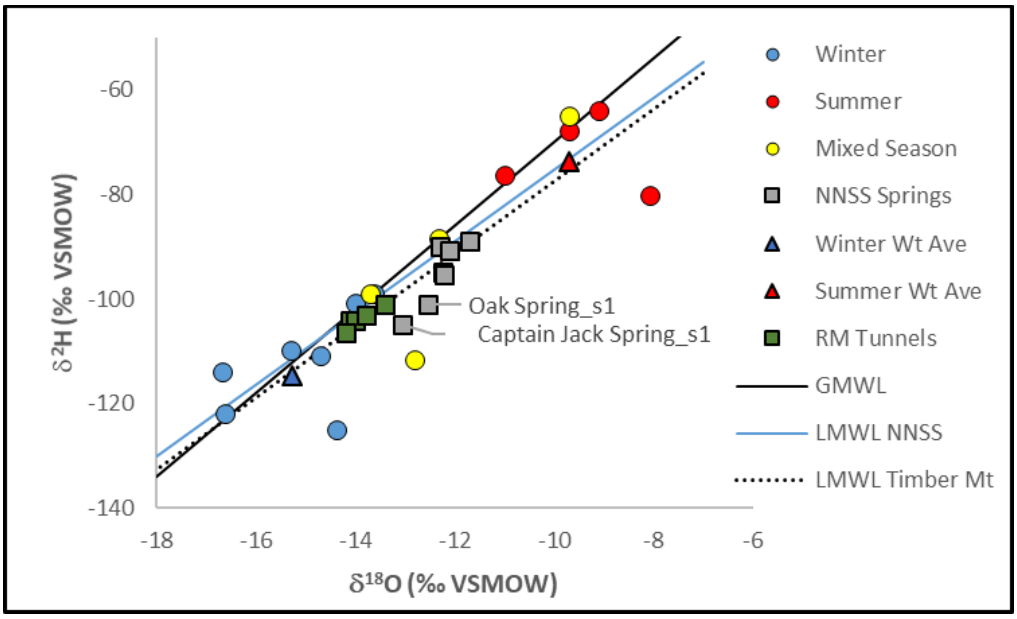

Figure 18. Isotopic signatures of precipitation samples from the bulk precipitation gauge at the Timber Mountain precipitation monitoring station from June 2010 through May 2019 and the isotopic signature of NNSS springs and Rainier Mesa tunnels. The NNSS springs plot between the winter and summer isotopic signatures. Rainier Mesa (RM) tunnel water is shown as green squares. The precipitation amount-weighted isotopic average for winter and summer precipitation are presented as triangles. The global meteoric water line (GMWL, $\delta^2H = 8\ \delta^{18}O + 10$ [Craig, 1961]), an NNSS local meteoric water line (LMWL, $\delta^2H = 6.87\ \delta^{18}O - 6.5$ [Ingraham *et al.*, 1991]), and a Timber Mountain LMWL ($\delta^2H = 6.8\ \delta^{18}O$ -7.89) are also shown.

Considering that Timber Mountain (2,272 m [7,456 ft] above mean sea level [amsl]) and Rainier Mesa (2,342 m [7,863 ft] amsl) are geographically close (roughly 20 km [12.5 miles]) and have similar elevations, it would be expected that precipitation falling on these two areas would have similar isotopic signatures and that the corresponding recharge would also have similar isotopic signatures. Therefore, the isotopic signature of Timber Mountain recharge should be similar to Rainier Mesa recharge because isotopically lighter precipitation is correlated with increasing elevation, most recharge is derived from winter precipitation that melts during the spring, the amount-weighted isotopic mean of winter precipitation at the Timber Mountain weather monitoring station is isotopically light, Rainier Mesa tunnel water and two Rainier Mesa springs are isotopically lighter than other NNSS springs, and Timber Mountain is geographically close and similar in elevation.

Timber Mountain is bisected by the southern boundary of the Pahute Mesa-Oasis Valley groundwater basin as described by Fenelon *et al.* (2016) (Figure 16). Five wells close to Timber Mountain fall into three isotopically distinct groups (Figure 19). ER-18-2_m1 is isotopically light and similar to wells in the Pahute Mesa-Oasis Valley groundwater basin. ER-EC-7_m1-2 and UE-18t_p1 are isotopically similar to the Rainier Mesa tunnel water and the isotopically light NNSS springs, Captain Jack Spring and Oak Spring. Two wells, ER-30-1_p2 and UE-29a 2_p1, are isotopically heavy and similar to the isotopically heavier NNSS springs. This suggests that Timber Mountain recharge may have only a small influence on the available wells depending on the groundwater flow path.

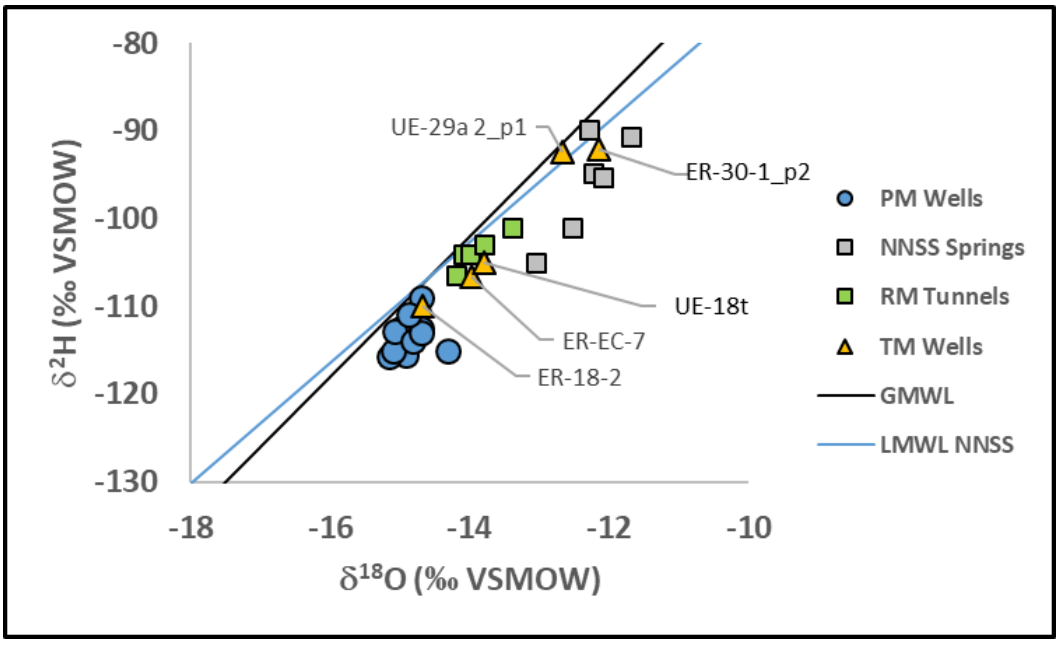

Figure 19. Isotopic signatures of wells surrounding Timber Mountain (Pahute Mesa [PM] wells and Timber Mountain [TM] wells) and the Rainier Mesa (RM) tunnel and NNSS springs. The global meteoric water line (GMWL, $\delta^2H = 8\ \delta^{18}O + 10$ [Craig, 1961]) and the NNSS local meteoric water line (LMWL, $\delta^2H = 6.87\ \delta^{18}O - 6.5$ [Ingraham *et al.*, 1991]) are also shown.

Chemically, recharge on Timber Mountain would be similar to the chemistry of NNSS springs and Rainier Mesa tunnel waters that have flowed through and interacted with volcanic rock over relatively short distances. Unfortunately, the Rainier Mesa tunnel water chemistry is affected by testing activities in the tunnels and is a combination of groundwater chemical compositions and interaction with anthropogenic materials in the tunnels (Russell *et al.*, in publication). Therefore, the chemistry of NNSS springs will be used as a surrogate to represent the chemical signature of Timber Mountain recharge.

The chemistry at wells ER-EC-7_m1-2, ER-30-1_p2, and UE-29a 2_p1 is similar to the NNSS springs (i.e., Timber Mountain recharge) with low Cl and low SO_4 (Figure 20). Pahute Mesa wells fall into two different groups, a low Cl and low SO_4 groundwater and a high Cl and high SO_4 groundwater. The low Cl-SO_4 group ranges in Cl from 4.7 to 20 mg/L and in SO_4 from 16.9 to 44 mg/L. The high Cl-SO_4 group ranges in Cl from 44 to 60 mg/L and in SO_4 from 80 to 94 mg/L. ER-18-2_m1 has low Cl, similar to NNSS springs, but has higher SO_4. UE-18t_p2 has low SO_4, like the NNSS springs, but much higher Cl. ER-18-2_m1 and UE-18t_p2 are close to each other and are both completed in the Rainier Mesa welded-tuff aquifer. The reason for the large differences in Cl and SO_4 between these two wells is unknown.

For water-rock reaction modeling of the mixing of Timber Mountain recharge with surrounding groundwater, the average chemistry of NNSS springs was used as a surrogate for groundwater recharge from Timber Mountain. The average isotopic signature of Rainier Mesa tunnel water, Captain Jack Spring, and Oak Spring was used as a surrogate for Timber Mountain recharge.

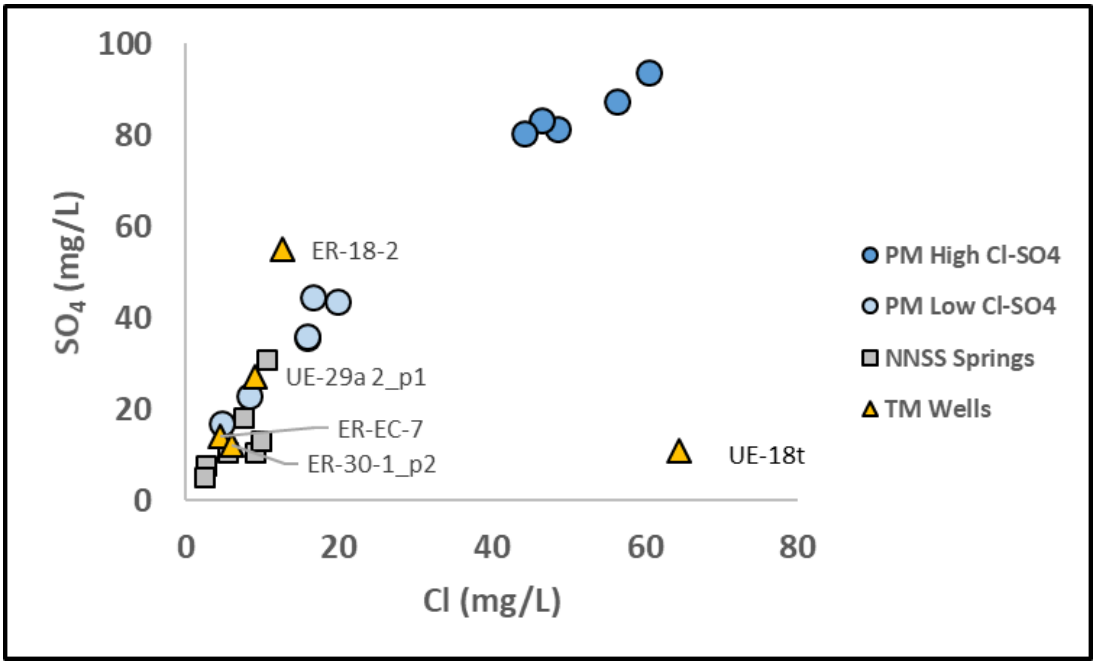

Figure 20. Cl and SO_4 concentrations in wells surrounding Timber Mountain (Pahute Mesa [PM] high Cl-SO_4 and PM low Cl-SO_4, and Timber Mountain [TM] wells) and NNSS springs.

Water-rock Reaction Modeling

Groundwater recharge on Timber Mountain would be expected to flow radially outward from the recharge area to the north and northwest into the Pahute Mesa-Oasis Valley groundwater basin and to the southwest, south, and east away from Timber Mountain. This conceptual model can be tested by modeling the water-rock reactions of recharge as it flows from Timber Mountain and examining the influence of Timber Mountain recharge on groundwater flow in the Pahute Mesa-Oasis Valley groundwater basin adjacent to the basin boundary.

Based on the chemical and isotopic relationships of Timber Mountain recharge to groundwater from wells surrounding Timber Mountain (Figures 19 and 20), different groundwater flow paths and the corresponding water-rock reactions can be tested. The water-rock reaction models tested are described below and the complete model outputs are included in Appendix A.

UE-29a 2_p1 and ER-30-1_p2

UE-29a 2_p1 and ER-30-1_p2 are isotopically heavier than Timber Mountain recharge and are similar to the isotopically heavier NNSS springs. Therefore, these two wells appear not to be derived from Timber Mountain recharge. No water-rock reaction models were run for these wells.

ER-EC-7_m1-2

Isotopically, ER-EC-7_m1-2 is like Timber Mountain recharge, so a direct flow path from Timber Mountain to ER-EC-7_m1-2 was evaluated. This scenario does not require any mixing with other groundwater. This scenario produced two successful models and the main water-rock reactions included the dissolution of calcite and SiO_2 (Table 5). Of note, the water-rock reaction models produced a poor match with carbon isotopes. The $\delta^{13}C$ signature used for Timber Mountain recharge (-14.1 ‰, the average of NNSS springs) is isotopically light, as would be expected for $\delta^{13}C$ in a recharge zone. ER-EC-7 has a $\delta^{13}C$ of -6.6 ‰. This suggests that either the water-rock reaction models do not include the correct carbon isotopic reactions or there is another groundwater mixing with Timber Mountain recharge to produce the observed water chemistry at ER-EC-7_m1-2. This unidentified groundwater would have to have similar $\delta^{2}H$ and $\delta^{18}O$ signatures to Timber Mountain recharge and ER-EC-7_m1-2 and would have to have a heavier $\delta^{13}C$ signature than ER-EC-7_m1-2.

Table 5. Water-rock reaction modeling results with Timber Mountain (TM) recharge flowing to ER-EC-7_m1-2. Positive values indicate mineral phase dissolution. Mineral phase changes are expressed as millimoles of mineral phase per kilogram of water (mmol/Kg).

Model #	**Calcite (mmol/Kg)**	**CO_2 Gas (mmol/Kg)**	**Ca/Mg Exchange (mmol/Kg)**	**SiO_2 (mmol/Kg)**
#1 and #2	0.4	0.1	0.1	0.3

ER-18-2_m1

Recharge from Timber Mountain flowing northeast toward ER-18-2_m1 requires mixing isotopically heavier recharge with an isotopically lighter Pahute Mesa groundwater. This scenario was tested by mixing either ER-20-4_m1, ER-EC-12_m2, ER-EC-14_m2, or UE-18r_o1 with Timber Mountain recharge.

The mixing scenario using ER-20-4_m1 produced four successful models using either δ^2H or $\delta^{18}O$ as the mixing constraint with 35 percent to 44 percent Timber Mountain recharge and 56 percent to 65 percent ER-20-4_m1 (Table 6). The main water-rock reactions included the exchange of Ca and Mg with Na on clay surfaces, dissolution of soil CO_2, and dissolution of calcite. The water-rock reaction models produced a poor match with carbon isotopes because of the isotopically heavy $\delta^{13}C$ signature at ER-18-2_m1 (-0.2 ‰).

The mixing scenario using ER-EC-12_m2 produced four successful models using either δ^2H or $\delta^{18}O$ as the mixing constraint with 31 percent to 33 percent Timber Mountain recharge and 67 percent to 69 percent ER-EC-12_m2 (Table 6). The main water-rock reactions included the exchange of Ca and Mg with Na on clay surfaces, dissolution of soil CO_2, and dissolution of calcite. The water-rock reaction models produced a poor match with carbon isotopes because of the isotopically heavy $\delta^{13}C$ signature at ER-18-2_m1 (-0.2 ‰).

The mixing scenario using ER-EC-14_m2 produced two successful models using δ^2H as the mixing constraint with 45 percent Timber Mountain recharge and 55 percent ER-EC-12_m2 (Table 6). There were no successful models using $\delta^{18}O$. The main water-rock reactions included the exchange of Ca and Mg with Na on clay surfaces, dissolution of soil CO_2, and dissolution of calcite. The water-rock reaction models produced a poor match with carbon isotopes because of the isotopically heavy $\delta^{13}C$ signature at ER-18-2_m1 (-0.2 ‰).

Table 6. Water-rock reaction modeling results with Timber Mountain (TM) recharge mixing with ER-20-4_m1, ER-EC-12_m2, ER-EC-14_m2, or UE-18r_o1 to produce the observed water chemistry at ER-18-2_m1. Positive values indicate mineral phase dissolution. Negative values indicate mineral phase precipitation. Mineral phase changes are expressed as millimoles of mineral phase per kilogram of water (mmol/Kg).

Model #	**Proportion of TM recharge (percent)**	**Proportion in Well (percent)**	**Calcite (mmol/Kg)**	**CO_2 Gas (mmol/Kg)**	**Ca/Mg Exchange (mmol/Kg)**	**SiO_2 (mmol/Kg)**
	TM Recharge	ER-20-4_m1				
δ^2H #1 and #2	44	56	5.5 to 5.9	5.9 to 6.3	6.7	-0.3
$\delta^{18}O$ #1 and #2	35	65	5.4 to 5.9	5.9 to 6.3	6.7	-0.4
	TM Recharge	ER-EC-12_m2				
δ^2H #1 and #2	31	69	5.3 to 5.6	5.7 to 6.0	6.4	-0.3
$\delta^{18}O$ #1 and #2	33	67	5.3 to 5.6	5.7 to 6.0	6.4	-0.3
	TM Recharge	ER-EC-14_m2				
δ^2H #1 and #2	45	55	5.4 to 5.7	5.6 to 5.9	6.6	-.01
$\delta^{18}O$				No Models		
	TM Recharge	UE-18r_o1				
δ^2H #1 and #2	12	88	4.8 to 5.1	4.8 to 5.2	6.2	0.2
$\delta^{18}O$ #1 and #2	19	81	4.8 to 5.2	4.9 to 5.3	6.2	0.2

ER-18-2_m1 has higher concentrations of Na^+ and HCO_3^- than other Pahute Mesa groundwater, as well as an elevated water temperature (43 °C). The well also has high concentrations of helium isotopes (^3He and ^4He), which indicates the presence of mantle CO_2 and possible upwelling of deep fluids along the structural margin of the Timber Mountain caldera (Navarro, 2020; LLNL, 2004). However, the similarity in δ^2H and $\delta^{18}O$ to other Pahute Mesa groundwater (Figure 19) suggests that the groundwater in ER-18-2 is deeply circulated Pahute Mesa groundwater and not other fluids from deeper in the crust. The presence of mantle CO_2 explains the elevated HCO_3^-, as indicated in the water-rock reaction models, which also explain the elevated Na^+ by dissolution of calcite fracture coatings coupled with Na-Ca exchange with zeolites and clays. The poor match of $\delta^{13}C$ in the models likely results from the models using the isotopically light carbon isotopic signature of soil gas instead of isotopically heavier mantle CO_2.

The mixing scenario using UE-18r_o1 produced four successful models using either δ^2H or $\delta^{18}O$ as the mixing constraint with 12 percent to 19 percent Timber Mountain recharge and 81 percent to 88 percent UE-18r_o1 (Table 6). The main water-rock reactions included the exchange of Ca and Mg with Na on clay surfaces, dissolution of soil CO_2, and dissolution of calcite. The water-rock reaction models produced a poor match with carbon isotopes because of the isotopically heavy $\delta^{13}C$ signature at ER-18-2_m1 (-0.2 ‰).

UE-18t_p1

Isotopically, UE-18t_p1 is like Timber Mountain recharge, so a direct flow path from Timber Mountain is suggested, but groundwater contours (Fenelon *et al.*, 2010, 2016) show that groundwater flows from Rainier Mesa toward Timber mountain and UE-18t_p1 is upgradient of Timber Mountain. Because the isotopic signature of Rainier Mesa tunnel water is used to represent Timber Mountain recharge, UE-18t also looks isotopically like Rainier Mesa recharge. Considering it is uncertain whether Timber Mountain recharge reaches ER-18-2_m1, it is even more uncertain whether Timber Mountain recharge reaches UE-18t_p1. Water-rock reaction models were run for Timber Mountain recharge to UE-18t_p1 without mixing and are presented in Appendix A, but the results are not discussed further.

UE-18r_o1

UE-18r_o1 is on the periphery of Timber Mountain within the Pahute Mesa-Oasis Valley groundwater basin. Recharge from Timber Mountain flowing northwest toward UE-18r_o1 requires mixing isotopically heavier recharge with an isotopically lighter Pahute Mesa groundwater. This scenario was tested by mixing either ER-20-4_m1, ER-EC-12_m2, or ER-EC-14_m2 with Timber Mountain recharge.

The mixing scenario using ER-20-4_m1 produced two successful models using either δ^2H or $\delta^{18}O$ as the mixing constraint with 19 percent to 36 percent Timber Mountain recharge and 64 percent to 81 percent ER-20-4_m1 (Table 7). The main water-rock reactions included the dissolution of soil CO_2, dissolution of calcite, exchange of Ca and Mg with Na on clay surfaces, and precipitation of SiO_2. The water-rock reaction models produced a fair match with carbon isotopes, with an average difference of approximately 2.0 ‰ (Appendix A).

The mixing scenario using ER-EC-12_m2 produced four successful models using either δ^2H or $\delta^{18}O$ as the mixing constraint with 17 percent to 21 percent Timber Mountain recharge and 79 percent to 83 percent ER-EC-12_m2 (Table 7). The main water-rock reactions included the dissolution of soil CO_2, dissolution of calcite, precipitation of SiO_2, and exchange of Ca and Mg with Na on clay surfaces. The water-rock reaction models produced a fair match with carbon isotopes, with an average difference of approximately 2.2 ‰ (Appendix A).

The mixing scenario using ER-EC-14_m2 produced one successful model using δ^2H as the mixing constraint with 37 percent Timber Mountain recharge and 63 percent ER-EC-12_m2 (Table 7). The main water-rock reactions included the dissolution of soil CO_2, dissolution of calcite, exchange of Ca and Mg with Na on clay surfaces, and precipitation of SiO_2. The water-rock reaction models produced a good match with carbon isotopes, with a difference of approximately 1.2 ‰ (Appendix A).

Water-rock reaction models using NETPATH and PHREEQC were also created for UE-18r_o1 by Navarro (2020). These models produced the observed water chemistry at UE-18r by mixing upgradient Pahute Mesa groundwater with other Pahute Mesa groundwater and did not require any recharge water from Timber Mountain. In the NETPATH models, δ^2H and $\delta^{18}O$ were not used as phases because the small variability observed in Pahute Mesa groundwater was within the reported analytical error of δ^2H and $\delta^{18}O$. Therefore, the mixing components in the NETPATH models were determined only by dissolution and precipitation of the phases used. In the PHREEQC models, δ^2H and $\delta^{18}O$ were used but allowed to vary by 10 percent (greater than analytical error). In these models, mixing components were determined by the dissolution and precipitation of the phases used and the matching of the δ^2H and $\delta^{18}O$.

Table 7. Water-rock reaction modeling results with Timber Mountain (TM) recharge mixing with ER-20-4_m1, ER-EC-12_m2, or ER-EC-14_m2 to produce the observed water chemistry at UE-18r_o1. Positive values indicate mineral phase dissolution. Negative values indicate mineral phase precipitation. Mineral phase changes are expressed as millimoles of mineral phase per kilogram of water (mmol/Kg).

Model #	Mixture (percent)	Mixture (percent)	Calcite (mmol/Kg)	CO_2 Gas (mmol/Kg)	Ca/Mg Exchange (mmol/Kg)	SiO_2 (mmol/Kg)
	TM Recharge	ER-20-4_m1				
δ^2H #1 and #2	36	64	0.8 to 0.9	1.2 to 1.3	0.7	-0.5
$\delta^{18}O$ #1 and #2	19	81	0.8	1.2 to 1.3	0.6	-0.7
	TM Recharge	ER-EC-12_m2				
δ^2H #2	21	79	0.6	0.9	0.2	-0.5
$\delta^{18}O$ #2	17	83	0.6	0.9	0.2	-0.6
	TM Recharge	ER-EC-14_m2				
δ^2H #2	37	63	0.7	0.8	0.5	-0.3
$\delta^{18}O$				No Models		

ER-EC-5_m1-3

ER-EC-5_m1-3 is on the periphery of Timber Mountain within the Pahute Mesa-Oasis Valley groundwater basin. Recharge from Timber Mountain flowing west toward ER-EC-5_m1-3 requires mixing isotopically heavier recharge with an isotopically lighter Pahute Mesa groundwater. This scenario was tested by mixing either ER-20-4_m1, ER-EC-12_m2, or ER-EC-14_m2 with Timber Mountain recharge.

The mixing scenario using ER-20-4_m1 produced four successful models using either δ^2H or $\delta^{18}O$ as the mixing constraint with 8 percent to 22 percent Timber Mountain recharge and 78 percent to 92 percent ER-20-4_m1 (Table 8). The main water-rock reaction included dissolution of calcite, dissolution of soil CO_2, exchange of Ca and Mg with Na on clay surfaces, and precipitation of SiO_2. The water-rock reaction models produced a good match with carbon isotopes, with an average difference of approximately 1.8 ‰ (Appendix A).

The mixing scenario using ER-EC-12_m2 produced four successful models using either δ^2H or $\delta^{18}O$ as the mixing constraint with 4 percent to 6 percent Timber Mountain recharge and 94 percent to 96 percent ER-EC-12_m2 (Table 8). The main water-rock reaction was dissolution of calcite and the water-rock reaction models produced a fair match with carbon isotopes, with an average difference of approximately 2.2 ‰ (Appendix A).

Table 8. Water-rock reaction modeling results with Timber Mountain (TM) recharge mixing with ER-20-4_m1, ER-EC-12_m2, or ER-EC-14_m2 to produce the observed water chemistry at ER-EC-5_m1-3. Positive values indicate mineral phase dissolution. Negative values indicate mineral phase precipitation. Mineral phase changes are expressed as millimoles of mineral phase per kilogram of water (mmol/Kg).

Model #	**Mixture (percent)**	**Mixture (percent)**	**Calcite (mmol/Kg)**	**CO_2 Gas (mmol/Kg)**	**Ca/Mg Exchange (mmol/Kg)**	**SiO_2 (mmol/Kg)**
	TM Recharge	ER-20-4_m1				
δ^2H #1 and #2	22	78	0.6 to 0.8	0.3 to 0.5	0.5	-0.1
$\delta^{18}O$ #1 and 2	8	92	0.5 to 0.7	0.3 to 0.5	0.4	-0.2
	TM Recharge	ER-EC-12_m2				
δ^2H #1 and #2	4	96	0.3	0.1	-0.1	0.0
$\delta^{18}O$ #1 and #2	6	94	0.3	0.1	-0.1	0.0
	TM Recharge	ER-EC-14_m2				
δ^2H #1 $\delta^{18}O$	23	77	0.4	-0.1 No Models	0.2	0.2

The mixing scenario using ER-EC-14_m2 produced one successful model using δ^2H as the mixing constraint with 23 percent Timber Mountain recharge and 77 percent ER-EC-12_m2 (Table 8). The main water-rock reaction was dissolution of calcite and the water-rock reaction models produced a good match with carbon isotopes with a difference of 0.4 ‰ (Appendix A).

Water-rock reaction models using NETPATH and PHREEQC were also created for ER-EC-5_m1-3 by Navarro (2020). These models produced the observed water chemistry at ER-EC-5_m1-3 by mixing upgradient Pahute Mesa groundwater with other Pahute Mesa groundwater and did not require any recharge water from Timber Mountain. In the NETPATH models, δ^2H and $\delta^{18}O$ were not used as phases because the small variability observed in Pahute Mesa groundwater was within the reported analytical error of δ^2H and $\delta^{18}O$. Therefore, mixing components in the NETPATH models were determined only by dissolution and precipitation of the phases used. In the PHREEQC models, δ^2H and $\delta^{18}O$ were used but allowed to vary by 10 percent (greater than analytical error). In these models, mixing components were determined by the dissolution and precipitation of the phases used and the matching of the δ^2H and $\delta^{18}O$.

ER-OV-3c_p1

ER-OV-3c_p1 is downgradient of Timber Mountain within the Pahute Mesa-Oasis Valley groundwater basin. Recharge from Timber Mountain flowing southwest toward ER-OV-3c_p1 requires mixing isotopically heavier recharge with an isotopically lighter Pahute Mesa groundwater. This scenario was tested by mixing either ER-20-4_m1, ER-EC-12_m2, ER-EC-14_m2, or ER-EC-05_m1-3 with Timber Mountain recharge.

The mixing scenario using ER-20-4_m1 produced four successful models using either δ^2H or $\delta^{18}O$ as the mixing constraint with 33 percent to 53 percent Timber Mountain recharge and 47 percent to 57 percent ER-20-4_m1 (Table 9). The main water-rock reactions included the dissolution of calcite, dissolution of soil CO_2, and exchange of Ca and Mg with Na on clay surfaces. The water-rock reaction models produced a poor match with carbon isotopes, with an average difference of approximately 3.1 ‰ (Appendix A).

The mixing scenario using ER-EC-12_m2 produced four successful models using either δ^2H or $\delta^{18}O$ as the mixing constraint with 31 percent to 42 percent Timber Mountain recharge and 58 percent to 68 percent ER-EC-12_m2 (Table 9). The main water-rock reaction was the dissolution of calcite, dissolution of soil CO_2, and exchange of Ca and Mg with Na on clay surfaces. Water-rock reaction models produced a poor match with carbon isotopes, with an average difference over 3.4 ‰ (Appendix A).

The mixing scenario using ER-EC-14_m2 produced two successful models using δ^2H as the mixing constraint with 54 percent Timber Mountain recharge and 46 percent ER-EC-14_m2 (Table 9). The main water-rock reactions included the dissolution of calcite, exchange of Ca and Mg with Na on clay surfaces, dissolution of SiO_2, and dissolution of soil CO_2. The water-rock reaction models produced a fair match with carbon isotopes, with a difference of approximately 2.6 ‰ (Appendix A).

The mixing scenario using ER-EC-5_m1-3 produced four successful models using either δ^2H or $\delta^{18}O$ as the mixing constraint with 31 percent to 40 percent Timber Mountain recharge and 60 percent to 68 percent ER-EC-5_m1-3 (Table 9). The main water-rock reactions included the dissolution of calcite, exchange of Ca and Mg with Na on clay surfaces, dissolution of soil CO_2, and dissolution of SiO_2. The water-rock reaction models produced a good match with carbon isotopes, with an average difference of less than 2 ‰ (Appendix A).

Table 9. Water-rock reaction modeling results with Timber Mountain (TM) recharge mixing with ER-20-4_m1, ER-EC-12_m2, ER-EC-14_m2, or ER-EC-5_m1-3 to produce the observed water chemistry at ER-OV-3c_p1. Positive values indicate mineral phase dissolution. Negative values indicate mineral phase precipitation. Mineral phase changes are expressed as millimoles of mineral phase per kilogram of water (mmol/Kg).

Model #	**Mixture (percent)**	**Mixture (percent)**	**Calcite (mmol/Kg)**	**CO_2 Gas (mmol/Kg)**	**Ca/Mg Exchange (mmol/Kg)**	**SiO_2 (mmol/Kg)**
	TM Recharge	ER-20-4_m1				
δ^2H #1 and #2	53	47	0.6 to 0.9	0.3 to 0.6	0.7	0.2
$\delta^{18}O$ #1 and #2	33	67	0.5 to 0.8	0.3 to 0.6	0.6	0.2
	TM Recharge	ER-EC-12_m2				
δ^2H #1 and #2	42	58	0.5 to 0.6	0.2 to 0.4	0.4	0.2
$\delta^{18}O$ #1 and #2	31	68	0.4 to 0.6	0.2 to 0.3	0.3	0.2
	TM Recharge	ER-EC-14_m2				
δ^2H #1 and #2	54	46	0.5 to 0.7	0.1 to 0.3	0.6	0.4
$\delta^{18}O$			No Models			
	TM Recharge	ER-EC-14_m2				
δ^2H #1 and #2	40	60	0.3 to 0.5	0.1 to 0.3	0.5	0.3
$\delta^{18}O$ #1 and #2	31	68	0.2 to 0.3	0.1 to 0.3	0.3	0.2

Summary Isotopic and Chemical Signatures of Timber Mountain Recharge and Water-rock Reaction Modeling

Stable isotopic data from precipitation at the Timber Mountain monitoring station were used to identify an appropriate isotopic signature for groundwater recharge at Timber Mountain by examining the precipitation isotopic data and isotopic data from NNSS springs and Rainier Mesa tunnels, as described previously. Water chemistry to represent Timber Mountain recharge was selected from nine NNSS springs that have short flow paths through volcanic rocks. The δ^2H and $\delta^{18}O$ signatures of Timber Mountain recharge and surrounding groundwaters were used to identify groundwater flow paths and groundwater mixing scenarios in which Timber Mountain recharge might be a significant component of the downgradient groundwater. Eight wells near Timber Mountain were selected for further analysis by water-rock reaction modeling to test the groundwater flow-path and mixing

scenarios. The eight wells included UE-29a2, ER-30-1_p2, ER-EC-7_m1-2, ER-18-2_m1, UE-18t_p1, UE-18r_o1, ER-EC-5, and ER-OV-3c. The results from examining the stable isotopic data, water chemistry data, and water-rock reaction modeling (Table 10) showed that:

- UE-29a2_p1 and ER-30-1_p2 are isotopically heavier than Timber Mountain recharge, so they likely have a different source of recharge than Timber Mountain.
- ER-EC-7_m1-2 is isotopically similar to Timber Mountain recharge and water-rock reaction modeling. This shows that the main reactions are the dissolution of calcite and SiO_2, which is consistent with a direct flow path from Timber Mountain to ER-EC-7.
- ER-18-2_m1 water chemistry can be produced by mixing 12 percent to 45 percent Timber Mountain recharge with Pahute Mesa groundwater and the main mineral phase changes are the dissolution of calcite and soil CO_2 and the exchange of Ca and Mg with Na on clay surfaces. There was a poor match with carbon isotopic data because of the isotopically heavy $\delta^{13}C$ signature at ER-18-2_m1.
- UE-18t_p1 is isotopically similar to Timber Mountain recharge, so a direct flow path is possible.
- UE-18r_o1 can be produced by mixing Timber Mountain recharge with Pahute Mesa groundwater with 17 percent to 37 percent Timber Mountain recharge and the main mineral phase changes are the dissolution of calcite and soil CO_2, exchange of Ca and Mg with Na on clay surfaces, and precipitation of SiO_2. There were fair to good matches with carbon isotopic data between the models.
- ER-EC-5_m1-3 can be produced by mixing Timber Mountain recharge with Pahute Mesa groundwater with 4 percent to 23 percent Timber Mountain recharge and the main mineral phase changes are the dissolution of calcite and soil CO_2 and the exchange of Ca and Mg with Na on clay surfaces. There were fair to good matches with carbon isotopic data between the models.
- ER-OV-3c_p1 can be produced by mixing Timber Mountain recharge with Pahute Mesa groundwater with 31 percent to 53 percent Timber Mountain recharge and dissolution of calcite and soil CO_2, and the main mineral phase change is the exchange of Ca and Mg with Na on clay surfaces. There were poor to good matches with carbon isotopic data between models depending on the well used to represent Pahute Mesa groundwater.
- If an isotopically heavier Timber Mountain recharge component is used, the percent of Timber Mountain recharge would be less.
- Because the isotopic signature of Timber Mountain was assumed to be similar to the isotopic signature of Rainier Mesa and because Rainier Mesa is regionally upgradient of Timber Mountain (Figure 16), the mixing component of Timber Mountain recharge cannot be differentiated isotopically from the Rainier Mesa recharge component.

Table 10. Summary water-rock reaction models for the component of Timber Mountain recharge in wells surrounding Timber Mountain.

Well	Percent TM Recharge	Mineral Phase Changes	Match $\delta^{13}C$
UE-29a2_p1	0	NA	NA
ER-30-1_p2	0	NA	NA
ER-EC-7_m1-2	100	Dissolution calcite and SiO_2	Poor
ER-18-2_m1	12 to 45	Dissolution calcite and CO_2, cation exchange	Poor
UE-18t_p1	0	NA	NA
UE-18r_o1	17-37	Dissolution calcite and CO_2, cation exchange, precipitation SiO_2	Fair to Good
ER-EC-5_m1-3	4 to 23	Dissolution calcite and CO_2, cation exchange	Fair to Good
ER-OV-3c_p1	31 to 53	Dissolution calcite and CO_2, cation exchange	Poor to Good

NA = not applicable.

Movement of Recharge via Connected Faults Influenced by Regional Stress

Conceptual models of flow and transport for Pahute Mesa emphasize the role of interconnected networks of fractures and faults in promoting preferential flow and radionuclide transport (NNSA, 2009; Pawloski *et al.*, 2010). Variability in the magnitude of recharge and its spatial distribution is likely to have a strong effect on the rate of transport and overall retention of contaminants. The network of faults in the region exerts control on the directionality of transport and provides zones for preferential transport. Changes in the recharge pattern combined with a modeling framework built using interactions between fault orientations and stress field directions allow for the study of primary controls and ranges for pathline configurations. This section explores the effect of the regional stress field on the hydraulic properties of the Pahute Mesa Phase II faults (U.S. Department of Energy, 2020) and Slate faults (Slate *et al.*, 1999) (Figure 21) and their influence on the configuration of pathlines originating from the Timber Mountain area.

Fault Dilation and Slip Tendencies

The dilation tendency (T_d) of a fault is defined as a dimensionless ratio that describes the amount of resolved normal stress acting on a fault plane normalized by the differential stress (max difference between *Shmin*, *Shmax*, and *Sv*) in the principal directions (Ferrill *et al.*, 1999). The slip tendency (*Ts*) is the ratio of shear stress relative to normal stress on a fault plane (Morris *et al.*, 1996). Values of dilation and slip tendencies vary in the range of 0 to 1, with higher tendency values indicating a higher potential for the fault to serve as a conduit.

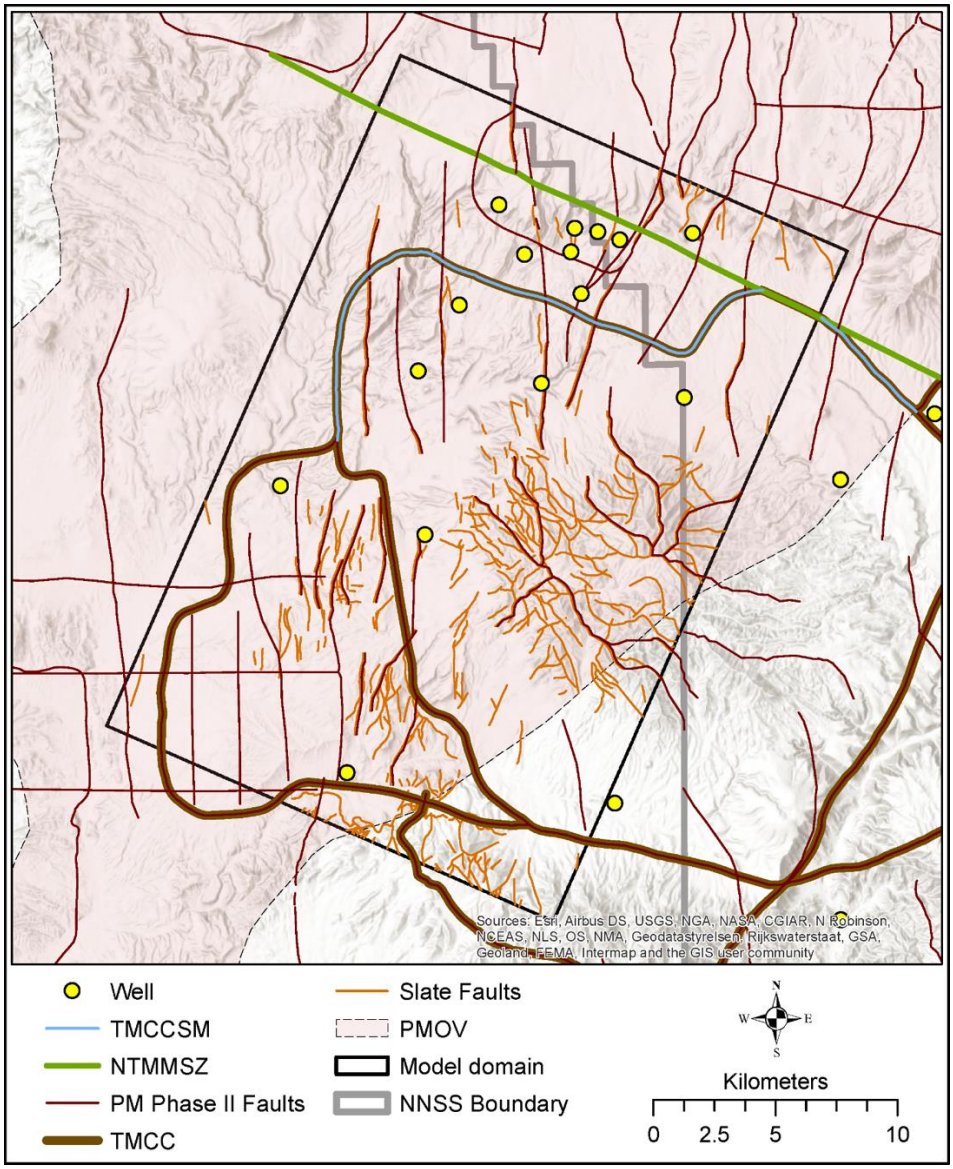

Figure 21. The Pahute Mesa Phase II faults (U.S. Department of Energy, 2020), Slate faults (Slate *et al*., 1999*)*, 20 km x 30 km (12.4 mi x 18.6 mi) modeling domain oriented at an azimuth of 21°, geologic features (TMCCSM, NTMMSZ, and TMCC), wells, and Pahute Mesa-Oasis Valley groundwater basin boundary (PMOV).

Figure 22 shows the dilation tendency and slip tendency values computed from 8,510 digitized segments of the Phase II Pahute Mesa faults (Figure 21) for the average computed stress field. Faults with the highest slip tendency trend northeast-southwest and faults with the lowest slip tendency trend northwest-southeast. The near vertical value of dip angle (80 °) (U.S. Department of Energy, 2020) used in this study greatly reduces the likelihood of the occurrence of critically stressed faults with $Ts \geq 0.6$. The possible enhancement of fault permeability in Pahute Mesa owing to the influence of the stress field is therefore chiefly guided by the dilation tendency rather than the slip tendency values.

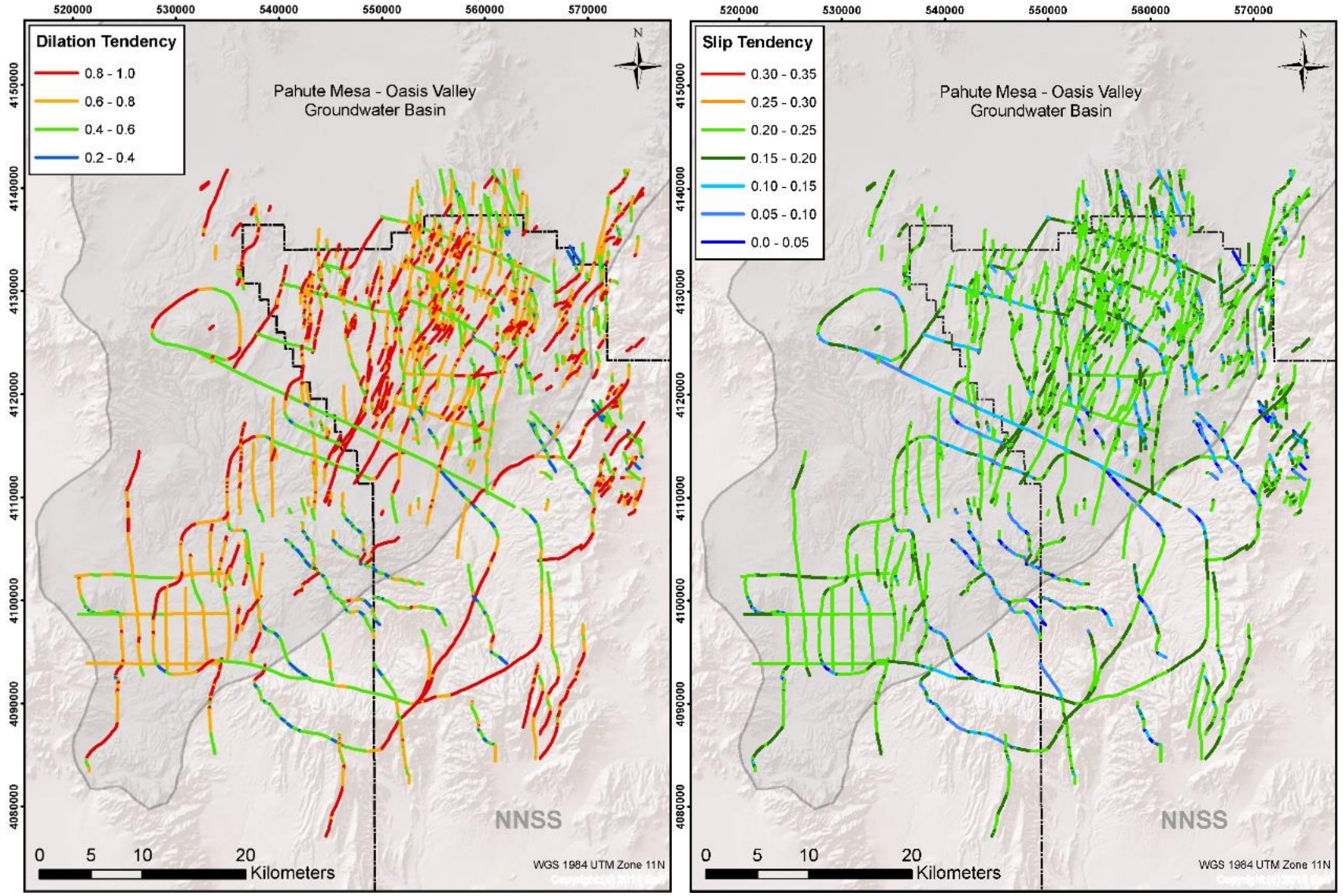

Figure 22. Computed dilation tendency (left) and slip tendency (right) for Pahute Mesa faults (adapted from Reeves *et al.* [2017]).

Objectives

The goal was to use computed dilation tendency values to assess the influence of the regional stress field on flow path configurations originating from the Timber Mountain area under different recharge conditions. Fault dilation and slip tendency values were used to infer permeability and connectivity in the system, which were then used in a continuum model to identify the principal flow paths originating from the Timber Mountain area. The study particularly focused on examining the propensity of groundwater to migrate in the northwardly direction from the Timber Mountain area against the general direction of regional groundwater movement. This study was designed to develop an understanding of the modeling scenarios under which the permeability-based stress field parameter in western Pahute Mesa could potentially corroborate the water-chemistry-based studies that show some degree of hydraulic connection between the recharge at the Timber Mountain and northerly wells, such as ER-18-2. The approach of this study was to:

1) Use the interpretation of the regional stress field in Pahute Mesa in the form of computed dilation and the fracture continuum methodology of mapping fractures on a continuum mesh (Parashar and Reeves, 2011; Reeves *et al.*, 2014) to compute effective hydraulic conductivity for a large 20 km x 30 km (12.4 mi x 18.6 mi) two-dimensional (2D) regular grid over a portion of Pahute Mesa, encompassing most of the Timber Mountain area.

2) Conduct two-dimensional MODFLOW and MODPATH simulations using the computed hydraulic properties of the fault system and under different recharge scenarios to study the configurations and sensitivity of flow paths originating from the Timber Mountain area.

Model Setup

A large-scale 20 km x 30 km (12.4 mi x 18.6 mi) domain (Figure 21) was constructed using MODFLOW-2005 (Harbaugh, 2005). The model domain was discretized into 1,200 rows and 800 columns with a cell size of 25 m x 25 m (82 ft x 82 ft), resulting in 960,000 grid cells in the 2D plane. The cell size was selected to adequately represent the geometry of the fault structures, fault connectivity, separation distances between the test locations, and the background cells representing the fractured stratigraphic units. The rectangular model domain was rotated to an azimuth of 23.7° to align the model with the direction of regional groundwater flow (Belcher and Sweetkind, 2010; Garcia *et al.*, 2017). This allowed for the application of no-flow boundary conditions at the two longer sides (east and west boundaries). Table 11 shows the coordinates of the four vertices of the rectangular domain, denoted by easting and northing pairs in UTM Zone 11 NAD83.

The set of faults included in the study (Figure 21) consists of both the Pahute Mesa Phase II structural features (i.e., faults, caldera margins, and associated structural zones) compiled by U.S. Department of Energy (2020) and non-duplicate faults and fault segments from Slate *et al.* (1999).

Table 11. Easting and northing coordinates (UTM WGS84) of the vertices of the 20 km x 30 km (12.4 mi x 18.6 mi) model domain.

	Easting (m)	**Northing (m)**
Vertex 1 – SW corner	525625.56	4096534.39
Vertex 2 – NW corner	537670.80	4124010.56
Vertex 3 – NE corner	555987.80	4115981.01
Vertex 4 – SE corner	543942.83	4088504.72

Assumptions

The model presented here assumes flow and transport occurs in a fully saturated system. The steady-state solution of the hydraulic head was computed for fixed values of the constant head boundary conditions. Recharge to the model was assumed to be steady. It was assumed that the direction of groundwater flow was approximately along the longitudinal direction (northeast-southwest) of the model domain. Therefore, the model used no-flow boundaries along the longitudinal edges of the model domain. The background rock matrix was assumed to be homogeneous and isotropic in its properties. The hydraulic properties of faults were assumed to be solely dependent on dilation tendency values.

The Pahute Mesa Phase II faults and the Slate faults were undifferentiated. The caldera margins were treated as faults. Transport was assumed to occur only through advection. Processes such as diffusion, dual-domain mass transfer between fractures and matrix blocks, adsorption, and decay were not included in the simulations. Transport was also confined to the two-dimensional plane. Simulations to generate flow path configurations in MODPATH were conducted by placing a fixed number of particles uniformly distributed in a given area.

Boundary Conditions

Because the model was oriented to align approximately with the direction of regional groundwater flow, the two side boundaries were modeled as no-flow boundaries. The time-variant specified-head package was used in MODFLOW to assign constant hydraulic head values to all cells at the northern and southern boundary of the model domain. The head values were extracted from the Death Valley regional groundwater model, DV1 (Belcher and Sweetkind, 2010). The model presented here is a single layer and it does not include vertical stratigraphy information. Therefore, the vertical variation of hydraulic head values of the DV1 model cannot be integrated with the 2D work presented here. The maximum hydraulic head values in the DV1 model along the vertical profiles at the northern and southern boundary locations were used to assign the constant head boundary conditions.

Parametrization

The fault segments were placed in one of these three categories based on the following rules (Parashar *et al.*, 2018):

- High aperture (1,000 microns [0.039 in]) if dilation tendency ≥ 0.80.
- Medium aperture (350 microns [0.014 in]) if 0.20 ≤ dilation tendency < 0.80.
- Low aperture (100 microns [0.004) if dilation tendency < 0.20.

Figure 23 shows the 20 km x 30 km (12.4 mi x 18.6 mi) model domain with the Pahute Mesa Phase II faults color coded to highlight the low-, medium-, and high-aperture faults. It can be seen that major features can have different aperture values as the location and orientation changes.

Using the cubic law for fractures (Klimczak *et al.*, 2010), the equivalent hydraulic conductivity for the low-, medium-, and high-aperture cases were computed. An isotropic background conductivity value of 1.157×10^{-7} m/s (3.795×10^{-7} ft/s) was used to parametrize the MODFLOW model cells that didn't intersect a fault. As discussed in the "Chloride Mass Balance" section, this background conductivity value produces a groundwater mound of 152 m (499 ft) at the center of Timber Mountain when recharge of 1.48 cm/yr (0.58 in/yr) is applied within a radius of 4 km (2.5 mi). This background conductivity value is also representative of the low end (fifth percentile) of the range of hydraulic conductivity values of the Topopah Spring Aquifer (Garcia *et al.*, 2017) and has been used in previous studies to model low background conductivity scenarios in Pahute Mesa (Parashar *et al.*, 2018).

Both spatially uniform and variable recharge conditions were used in the MODFLOW simulations. For the uniform recharge distribution, a low value of 0.52 cm/yr (0.20 in/yr), medium value of 1.48 cm/yr (0.58 in/yr), and a high value of 2.44 cm/yr (0.86 in/yr) were used. For spatially variable recharge, estimates were obtained from the net infiltration model 5 of Middleton *et al.* (2019) for the Pahute Mesa-Oasis Valley area (Figure 24). Middleton *et al.* (2019) used the INFIL3.0 model (USGS, 2008a,b) to estimate long-term net infiltrations rates below the root zone, with their model 5 recommended for further use (hereafter referred to as INFIL Model 5). The INFIL Model 5 recharge values are considerably lower than the estimates used here for uniform recharge conditions. However, the uniform recharge values were only applied over a section of the model domain representing the Timber Mountain area. Spatially uniform recharge values ranging from 0.52 cm/yr to 2.44 cm/yr (0.20 in/yr to 0.86 in/yr) were only applied to the Timber Mountain area, whereas the rest of the model domain did not receive any recharge owing to their relatively lower elevation. In the case of spatially variable recharge models, the INFIL Model 5 recharge distributions covered the model domain in its entirety. Values of recharge for most of the model cells were very small. The maximum value of approximately 2.5 cm/yr (0.98 in/yr) recharge only occurred for a very small discontinuous portion of the model, as shown in the right and top left areas of Figure 24.

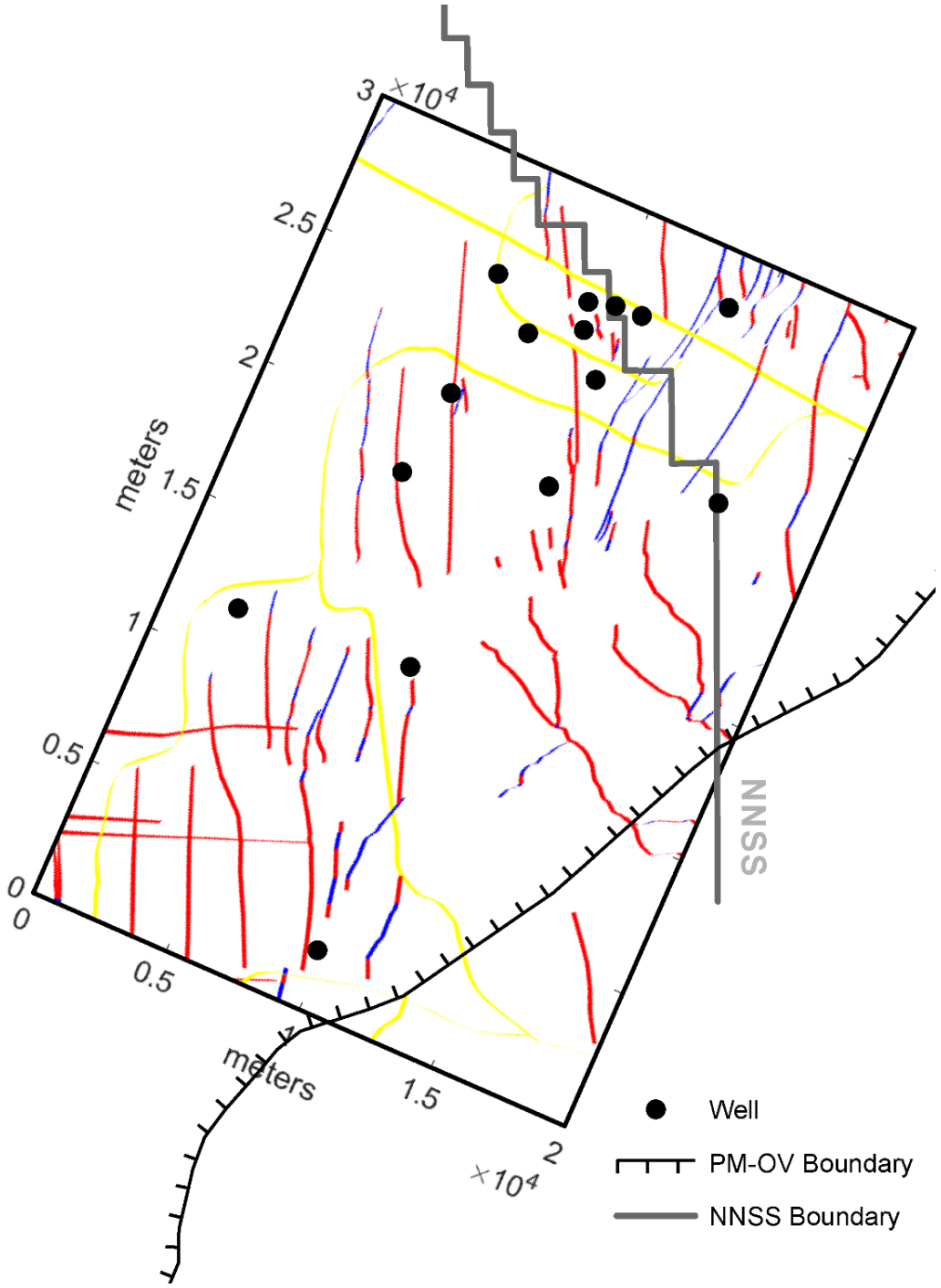

Figure 23. The 20 km x 30 km (12.4 mi x 18.6 mi) model domain with color-coded Pahute Mesa Phase II faults showing high aperture (blue), medium aperture (red), and low aperture (yellow) features.

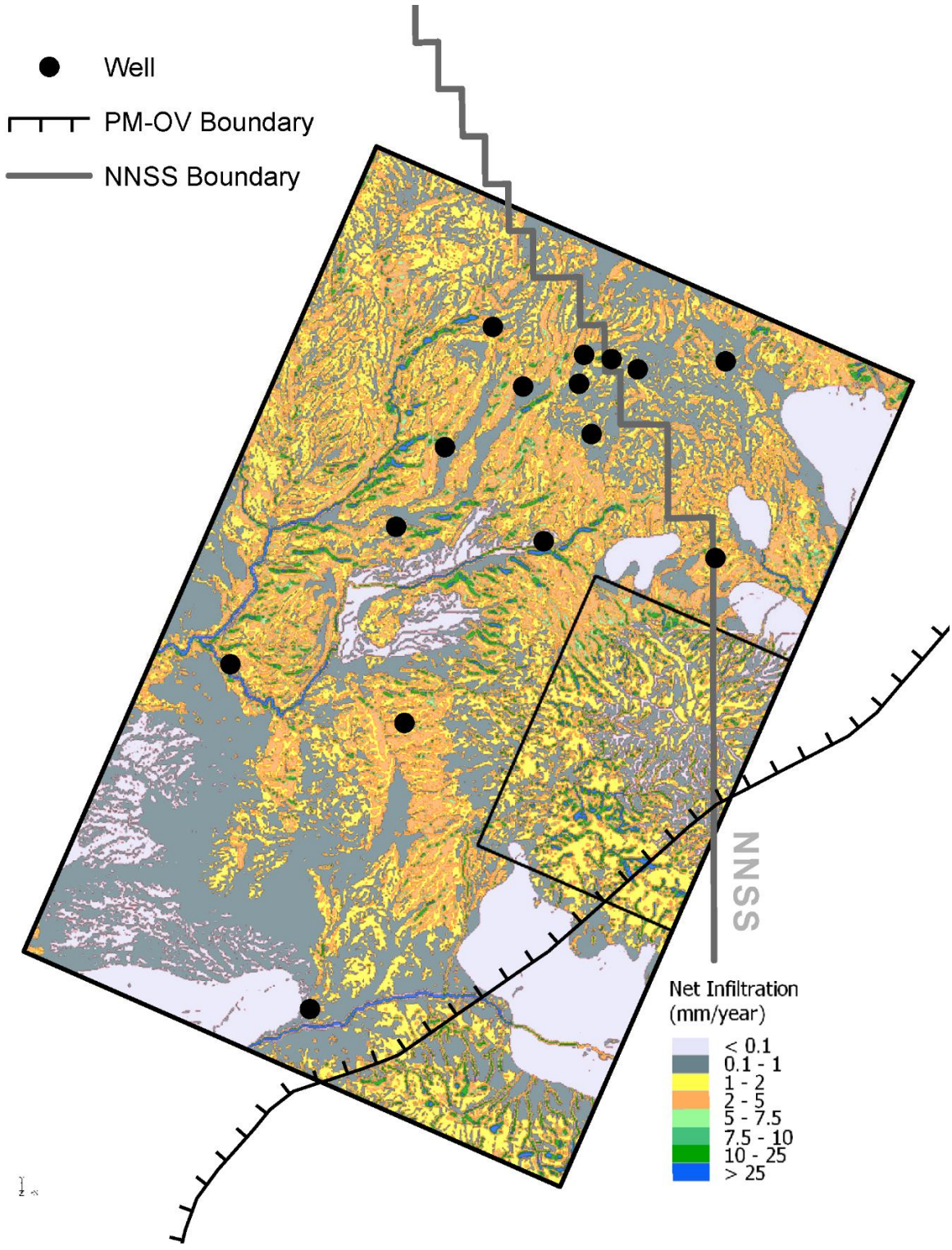

Figure 24. Recharge estimates (in millimeters per year) from INFIL Model 5 (revised from Middleton *et al.*, 2019). The rectangular box along the right edge of the domain represents the larger region over which particles are released to examine pathways migrating away from the Timber Mountain.

Modeling Scenarios

Four modeling scenarios were constructed to account for the uncertainty in recharge estimates and the MODFLOW model runs were repeated for each of those scenarios using head boundary conditions extracted from the Death Valley regional groundwater flow model (Belcher and Sweetkind, 2010). The results from the MODFLOW models were then used to conduct particle tracking studies using MODPATH (Pollock, 2012). Although MODPATH is designed to simulate flow paths by tracking particles from cell to cell until the particles reach a boundary, it does not provide information on travel times. Therefore, the transport study presented in this report only provides insight into possible pathways. The timescale of transport occurring through these pathways cannot be inferred from the results. Particles were released uniformly according to the following two methods:

1) Particles were only released within a small subarea, roughly corresponding to the higher elevation area of the Timber Mountain region. The intent here was to examine the flow paths originating from the areas receiving the highest amount of recharge. These higher elevation areas are represented by the box show in Figure 25 and roughly correspond to areas 6,500 ft amsl (1,981.2 m amsl). However, the shape is approximated as a square and not as elevation contour lines. The expanse of this area is only a small portion (less than half) of the recharge radius mountain topography shown in Figure 14. This method was only implemented for the uniform recharge conditions because the spatially variable recharge scenario, modeled using INFIL Model 5 estimates, have significantly lower recharge values and a clearly defined spatial distribution as shown in Figure 24.

2) Particles were released within the greater region to examine the many pathways away from Timber Mountain that groundwater may follow (Figure 24). This area is also represented by the box shown in Figures 26 and 27. Because the intent here is to examine patterns of pathlines leaving the Timber Mountain area, the particles were only released along the edges of the box.

Results and Discussion: Time and Spatial Variability of Recharge

Figure 24 shows the pattern of the hydraulic head contour lines and pathlines originating from the higher elevation areas within the Timber Mountain region for the modeling scenario of low, medium, and high values of uniformly distributed recharge. The hydraulic head contour lines were plotted for a fixed interval of 11 m (36 ft). The contour exhibit closed patterns in the Timber Mountain area indicative of mound formation for high recharge values. The spacing between the two adjacent contour lines varies greatly, with certain regions—particularly areas south of Timber Mountain—marked by a steep gradient that suggests relatively faster movement of radionuclides in those areas.

The qualitative nature of the pathline patterns is only mildly influenced by the amount of uniformly distributed recharge. Recharge under these uniformly distributed modeling scenarios are only applied to the Timber Mountain area. The recharge outside of Timber mountain area is assumed to be zero. As the recharge values increase, the pathlines originating from the higher elevation areas tend to shift westward from Timber Mountain. There is no indication that the recharge water can potentially migrate northward from the

higher elevations of Timber Mountain. Regardless of the magnitude of the recharge, the pathlines after traveling some distance, align themselves with the general direction of the regional groundwater flow and leave the model domain via its southern boundary. Analyzing the fault maps within the model domain (Figure 21) and their dilation tendency values (Figure 22) reveals that the Slate faults in the general area of Timber Mountain are of relatively minor importance compared with the dominant connections provided by the PM Phase II faults. The set of PM Phase II faults in the Timber Mountain area are largely oriented east-west. Therefore, the connected pathway provided by the PM Phase II faults in conjunction with the no-flow boundary condition applied to the east side of the model boundary promotes flow path configurations that migrate in the westward direction. The amount by which the pathlines migrate to the west increases with increases in the magnitude of recharge because higher recharge means the availability of a larger amount of water, which can be transmitted via the optimally oriented PM Phase II faults.

Figure 25 shows the pattern of the hydraulic head contour lines and pathlines originating from the Timber Mountain region for the modeling scenario of low, medium, and high values of uniformly distributed recharge. For these simulations, particles were released uniformly along the edges of a much larger area representative of the Timber Mountain region, as indicated by the black rectangle on the southeast side of the model domain in Figure 25. The uniformly distributed recharge values were only applied to the model cells within this rectangular area; cells outside of this subarea were not subjected to any recharge. By placing particles along the edges and not in the interior of the rectangular area, one can visually distinguish between pathlines migrating away from the Timber Mountain area and pathlines that can possibly travel through the Timber Mountain region under the influence of computed hydraulic gradients.

The patterns of hydraulic head contour lines in Figure 25 are undifferentiated from the patterns of Figure 24 because the recharge area and the magnitude of recharge did not change between these two sets of simulations. The much larger area for particle's initial release gives rise to pathline configurations showing significant variability with increasing recharge. For the low recharge value of 0.52 cm/yr (0.20 in/yr), the pathlines for the most part flow directly to the south. This creates a scenario in which pathlines originating from the edges of the rectangular particle release area can travel through the Timber Mountain region (as shown by the pathlines traversing directly southward for the low recharge case in Figure 26). The model does not show northward movement of pathlines in the case of low recharge values. However, medium (1.48 cm/yr [0.58 in/yr]) and higher (2.44 cm/yr [0.96 in/yr]) values of recharge lead to a subset of pathlines trending in the northward direction for some distance. The extent of migration to the north increases with increasing recharge. The simulations in their current form do not give information about the locations within the Timber Mountain region that are hydraulically connected to northern areas under higher recharge values, nor do they allow for the computation of the percentage of Timber Mountain recharge that can potentially migrate to the north. However, these simulations under spatially uniform recharge conditions do point to the possibility of some hydraulic connection between Timber Mountain recharge and the area surrounding ER-18-2. These subsets of pathlines provide corroboration to the water-chemistry-based evidence of a likely

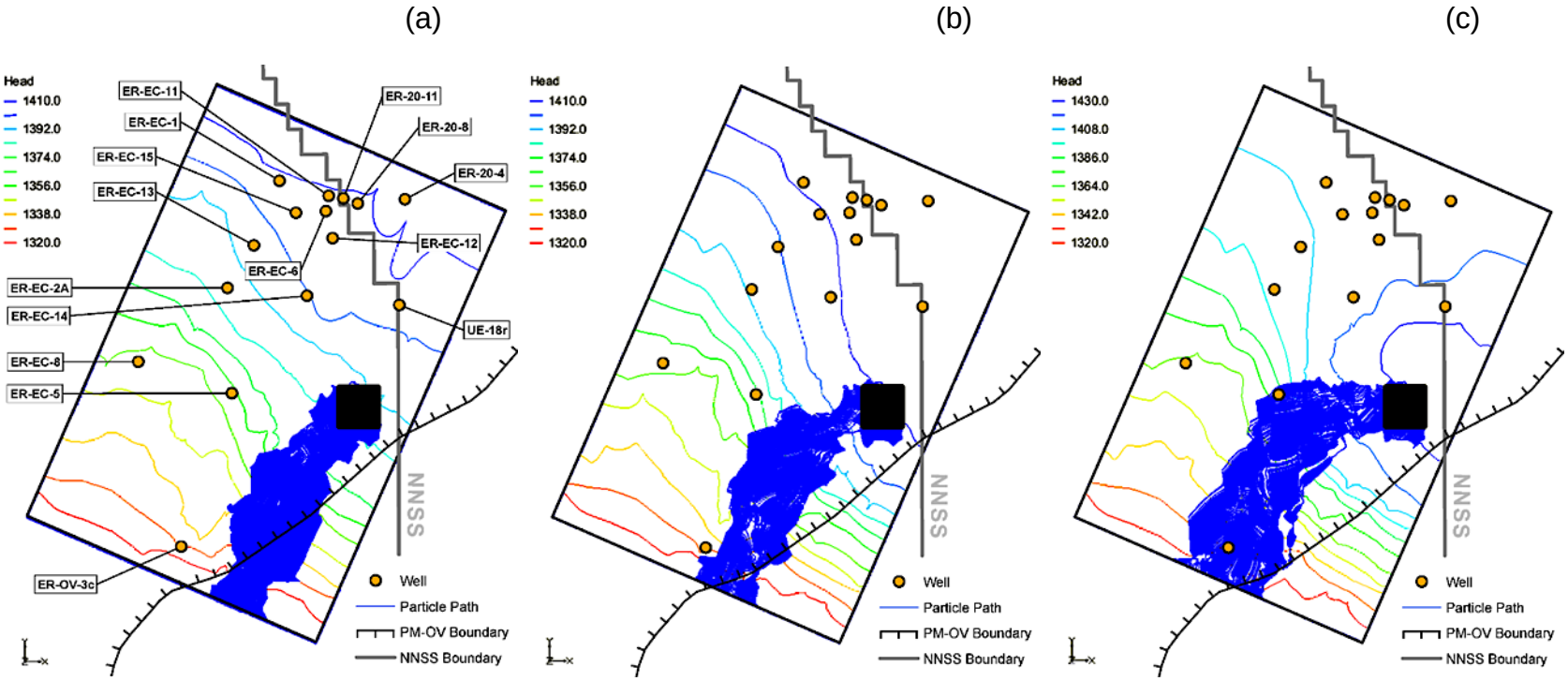

Figure 25. Projected pathlines originating from a higher elevation subarea within Timber Mountain for (a) low recharge estimates of 0.52 cm/yr (0.20 in/yr), (b) medium recharge estimates of 1.48 cm/yr (0.58 in/yr), and (c) high recharge estimates of 2.44 cm/yr (0.96 in/yr). Head values are shown in meters.

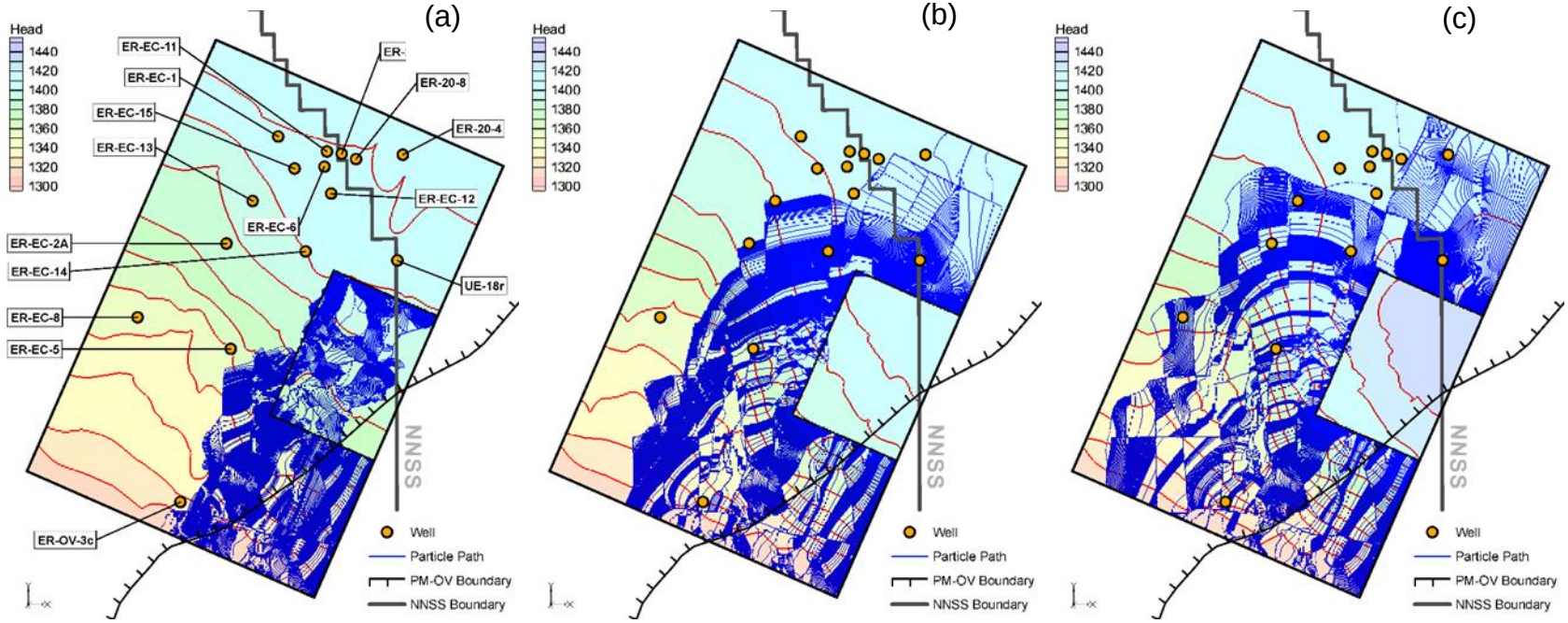

Figure 26. Projected pathlines originating from Timber Mountain for (a) low recharge estimates of 0.52 cm/yr (0.20 in/yr), (b) medium recharge estimates of 1.48 cm/yr (0.58 in/yr), and (c) high recharge estimates of 2.44 cm/yr (0.96 in/yr). Head values are shown in meters. Particles are initially released on the edge of the rectangular area for generation of pathlines. The pathlines move through the interior of the Timber Mountain area for low recharge conditions (left) and move strictly outward for medium and high recharge conditions.

hydraulic connection between the Timber Mountain recharge and areas to its north. However, results from Middleton *et al.* (2019) suggest that the amount of infiltration on Timber Mountain is small because of the presence of clayey soils with low soil hydraulic conductivity and steep slopes, which infers that there is a minimal amount of radial flow outward from Timber Mountain.

The pathlines trending to the north also realign with the general direction of groundwater movement and follow a configuration pattern that eventually causes the pathlines to exit the model through its southern boundary. The strictly outward movement of the pathlines for medium and high recharge values compared with the pathlines moving through the interior of Timber Mountain in the case of low recharge also indicates that the model produces significant hydraulic head mounds as the recharge values increase.

Figure 27 shows the pattern of the hydraulic head contour lines and pathlines originating from the Timber Mountain region for the modeling scenario of recharge estimates based on the INFIL Model 5 (shown in Figure 24). The recharge values are spatially variable here and are applied over the entire model domain. The pathline configurations are strikingly similar in this case to those obtained for the low estimates of uniformly distributed recharge (i.e., Figures 27 and 26a have similar patterns of pathlines). The pathlines in this case do not migrate much to the west. The average recharge value under this spatially variable condition is comparable to the lowest recharge value used for the spatially uniform recharge condition. The limited migration of pathlines to the west follows the general trend of less variability with decreasing magnitude of recharge.

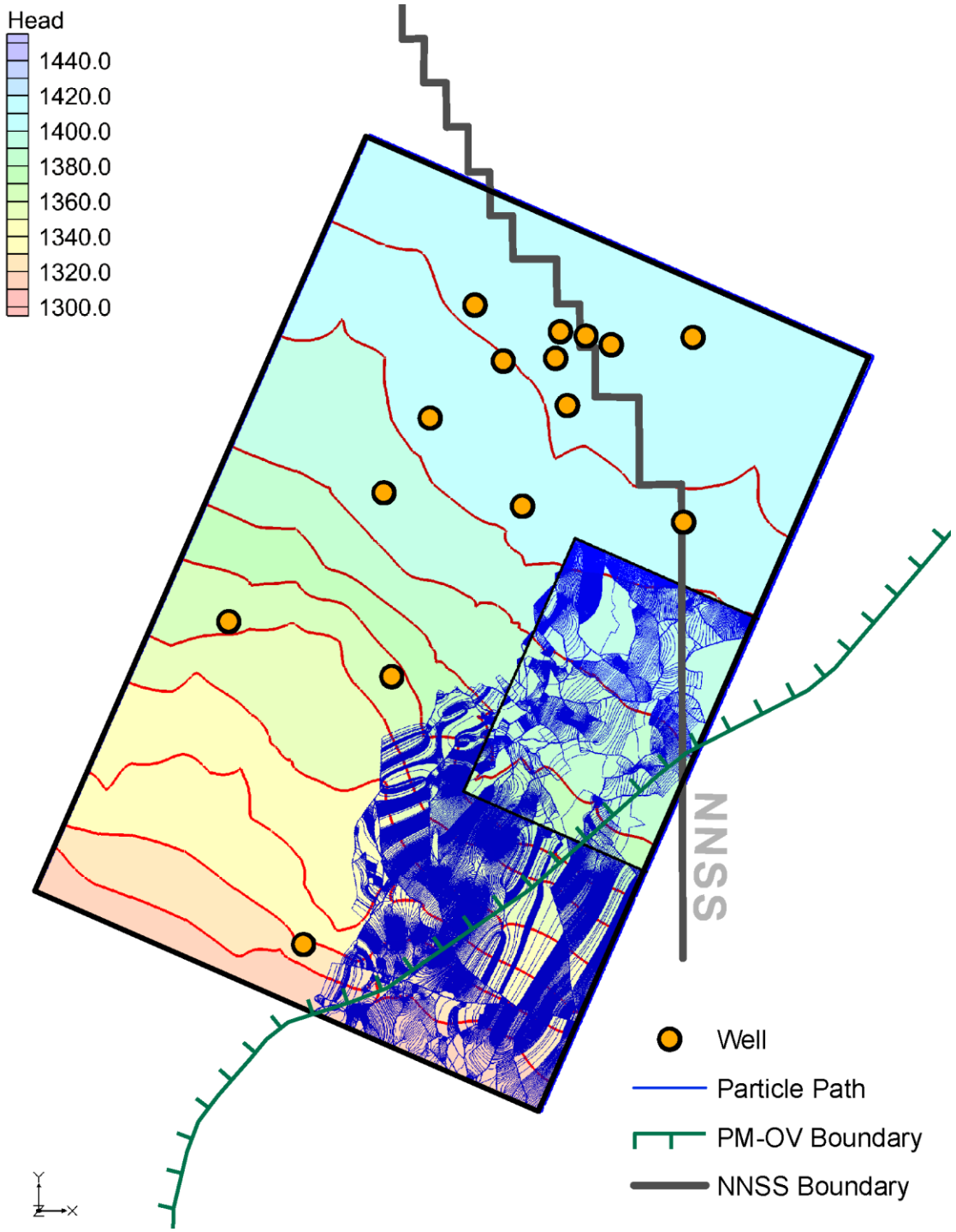

Figure 27. Projected pathlines originating from Timber Mountain for INFIL Model 5 derived recharge estimates. Head values are shown in meters. Particles are initially released on the edge of the rectangular area to generate pathlines.

CONCLUSIONS

The effect of Timber Mountain recharge on groundwater flow in the surrounding Pahute Mesa-Oasis Valley groundwater basin was evaluated using several methodologies. Weather and soil moisture data from the Timber Mountain monitoring site showed that shallow soil at the site became fully saturated six times during nine winters between 2010 and 2019. At full saturation, drainage was suggested immediately following significant winter/spring rainfall events and during snowmelt. Using the chloride mass-balance method, recharge at Timber Mountain was estimated to be 1.48 ± 0.96 cm/yr (0.58 ± 0.35 in/yr) (5.5 percent of annual precipitation).

Stable isotopic data, water chemistry data, and water-rock reaction modeling suggest that Timber Mountain recharge was approximately 10 percent to 45 percent of the groundwater in ER-18-2, which is upgradient of Timber Mountain relative to the general southwest groundwater flow in the Pahute Mesa-Oasis Valley groundwater basin. Results suggested that Timber Mountain recharge was approximately 15 percent to 40 percent of the groundwater at UE-18r_o1, northwest of Timber Mountain and roughly perpendicular to the southwesterly groundwater flow in the basin. Timber Mountain recharge at ER_EC-5_m1-3, west of Timber Mountain, was approximately 5 percent to 20 percent, whereas ER-OV-3c and ER-EC-7 may have a larger component of Timber Mountain recharge, approximately 30 percent to 50 percent and 100 percent, respectively. These results are consistent with groundwater recharge from Timber Mountain flowing radially outward to the north and northwest into the Pahute Mesa-Oasis Valley groundwater basin, and to the southwest, south, and east away from Timber Mountain.

The 2-D MODFLOW and MODPATH simulations of groundwater flow along faults while applying the regional stress field under different recharge scenarios provided insights into the configuration of groundwater pathlines originating from Timber Mountain. For the scenario of uniformly distributed recharge for low, medium, and high amounts of recharge based on the chloride mass-balance method and release of particles only at the highest elevations, the pattern of pathlines was only mildly influenced by the amount of recharge. As the recharge values increased, the pathlines from the higher elevations shifted westward from Timber Mountain and there was no recharge that migrated northward. Regardless of the magnitude of the recharge, the pathlines eventually aligned with the general direction of the regional groundwater flow and left the model domain at the southern boundary.

For the scenario of uniformly distributed recharge for low, medium, and high amounts of recharge based on the chloride mass-balance method and the release of particles over a much larger area of Timber Mountain, the much larger area of particle release produced pathlines with significant variability with increasing recharge. For low recharge, the pathlines flowed directly to the south. For medium and high recharge, a subset of pathlines trended northeastward and the extent of migration northeastward increased with increasing recharge. These simulations indicated some hydraulic connection between Timber Mountain recharge with the area to the northeast around ER-18-2, which is consistent with the results from the water-rock geochemical reaction modeling. The northern pathlines eventually realigned with the general southwestward direction of groundwater flow and exited the southern boundary of the model domain.

For the third scenario in which recharge amount and distribution were from the INFIL Model 5, the pathlines were more spatially confined and did not migrate very far westward. The average recharge was significantly less for this scenario, and the pathlines followed patterns similar to those obtained for low estimates of uniformly distributed recharge.

Based on the methods applied here, the results indicate that Timber Mountain produces enough groundwater recharge to form a groundwater mound and that recharge flows outward radially from Timber Mountain. Water chemistry and isotopic interpretations along with water-rock geochemical reaction modeling results are consistent with groundwater flow modeling scenarios. This suggests that groundwater recharge from Timber Mountain could flow northwestward to some extent toward ER-18-2 against the general southwestward groundwater flow of the Pahute Mesa-Oasis Valley groundwater basin.

REFERENCES

Belcher, W.R., P.E. Elliott, and A.L. Geldon, 2001. Hydraulic-Property Estimates for Use with a Transient Ground-Water Flow Model of the Death Valley Regional Ground-Water Flow System, Nevada and California. U.S. Geological Survey Water-Resources Investigations Report 01-4120.

Belcher, W., and D. Sweetkind, 2010. Death Valley Regional Groundwater Flow System, Nevada and California Hydrogeologic Framework and Transient Groundwater Flow Model. U.S. Geological Survey Professional Paper 1711.

Beria, H., J.R. Larsen, N.C. Ceperley, A. Michelon, T. Vennemann, and B. Schaefli, 2018. Understanding Snow Hydrologic Processes through the Lens of Stable Water Isotopes. *WIREs Water* 5:e1311, https://doi.org/10.1002/wat2.1311.

Botros, F.E., A.E. Hassan, D.M. Reeves, and G. Pohll, 2008. On Mapping Fracture Networks onto Continuum. *Water Resources Research* 44, W08435, doi:10.1029/2007WR006092.

Byers, F.M., Jr., W.J. Carr, R.L. Christiansen, P.W. Lipman, P.P. Orkild, and W.D. Quinlivan. 1976a. Geologic Map of the Timber Mountain Caldera Area, Nye County, Nevada, Map, I-891, scale 1:48,000. Reston, VA: U.S. Geological Survey.

Byers, F.M., Jr., J.W. Carr, P.P. Orkild, W.D. Quinlivan, and K.A. Sargent, 1976b. Volcanic Suites and Related Cauldrons of Timber Mountain-Oasis Valley Caldera Complex, Southern Nevada. U.S. Geological Survey Professional Paper 919.

Carr, J.W., and W.D. Quinlivan, 1964. Geology of the Timber Mountain Quadrangle, Nye County, Nevada. U.S. Geological Survey Technical Letter NTS-84.

Craig, H., 1961. Isotopic Variations in Natural Waters. *Science* 133:1702-1703.

Christiansen, R.L., P.W. Lipman, W.J. Carr, F.M. Byers Jr., P.P. Orkild, K.A. Sargent, 1977. Timber Mountain-Oasis Valley caldera complex of southern Nevada. Geological Society of America Bulletin 88:943-959.

Cooper, C.A., R.L. Hershey, J.M. Healey, and B.F. Lyles, 2013. Estimation of Groundwater Recharge at Pahute Mesa Using the Chloride Mass-Balance Method. Desert Research Institute Report No. 45251, Reno, NV.

Earman, S., A.R. Campbell, F.M. Phillips, and B.D. Newman, 2006. Isotopic exchange between snow and atmospheric water vapor: Estimation of snowmelt component of groundwater recharge in the southwestern United States. *Journal of Geophysical Research* 111, D090302, doi: 10.1029/2005JD006470.

Fenelon, J.M., K.J. Halford, and M.T. Moreo, 2016. Delineation of the Pahute Mesa-Oasis Valley Groundwater Basin, Nevada. U.S. Geological Survey Scientific Investigation Report 2015-5175.

Fenelon, J.M., D.S. Sweetkind, and R.J. Laczniak, 2010. Groundwater Flow Systems at the Nevada Test Site, Nevada—A Synthesis of Potentiometric Contours, Hydrostratigraphy, and Geologic Structures. U.S. Geological Survey Professional Paper 1771.

Ferrill, D.A., J. Winterle, G. Wittmeyer, D. Sims, S. Colton, A. Armstrong, and A.P. Morris, 1999. Stressed rock strains groundwater at Yucca Mountain, Nevada. GSA Today 9:5:1-7.

Garcia, C.A., T.R. Jackson, K.J. Halford, D.S. Sweetkind, N.A. Damar, J.M Fenelon, and S.R. Reiner, 2017. Hydraulic Characterization of Volcanic Rocks in Pahute Mesa Using an Integrated Analysis of 16 Multiple-Well Aquifer Tests, Nevada National Security Site, 2009-14. U.S. Geological Survey Scientific Investigations Report 2016-5151.

Grauch, V.J.S., D.A. Sawyer, C.J. Fridrich, and M.R. Hudson, 1999. Geophysical Framework of the Southern Nevada Volcanic Field and Hydrogeologic Implications. U.S. Geological Survey Professional Paper 1608.

Harbaugh, A.W., 2005. MODFLOW-2005. The U.S. Geological Survey Modular Ground-Water Model - The Ground-Water Flow Process. U.S. Geological Survey Techniques and Methods 6-A16.

Hardebeck, J.L., and A.J. Michael, 2006. Damped regional stress inversions: Methodology and examples for southern California and the Coalinga aftershock sequence. *Journal of Geophysical Research* 111:B11310 doi:10.1029/2005JB004144.

Hillel, D., 1980. Fundamentals of Soil Physics. Academic Press, Inc., Orlando, FL. ISBN: 0123485606.

Ingraham, N.L., B.F. Lyles, R.L. Jacobson, and J.W. Hess, 1991. Stable isotopic study of precipitation and spring discharge in southern Nevada. *Journal of Hydrology* 125:243-258.

Klimczak, C., R.A. Schultz, R. Parashar, and D.M. Reeves, 2010. Cubic law with aperture-length correlation: Implications for network scale fluid flow. *Hydrogeology Journal* 18:851-862.

Kwicklis, E.M., T.P. Rose, and F.C. Benedict Jr., 2005. Evaluation of Groundwater Flow in the Pahute Mesa-Oasis Valley Flow System Using Groundwater Chemical and

Isotopic Data. Los Alamos National Laboratory, LA-UR-05_4344, Los Alamos, NM.LLNL, 2004. Memo to Bob Bangerter, UGTA Project Manager, NNSA/NSO from Environmental Radiochemistry Group, Chemical and Biology & Nuclear Science Division, Lawrence Livermore National Laboratory, Isotopic Analyses: Environmental Monitoring Well ER-18-2, February 13, 2004.

Lyles, B.F., G. McCurdy, and J. Healey, 2016. 2015 Annual Report Timber Mountain Environmental Monitoring Station. Desert Research Institute Letter Report, DOE/NV/0000939-32.

Lyles, B.F., G. McCurdy, J. Healey, and K. Heintz, 2018a. 2016 Annual Report Timber Mountain Environmental Monitoring Station. Desert Research Institute Letter Report, DOE/NV/0003590-13.

Lyles, B.F., G. McCurdy, and J. Healey, 2018b. 2017 Annual Report Timber Mountain Environmental Monitoring Station. Desert Research Institute Letter Report, DOE/NV/0003590-17.

Lyles, B.F., G. McCurdy, and J. Healey, 2018c. 2018 Annual Report Timber Mountain Environmental Monitoring Station. Desert Research Institute Letter Report, DOE/NV/0003590-23.

Lyles, B.F., G. McCurdy, K. Heintz, and J. Healey, 2019. 2019 Annual Report Timber Mountain Environmental Monitoring Station. Desert Research Institute Letter Report, DOE/NV/0003590-41.

Middleton, R.S., E.M. Kwicklis, K.H. Birdsell, K.E. Bennet, D.G Levitt, and J. Hevesi, 2019. Net Infiltration Models for the Pahute Mesa Area. Los Alamos National Laboratory LA-UR-16-27513.

Morris, A., D.A. Ferrill, and D.B. Henderson, 1996. Slip tendency analysis and fault reactivation. *Geology* 24:275-278.

National Oceanic and Atmospheric Administration (NOAA), 2014. Precipitation Frequency Data Server. http://hdsc.nws.noaa.gov/hdsc/pfds/ (accessed July 2019).

Navarro, 2020. Phase II Geochemical and Isotopic Evaluation of Groundwater Flow in the Pahute Mesa-Oasis Valley Flow System, Nevada. Revision No. 1. Prepared for U.S. Department of Energy, Las Vegas, NV, N/0002653-069, September 2020.

Navarro, 2019. Written communication. Subject: "UGTA Chemistry Database," UGTA Technical Data Repository Database Identification Number UGTA-4-1197. Las Vegas, NV. As accessed on March 7, 2019.

National Nuclear Security Administration, 2009. Phase II Corrective Action Investigation Plan Action Units 101 and 102: Central and Western Pahute Mesa, Nevada Test Site, Nye County, Nevada. U.S. Department of Energy, DOE/NV-1312.

Parkhurst, D.L., and S.R. Charlton, 2008. NETPATHXL-An Excel Interface to the Program NETPATH. U.S. Geological Survey Techniques and Methods 6-A26.

Pawloski, G.A., J. Wurtz, and S.L. Drellack, 2010. The Underground Test Area Project of the Nevada Test Site: Building confidence in groundwater flow and transport models at

Pahute Mesa through focused characterization studies. Waste Management 2010 Conference (WM2010), Phoenix, Arizona, March 7-10, 2010, LLNL-CONF-422250.

Parashar, R., and D.M. Reeves, 2011. Computation of flow and transport in fracture networks on a continuum grid. MODFLOW and More 2011: Integrated Hydrologic Modeling, Golden, CO, June 5-8.

Parashar, R., H.V. Pham, and D.M. Reeves, 2018. Investigation of Primary Flow Paths in Western Pahute Mesa Using Models Accounting for the Influence of Regional Stress on Fault Permeability. U.S. Department of Energy letter report. DOE/NV/0003590-24.

Plummer, N.L., E.C. Prestemon, and E.L. Parkhurst, 1994. An Interactive Code (NETPATH) for Modeling Net Geochemical Reactions along a Flowpath, Version 2.0. U.S. Geological Survey, Water Resources Investigations Report 91-1169, Reston, VA.

Pollock, D.W., 2012. User Guide for MODPATH Version 6 - A Particle Tracking Model for MODFLOW. U.S. Geological Survey Techniques and Methods 6-A41.

Reeves, D.M., D.A. Benson, M.M. Meerschaert, 2008. Transport of conservative solutes in simulated fracture networks: 1. Synthetic data generation. Water Resources Research 44, W05404, doi:10.1029/2007WR006069.

Reeves, D.M., R. Parashar, K. Pohlmann, C. Russell, and J. Chapman, 2014. Development and calibration of dual-permeability flow models with discontinuous fault networks. *Vadose Zone Journal* 13(8), doi:10.2136/vzj2013.10.0183.

Reeves, D.M., K.D. Smith, R. Parashar, C. Collins, and K.V. Heintz, 2017. Investigating the Influence of Regional Stress on Fault and Fracture Permeability at Pahute Mesa, Nevada National Security Site. DOE/NV/0000939-41.

Rose, T.P., F.C. Benedict, Jr., J.M. Thomas, W.S. Sicke, R.L. Hershey, J.B Paces, I.M. Farnham, and Z.E. Peterman, 2006. Geochemical Data Analysis and Interpretation of the Pahute Mesa—Oasis Valley Groundwater Flow System, Nye County, Nevada, August 2002. Lawrence Livermore National Laboratory, UCRL-TR-224559, Livermore, CA.

Russell, C.E., C. Collins, R.H. French, and P. Rivera, *in publication*. Evaluation of Monitoring Data from Water Impounded within U12n and U12t Tunnels, Rainier and Aqueduct Mesas, Nevada National Security Site, Desert Research Institute Publication No. 45XXX.

Russell, C.E., and T. Minor, 2002. Reconnaissance estimates of recharge based on an elevation-dependent chloride mass-balance approach. Desert Research Institute Publication no. 45164, Las Vegas and Reno, Nevada, also DOE/NV/11508-37, p. 57 plus one appendix.

Sawyer, D.A., R.J. Fleck, M.A. Lanphere, R.G. Warren, D.E. Broxton, and M.R. Hudson. 1994. Episodic caldera volcanism in the Miocene Southwestern Nevada Volcanic Field: Revised stratigraphic caldera framework, $^{40}Ar/^{39}Ar$ geochronology, and implications for magmatism and extension. *Geological Society of America Bulletin* 106:1304–1318.

Simpson, E.S., D.B. Thorud, and I. Friedman, 1972. Distinguishing seasonal recharge to groundwater by deuterium analysis in southern Arizona. In: World water balance. Proceedings Reading Symposium 1970. International Association of Scientific Hydrology-UNESCO-WMO pp. 623-633.

Slate, J.L., M.E. Berry, P.D. Rowley, C.J. Fridrich, K.S. Morgan, J.B Workman, O.D. Young, G.L. Dixon, V.S. Williams, E.H. McKee, D.A. Ponce, T.G. Hildenbrand, W.C. Swadley, S.C. Lundstrom, E.B. Ekren, R.G. Warren, J.C. Cole, R.J. Fleck, M.A. Lanphere, D.A. Sawyer, S.A. Minor, D.J. Grunwald, R.J. Laczniak, C.M. Menges, J.C. Yount, and A.S. Jayko, 1999. Digital Geologic Map of the Nevada Test Site and Vicinity, Nye, Lincoln, and Clark Counties, Nevada, and Inyo County, California. U.S. Geological Survey Open-File Report 99-554-A.

Thomas, J.M, F.C. Benedict, Jr., T.P. Rose, R.L. Hershey, J.B. Paces, Z.E. Peterman, I.M. Farnham, K.H. Johannesson, A.K. Singh, K.J. Stetzenbach, G.B. Hudson, J.M. Kenneally, G.F. Eaton, and D.K. Smith, 2002. Geochemical and Isotopic Interpretations of Groundwater Flow in the Oasis Valley Flow System, Southern Nevada. Desert Research Institute, Publication No. 45190, Reno, NV.

U.S. Department of Energy, 2020. Pahute Mesa-Oasis Valley Hydrostratigraphic Framework Model for Corrective Action Units 101 and 101: Central and Western Pahute Mesa, Nye County, Nevada. Environmental Management Nevada Program, Revision No. 0, March 2020, DOE/EMNV-0014.

U.S. Geological Survey (USGS), 2008a. Documentation of Computer Program INFIL3.0 – A Distributed-Parameter Watershed Model to Estimate Net Infiltration Below the root Zone. U.S. Geological Survey Scientific Investigations Report 2008-5006, p. 99.

U.S. Geological Survey, 2008b. Computer Program INFIL3.0 – A Distributed-Parameter Watershed Model to Estimate Net Infiltration Below the root Zone, access at https://water.usgs.gov/nrp/gwsoftware/Infil/Infil.html.

Warren, R.G., G.L. Cole, and D. Walther, 2000. A Structural Block Model for the Three-Dimensional Geology of the Southwestern Nevada Volcanic Field. Los Alamos National Laboratory Report LA-UR-00-5866.

Winograd, I.J., and A.C. Riggs, 1984. Recharge to the Spring Mountains, Nevada: isotopic evidence. *Geological Society of America Abstracts with Programs* 16(6):698.

Winograd, I.J., A.C. Riggs, and T.B. Coplen, 1998. The relative contributions of summer and cool-season precipitation to groundwater recharge, Spring Mountains, Nevada, USA. *Hydrogeology Journal* 6:77-93.

Zablocki, C.J., 1979. Some Reconnaissance-Type Electrical Surveys of Timber Mountain Caldera, Nye County, Nevada. U.S. Geological Survey Open-file Report 79-1695.

APPENDIX A. MEAN WATER CHEMISTRY AND ISOTOPIC DATA FOR GROUNDWATER WATER-ROCK REACTION MODELING

Table A-1. Timber Mountain recharge input chemical, isotopic, and precipitation data.

Bulk Precipitation Gauge, Timber Mountain Weather Station					
Start Date	**Sample Collection Date**	**$\delta^{18}O$ (‰)**	**$\delta^{2}H$ (‰)**	**Precipitation (inches)**	**Season**
12/1/2010	5/16/2011	-16.6	-122	8.875	winter
5/6/2011	9/20/2011	-9.7	-68	2.125	summer
9/20/2011	8/2/2012	-	-	5	fall/winter/spring/summer
8/2/2011	12/4/2012	-13.7	-99	4.31	fall/winter
12/4/2012	5/16/2013	-9.7	-65	4.625	winter (short)
5/16/2013	11/19/2013	-12.81	-111.6	4.125	summer/fall
11/19/2013	5/5/2014	-16.67	-114	2.875	winter
5/5/2014	9/25/2014	-8.08	-80.38	2.813	summer
9/25/2014	7/1/2015	-14.36	-124.99	7	winter/summer
7/1/2015	11/4/2015	-11	-76.42	6.5	summer/fall
11/4/2015	7/28/2016	-12.3	-88.6	8.02	winter/summer
7/28/2016	11/18/2016	-	-	-	summer/fall
11/18/2016	2/9/2017	-14.7	-111	4.125	winter (short)
2/9/2017	6/28/2017	-13.6	-99	4.375	winter (short)
6/28/2017	9/19/2017	-	-	-	summer
9/19/2017	5/3/2018	-14	-101	3.67	winter
5/3/2018	10/25/2018	-9.1	-64	-	summer
10/25/2018	5/15/2019	-15.3	-110	-	winter

Table A-2. Rainier Mesa tunnels isotopic data.

Tunnel Name	Sample Date	$\delta^{18}O$ (‰)	$\delta^{2}H$ (‰)
U-12n Ext. Drift GSP	10/30/2006	-14.1	-104
U-12n Main Drift GSP	10/31/2006	-14.0	-104
U-12t Main Drift GSD	11/02/2006	-14.2	-106
U-12t Main Drift GSD	11/02/2006	-14.2	-107
U-12n Vent Hole 2	10/05/2011	-13.8	-103
U-12n Vent Hole 2	10/05/2011	-	-103
U-12n.10 Vent Hole	08/20/2008	-13.4	-101

Table A-3. NNSS springs chemical and isotopic data.

Spring Name		SO_4 (mg/L)	$\delta^{18}O$ (‰)	$\delta^{2}H$ (‰)	Cl (mg/L)
Captain Jack Spring_s1	AVERAGE	10.4	-13.1	-105	5.54
Captain Jack Spring_s1	STD	4.3	1.0	6	1.15
Oak Spring_s1	AVERAGE	10.5	-12.5	-101	9.16
Oak Spring_s1	STD	1.2	0.3	7	0.65
Topopah Spring_s1	AVERAGE	7.59	-12.3	-90	2.77
Topopah Spring_s1	STD	1.99	0.6	3	1.09
Tippipah Sp_s1	AVERAGE	18.2	-12.2	-95	7.60
Tippipah Sp_s1	STD	2.6	1.0	4	0.57
Whiterock Spring	AVERAGE	30.9	-12.2	-95	10.6
Whiterock Spring	STD	5.3	1.7	2	2.2
John’s Spring	2/23/2011	13.2	-12.1	-91	9.9
Cottonwood Spring	3/16/2011	5.1	-11.7	-89	2.5

Table A-4. Mean, standard deviation (SD), and number of samples (n) of δ^2H and $\delta^{18}O$; sample elevation; and catchment peak elevation for select NNSS springs and Rainier Mesa tunnels (table ordered by increasing $\delta^{18}O$).

Sample Location	Sample Elevation (m above sea level)	Catchment Peak	Peak Elevation (m above sea level)	δ^2H			$\delta^{18}O$		
				Mean (‰)	SD (‰)	n	Mean (‰)	SD (‰)	n
U-12t Main Drift GSD	1,711	Rainier Mesa Ridgeline	2,163	-107	0.7	2	-14.2	0.0	2
U-12n Ext. Drift GSP	1,844	Rainier Mesa Ridgeline	2,291	-104	-	1	-14.1	-	1
U-12n Main Drift GSP	1,844	Rainier Mesa Ridgeline	2,291	-104	-	1	-14.0	-	1
U-12n Vent Hole 2	1,860	Rainier Mesa Ridgeline	2,309	-103	0.0	2	-13.8	-	1
U-12n 10 Vent Hole	1,841	Rainier Mesa Ridgeline	2,291	-101	-	1	-13.4	-	1
Captain Jack Spring	1,793	Unnamed peak Eleana Range	1,954	-105	5.7	4	-13.1	1.0	9
Oak Spring	1,783	Oak Spring Butte	2,122	-101	7.0	2	-12.5	0.3	5
Topopah Spring	1,774	Shoshone Mountain	2,151	-90	3.0	2	-12.3	0.6	8
Whiterock Spring	1,539	Quartzite Ridge	2,167	-95	1.7	38	-12.2	1.7	53
Tippipah Spring	1,585	Unnamed peak north of Shoshone Mountain	2,018	-95	3.5	3	-12.2	1.0	6
Cottonwood Spring	1,292	Unnamed ridge west of Fortymile Wash	1,305	-89	-	1	-11.7	-	1

Table A-5. Percent summer versus winter isotopic signature of springs and Rainier Mesa tunnels.

	$\delta^{18}O$ (%)	$\delta^{2}H$ (%)	$\delta^{18}O$ and $\delta^{2}H$ (%)	Season
John's Spring	43	42	42.4	winter
	57	58	57.6	summer
Oak Spring	51	67	58.9	winter
	49	33	41.1	summer
Whiterock Spring	45	53	49.0	winter
	55	47	51.0	summer
Captain Jack Spring	60	77	68.4	winter
	40	23	31.6	summer
Tippipah Spring	45	52	48.6	winter
	55	48	51.4	summer
Topopah Spring	46	40	43.0	winter
	54	60	57.0	summer
Cottonwood Spring	36	38	36.7	winter
	64	63	63.3	summer
U-12n Ext. Drift GSP	79	74.2	76.5	winter
	21	25.8	23.5	summer
U-12n Main Drift GSP	77	74.2	75.6	winter
	23	25.8	24.4	summer
U-12t Main Drift GSD	81	80.3	80.5	winter
	19	19.7	19.5	summer
U-12n Vent Hole 2	73	71.7	72.6	winter
	27	28.3	27.4	summer
U-12n.10 Vent Hole	66	66.9	66.6	winter
	34	33.1	33.4	summer

Table A-6. NETPATH input chemical and isotopic data.

Well Name	Temp (°C)	EC (ms/cm)	pH	Ca (mg/L)	Mg (mg/L)	Na (mg/L)	K (mg/L)	Cl (mg/L)	SO_4 (mg/L)	HCO_3 (mg/L)	F (mg/L)	SiO_2 (mg/L)	Fe (mg/L)	Al (mg/L)	$\delta^{13}C$ (‰)	^{14}C (pMC)	$\delta^{2}H$ (‰)	$\delta^{18}O$ (‰)
TM Recharge	13.2	-	7.25	9.04	2.00	27.0	4.70	6.87	13.7	87	0.22	49.5	0.034	0.009	-14.1	97.5	-104	-13.9
ER-EC-7_m1-2	28.5	256	7.84	21.0	1.87	28.1	2.76	4.53	13.9	118	1.16	42.5	0.001	0.006	-6.6	41.4	-107	-14.0
ER-EC-5_m1-3	29.7	405	8.00	20.2	0.51	74.2	1.57	15.9	35.8	168	4.66	40.9	0.003	0.008	-2.8	6.9	-113	-15.0
ER-E-2A_m3	35.9	664	8.33	8.17	0.20	127.8	2.74	56.5	87.5	175	4.27	45.5	0.025	0.009	-1.8	9.8	-116	-14.9
ER-EC-13_m2	41.2	705	8.20	10.1	0.09	136.0	3.80	60.4	93.7	175	5.40	53.7	0.081	0.005	-2.5	12.5	-116	-15.2
ER-EC-14_m2	33.8	450	7.90	13.0	0.38	75.4	2.06	20.0	43.5	164	6.35	42.8	0.005	0.005	-2.6	7.2	-115	-14.3
ER-18-2_m1	46.3	1417	7.85	5.50	0.22	355.5	3.51	12.8	54.9	864	13.0	42.5	0.022	0.012	-0.2	1.0	-110	-14.7
UE-29a 2_p1	22.8	248	7.51	11.5	0.92	40.5	2.17	9.16	27.1	106	0.83	62.9	0.017	0.004	-12.2	66.5	-92	-12.7
UE-29a 1_p1	22.0	267	7.51	15.8	7.95	39.0	3.38	8.92	18.1	105	0.73	52.9	0.005	0.004	-11.5	75.5	-92	-12.4
ER-30-1_p2	24.3	291	9.28	2.59	0.07	65.3	1.33	6.16	12.0	128	1.14	28.7	0.100	0.005	-8.1	39.2	-92	-12.2
UE-18t (2016 ft)	30.4	293	8.12	3.74	0.22	59.4	2.32	3.17	12.2	149	8.43	32.5	5.500	0.371	-5.9	-	-	-14.6
UE-18t (1988 ft)	25.0	642	8.63	22.2	1.00	141.0	8.16	64.4	10.8	331	-	7.00	0.005	0.005	-	-	-105	-13.8
ER-20-4_m1	41.1	250	8.35	4.21	0.05	52.0	1.19	4.71	16.9	104	7.99	49.4	0.000	0.005	-3.4	18.6	-115	-15.1
ER-EC-12_m2	38.8	396	8.53	3.30	0.02	79.3	0.49	16.0	35.8	144	4.67	32.0	0.207	0.020	-5.3	15.9	-113	-15.1
ER-EC-4_m2-3	35.9	765	7.89	27.4	4.33	128.3	10.3	80.8	111	151	3.30	74.1	0.051	0.004	-1.5	5.9	-113	-14.7
ER-EC-8_m1-3	36.7	635	8.07	10.1	0.42	118.5	6.10	48.5	81.3	181	5.43	50.7	0.001	0.004	-1.2	12.1	-114	-14.8
ER-OV-01_p1	25.7	665	8.42	6.14	0.08	135.1	7.02	46.5	83.2	193	2.45	65.7	0.003	0.043	-2.0	5.0	-113	-14.7
ER-OV-6a_p1	28.6	672	8.42	2.39	0.24	136.5	7.59	44.3	80.3	193	3.67	51.4	0.008	0.011	-2.2	6.0	-113	-14.7
ER-OV-3c_p1	24.0	431	8.24	15.5	0.37	78.7	1.23	16.7	44.4	170	4.82	40.8	0.002	0.007	-3.2	6.8	-109	-14.7
UE-18r_o1	26.3	-	7.88	18.8	0.64	76.2	4.70	8.28	23.0	231	2.66	47.0	0.047	0.008	-4.5	8.2	-111	-14.9

Table A-7. NETPATH model input constraints and phases.

Constraint	**Ca (moles)**	**Mg (moles)**	**Na (moles)**	**K (moles)**	**C (moles)**	**Cl (moles)**	**S (moles)**	**Si (moles)**	**Fe (moles)**	**Al (moles)**
Phase										
Calcite	1				1					
Dolomite	1	1			2					
Gypsum	1						1			
Pyrite							2		1	
NaCl			1			1				
SiO_2								1		
Exchange*	1-X	-X	2							
TM-Glass	0.024	0.005	0.383	0.368				4.173	0.026	0.789
TM-Clay	0.141	0.138	0.161	0.017				3.462	0.050	2.438
Goethite									1	
CO_2 Gas					1					

*Mole fraction calculated by NETPATH for each well input water chemistry.

Table A-8. Mineral saturation index computed by NETPATH.

Saturation Index = LOG (Ion Activity Product/Solubility Product)																
Well Name	**Calcite**	**Dolomite**	**Gypsum**	**SiO_2 (a)**	**Quartz**	**Kaolinite**	**Albite**	**Anorthite**	**Kspar**	**Kmica**	**Ca-Mont**	**Illite**	**Hematite**	**Goethite**	**$Fe(OH)_3$ (a)**	**PCO_2**
TM Recharge	-1.45	-3.38	-3.11	-0.27	1.08	5.62	0.03	-2.96	1.76	10.00	5.09	3.94	7.26	3.53	-2.80	-2.43
ER-EC-7_m1-2	-0.12	-0.91	-2.81	-0.47	0.78	2.18	-1.28	-3.41	0.01	5.43	1.20	0.48	9.65	3.57	-2.20	-2.76
ER-EC-5_m1-3	0.14	-0.93	-2.47	-0.50	0.74	1.89	-0.90	-3.34	-0.29	4.92	0.88	0.00	11.42	4.37	-1.36	-2.76
ER-E-2A_m3	0.12	-0.92	-2.54	-0.52	0.68	0.65	-0.91	-3.82	-0.36	3.72	-0.50	-0.98	15.08	5.76	0.24	-3.03
ER-EC-13_m2	0.15	-1.29	-2.42	-0.48	0.69	0.02	-1.19	-4.18	-0.59	2.87	-1.18	-1.74	15.92	5.83	0.48	-2.87
ER-EC-14_m2	-0.10	-1.31	-2.57	-0.51	0.70	1.22	-1.29	-4.03	-0.62	4.00	0.05	-0.80	11.70	4.22	-1.37	-2.64
ER-18-2_m1	0.18	-0.52	-3.07	-0.61	0.53	0.67	-1.03	-4.19	-0.93	3.51	-0.76	-1.44	13.32	4.19	-0.99	-1.80
UE-29a 2_p1	-0.86	-2.49	-2.77	-0.25	1.03	3.44	-0.45	-3.60	0.64	6.80	2.77	1.61	9.35	3.84	-2.14	-2.52
UE-29a 1_o1	-0.77	-1.53	-2.87	-0.32	0.97	3.33	-0.69	-3.68	0.63	6.80	2.55	1.72	8.06	3.25	-2.75	-2.54
ER-30-1_p2	0.27	-0.67	-3.85	-0.72	0.56	-1.02	-1.62	-5.11	-0.96	1.69	-2.57	-2.53	16.76	7.43	1.51	-4.22
UE-18t 2016	-0.48	-1.79	-3.60	-0.61	0.63	4.68	0.33	-0.94	1.20	9.42	3.92	3.25	18.65	7.94	2.23	-2.92
UE-18t 1988	0.97	0.97	-3.04	-1.25	0.02	-0.83	-2.91	-5.24	-1.81	2.11	-3.13	-2.91	13.92	5.96	0.07	-3.14
ER-20-4_m1	-0.20	-1.89	-3.39	-0.52	0.65	-0.39	-1.74	-4.59	-1.22	1.91	-1.72	-2.45	7.54	1.64	-3.71	-3.23
ER-EC-12_m2	-0.07	-1.84	-3.23	-0.70	0.48	0.32	-1.41	-3.87	-1.44	2.74	-1.11	-2.00	17.15	6.60	1.18	-3.29
ER-EC-4_m2-3	0.13	-0.10	-1.96	-0.29	0.91	1.18	-0.63	-3.65	0.49	4.65	0.35	0.09	13.82	5.13	-0.38	-2.67
ER-EC-8_m1-3	-0.01	-0.95	-2.47	-0.47	0.73	0.50	-1.16	-4.32	-0.25	3.60	-0.67	-1.07	10.94	3.64	-1.85	-2.75
ER-OV-01_p1	0.00	-1.56	-2.68	-0.27	0.99	3.34	0.91	-1.96	1.96	8.11	2.89	2.52	12.95	5.42	-0.45	-3.15
ER-OV-6a_p1	-0.37	-1.35	-3.10	-0.41	0.84	1.58	-0.19	-3.87	0.86	5.55	0.62	0.52	14.03	5.75	-0.01	-3.13
ER-OV-3c_p1	0.19	-0.91	-2.49	-0.46	0.82	1.99	-0.56	-3.39	-0.02	5.12	1.07	0.25	11.78	4.96	-0.97	-3.03
UE-18r _o1	0.09	-0.93	-2.69	-0.41	0.85	2.63	-0.49	-3.17	0.62	6.33	1.79	1.09	12.61	5.20	-0.64	-2.52

NETPATH Modeling Results

Positive mineral phase values indicate mineral dissolution, negative mineral phase values indicated mineral precipitation

Initial Well : TM Recharge
Final Well : ER-EC-7_m1-2

	Final	Initial
C	1.9422	1.4314
S	0.1450	0.1426
CA	0.5247	0.2256
MG	0.0770	0.0822
NA	1.2208	1.1766
K	0.0705	0.1203
CL	0.1279	0.1938
SI	0.7075	0.8237
FE	0.0000	0.0006
AL	0.0002	0.0003

CALCITE	CA	1.0000	C	1.0000	RS	4.0000	I1	0.0000	I2 0.0000
DOLOMITE	CA	1.0000	MG	1.0000	C	2.0000	RS	8.0000	I1 0.0000
	I2	0.0000							
GYPSUM	CA	1.0000	S	1.0000	RS	6.0000	I3	22.0000	
PYRITE	FE	1.0000	S	2.0000	RS	0.0000	I3	-60.0000	
NaCl	NA	1.0000	CL	1.0000					
SiO2	SI	1.0000							
EXCHANGE	CA	-0.8720	NA	2.0000	MG	-0.1280			
TM-Glass	K	0.3680	NA	0.3830	CA	0.0240	MG	0.0050	FE 0.0260
	AL	0.7890	SI	4.1730					
TM-Clay	K	0.0170	NA	0.1610	CA	0.1410	MG	0.1380	FE 0.0500
	AL	2.4380	SI	3.4620					
GOETHITE	FE	1.0000	RS	3.0000					
CO2 GAS	C	1.0000	RS	4.0000	I1	-12.0000	I2	100.0000	

MODEL 1

CALCITE		0.36366
DOLOMITE		-0.00062
GYPSUM	+	0.00088
PYRITE	+	0.00075
NaCl	+	-0.06592 (Constraint ignored)
SiO2		0.30333
EXCHANGE		0.07777
TM-Glass	+	-0.13741 (Constraint ignored)
TM-Clay	-	0.04444 (Constraint ignored)
CO2 GAS		0.14839

	Computed	Observed
Carbon-13	-11.2931	-6.6283
C-14 (% mod)	79.4042*	41.3500

Adjusted C-14 age in years: 5394.* * = based on Original Data

MODEL 2

CALCITE		0.36454
DOLOMITE		-0.00062
PYRITE	+	0.00119
NaCl	+	-0.06592 (Constraint ignored)
SiO2		0.30333
EXCHANGE		0.07777
TM-Glass	+	-0.13741 (Constraint ignored)
TM-Clay	-	0.04444 (Constraint ignored)
GOETHITE	-	-0.00044
CO2 GAS		0.14752

	Computed	Observed
Carbon-13	-11.2876	-6.6283
C-14 (% mod)	79.3590*	41.3500

Adjusted C-14 age in years: 5389.* * = based on Original Data

Initial Well 1 : TM Recharge
Initial Well 2 : ER-20-4_m1
Final well : ER-18-2_m1

```
          Final    Initial 1   Initial 2
 C      14.1751      1.4314      1.7079
 S       0.5720      0.1426      0.1760
 CA      0.1375      0.2256      0.1051
 MG      0.0092      0.0822      0.0019
 NA     15.4843      1.1766      2.2610
 K       0.0898      0.1203      0.0304
 CL      0.3605      0.1938      0.1330
 SI      0.7087      0.8237      0.8232
 FE      0.0004      0.0006      0.0000
 AL      0.0004      0.0003      0.0002
 D    -110.0000   -103.7000   -115.0000

 CALCITE  CA   1.0000 C    1.0000 RS   4.0000 I1   0.0000 I2   0.0000
 DOLOMITE CA   1.0000 MG   1.0000 C    2.0000 RS   8.0000 I1   0.0000
          I2   0.0000
 GYPSUM   CA   1.0000 S    1.0000 RS   6.0000 I3  22.0000
 PYRITE   FE   1.0000 S    2.0000 RS   0.0000 I3 -60.0000
 NaCl     NA   1.0000 CL   1.0000
 SiO2     SI   1.0000
 EXCHANGE CA  -0.9372 NA   2.0000 MG  -0.0628
 TM-Glass K    0.3680 NA   0.3830 CA   0.0240 MG   0.0050 FE   0.0260
          AL   0.7890 SI   4.1730
 TM-Clay  K    0.0170 NA   0.1610 CA   0.1410 MG   0.1380 FE   0.0500
          AL   2.4380 SI   3.4620
 GOETHITE FE   1.0000 RS   3.0000
 CO2 GAS  C    1.0000 RS   4.0000 I1 -12.0000 I2 100.0000

            MODEL   1
  Init 1    + F        0.44248
  Init 2    + F        0.55752
  CALCITE              5.49141
  DOLOMITE             0.39714
  GYPSUM    +          0.41081
  NaCl      +          0.20057
  SiO2                -0.28028
  EXCHANGE             6.74232
  TM-Glass  +          0.05415
  TM-Clay   -         -0.01744
  GOETHITE  -         -0.00042
  CO2 GAS              6.30389
                Computed    Observed
Carbon-13       -6.1935     -0.2117
C-14 (% mod)    50.0751*     1.0000
-------------------------------------------------------------------------
Adjusted C-14 age in years:  32352.*     * = based on Original Data

            MODEL   2
  Init 1    + F        0.44248
  Init 2    + F        0.55752
  CALCITE              5.90223
  DOLOMITE             0.39714
  PYRITE    +          0.20541
  NaCl      +          0.20057
  SiO2                -0.28028
  EXCHANGE             6.74232
  TM-Glass  +          0.05415
  TM-Clay   -         -0.01744
  GOETHITE  -         -0.20583
  CO2 GAS              5.89308
                Computed    Observed
Carbon-13       -5.8457     -0.2117
C-14 (% mod)    47.1770*     1.0000
-------------------------------------------------------------------------
Adjusted C-14 age in years:  31859.*     * = based on Original Data
```

Initial Well 1 : TM Recharge
Initial Well 2 : ER-20-4_m1
Final well : ER-18-2_m1

	Final	Initial 1	Initial 2
C	14.1751	1.4314	1.7079
S	0.5720	0.1426	0.1760
CA	0.1375	0.2256	0.1051
MG	0.0092	0.0822	0.0019
NA	15.4843	1.1766	2.2610
K	0.0898	0.1203	0.0304
CL	0.3605	0.1938	0.1330
SI	0.7087	0.8237	0.8232
FE	0.0004	0.0006	0.0000
AL	0.0004	0.0003	0.0002
18	-14.6833	-13.9000	-15.1000

CALCITE	CA	1.0000	C	1.0000	RS	4.0000	I1	0.0000	I2	0.0000
DOLOMITE	CA	1.0000	MG	1.0000	C	2.0000	RS	8.0000	I1	0.0000
	I2	0.0000								
GYPSUM	CA	1.0000	S	1.0000	RS	6.0000	I3	22.0000		
PYRITE	FE	1.0000	S	2.0000	RS	0.0000	I3	-60.0000		
NaCl	NA	1.0000	CL	1.0000						
SiO2	SI	1.0000								
EXCHANGE	CA	-0.9372	NA	2.0000	MG	-0.0628				
TM-Glass	K	0.3680	NA	0.3830	CA	0.0240	MG	0.0050	FE	0.0260
	AL	0.7890	SI	4.1730						
TM-Clay	K	0.0170	NA	0.1610	CA	0.1410	MG	0.1380	FE	0.0500
	AL	2.4380	SI	3.4620						
GOETHITE	FE	1.0000	RS	3.0000						
CO2 GAS	C	1.0000	RS	4.0000	I1	-12.0000	I2	100.0000		

MODEL 1		
Init 1	+	F 0.34725
Init 2	+	F 0.65275
CALCITE		5.44690
DOLOMITE		0.40205
GYPSUM	+	0.40763
NaCl	+	0.20636
SiO2		-0.35235
EXCHANGE		6.68389
TM-Glass	+	0.07778
TM-Clay	-	-0.02508
GOETHITE	-	-0.00059
CO2 GAS		6.31226

	Computed	Observed
Carbon-13	-6.1039	-0.2117
C-14 (% mod)	49.4104*	1.0000

Adjusted C-14 age in years: 32241.* * = based on Original Data

MODEL 2		
Init 1	+	F 0.34725
Init 2	+	F 0.65275
CALCITE		5.85453
DOLOMITE		0.40205
PYRITE	+	0.20382
NaCl	+	0.20636
SiO2		-0.35235
EXCHANGE		6.68389
TM-Glass	+	0.07778
TM-Clay	-	-0.02508
GOETHITE	-	-0.20441
CO2 GAS		5.90462

	Computed	Observed
Carbon-13	-5.7588	-0.2117
C-14 (% mod)	46.5347*	1.0000

Adjusted C-14 age in years: 31746.* * = based on Original Data

Initial Well 1 : TM Recharge
Initial Well 2 : ER-EC-12_m2
Final well : ER-18-2_m1

```
          Final    Initial 1   Initial 2
 C      14.1751      1.4314      2.3671
 S       0.5720      0.1426      0.3729
 CA      0.1375      0.2256      0.0823
 MG      0.0092      0.0822      0.0009
 NA     15.4843      1.1766      3.4501
 K       0.0898      0.1203      0.0126
 CL      0.3605      0.1938      0.4510
 SI      0.7087      0.8237      0.5332
 FE      0.0004      0.0006      0.0037
 AL      0.0004      0.0003      0.0007
 D    -110.0000   -103.7000   -112.8500

 CALCITE  CA   1.0000 C    1.0000 RS   4.0000 I1   0.0000 I2   0.0000
 DOLOMITE CA   1.0000 MG   1.0000 C    2.0000 RS   8.0000 I1   0.0000
          I2   0.0000
 GYPSUM   CA   1.0000 S    1.0000 RS   6.0000 I3  22.0000
 PYRITE   FE   1.0000 S    2.0000 RS   0.0000 I3 -60.0000
 NaCl     NA   1.0000 CL   1.0000
 SiO2     SI   1.0000
 EXCHANGE CA  -0.9372 NA   2.0000 MG  -0.0628
 TM-Glass K    0.3680 NA   0.3830 CA   0.0240 MG   0.0050 FE   0.0260
          AL   0.7890 SI   4.1730
 TM-Clay  K    0.0170 NA   0.1610 CA   0.1410 MG   0.1380 FE   0.0500
          AL   2.4380 SI   3.4620
 GOETHITE FE   1.0000 RS   3.0000
 CO2 GAS  C    1.0000 RS   4.0000 I1 -12.0000 I2 100.0000

            MODEL   1
  Init 1    + F        0.31148
  Init 2    + F        0.68852
  CALCITE              5.31304
  DOLOMITE             0.38676
  GYPSUM    +          0.27086
  NaCl      +         -0.01040      (Constraint ignored)
  SiO2                -0.28206
  EXCHANGE             6.35648
  TM-Glass  +          0.12033
  TM-Clay   -         -0.03901
  GOETHITE  -         -0.00353
  CO2 GAS              6.01288
                Computed    Observed
Carbon-13       -6.1466     -0.2117
C-14 (% mod)    47.3124*     1.0000
-------------------------------------------------------------------------
Adjusted C-14 age in years:  31883.*     * = based on Original Data

            MODEL   2
  Init 1    + F        0.31148
  Init 2    + F        0.68852
  CALCITE              5.58390
  DOLOMITE             0.38676
  PYRITE    +          0.13543
  NaCl      +         -0.01040      (Constraint ignored)
  SiO2                -0.28206
  EXCHANGE             6.35648
  TM-Glass  +          0.12033
  TM-Clay   -         -0.03901
  GOETHITE  -         -0.13896
  CO2 GAS              5.74202
                Computed    Observed
Carbon-13       -5.9173     -0.2117
C-14 (% mod)    45.4015*     1.0000
-------------------------------------------------------------------------
Adjusted C-14 age in years:  31542.*     * = based on Original Data
```

Initial Well 1 : TM Recharge
Initial Well 2 : ER-EC-12_m2
Final well : ER-18-2_m1

```
          Final    Initial 1   Initial 2
 C      14.1751      1.4314      2.3671
 S       0.5720      0.1426      0.3729
 CA      0.1375      0.2256      0.0823
 MG      0.0092      0.0822      0.0009
 NA     15.4843      1.1766      3.4501
 K       0.0898      0.1203      0.0126
 CL      0.3605      0.1938      0.4510
 SI      0.7087      0.8237      0.5332
 FE      0.0004      0.0006      0.0037
 AL      0.0004      0.0003      0.0007
 18    -14.6833    -13.9000    -15.0700

 CALCITE  CA   1.0000 C    1.0000 RS   4.0000 I1   0.0000 I2   0.0000
 DOLOMITE CA   1.0000 MG   1.0000 C    2.0000 RS   8.0000 I1   0.0000
          I2   0.0000
 GYPSUM   CA   1.0000 S    1.0000 RS   6.0000 I3  22.0000
 PYRITE   FE   1.0000 S    2.0000 RS   0.0000 I3 -60.0000
 NaCl     NA   1.0000 CL   1.0000
 SiO2     SI   1.0000
 EXCHANGE CA  -0.9372 NA   2.0000 MG  -0.0628
 TM-Glass K    0.3680 NA   0.3830 CA   0.0240 MG   0.0050 FE   0.0260
          AL   0.7890 SI   4.1730
 TM-Clay  K    0.0170 NA   0.1610 CA   0.1410 MG   0.1380 FE   0.0500
          AL   2.4380 SI   3.4620
 GOETHITE FE   1.0000 RS   3.0000
 CO2 GAS  C    1.0000 RS   4.0000 I1 -12.0000 I2 100.0000

            MODEL   1
  Init 1    + F        0.33051
  Init 2    + F        0.66949
  CALCITE              5.32518
  DOLOMITE             0.38625
  GYPSUM    +          0.27525
  NaCl      +         -0.00551      (Constraint ignored)
  SiO2                -0.27034
  EXCHANGE             6.37661
  TM-Glass  +          0.11468
  TM-Clay   -         -0.03718
  GOETHITE  -         -0.00341
  CO2 GAS              6.01958
                Computed    Observed
 Carbon-13       -6.1624     -0.2117
 C-14 (% mod)    47.4963*     1.0000
--------------------------------------------------------------------------
 Adjusted C-14 age in years:  31915.*     * = based on Original Data

            MODEL   2
  Init 1    + F        0.33051
  Init 2    + F        0.66949
  CALCITE              5.60042
  DOLOMITE             0.38625
  PYRITE    +          0.13762
  NaCl      +         -0.00551      (Constraint ignored)
  SiO2                -0.27034
  EXCHANGE             6.37661
  TM-Glass  +          0.11468
  TM-Clay   -         -0.03718
  GOETHITE  -         -0.14104
  CO2 GAS              5.74433
                Computed    Observed
 Carbon-13       -5.9294     -0.2117
 C-14 (% mod)    45.5546*     1.0000
--------------------------------------------------------------------------
 Adjusted C-14 age in years:  31570.*     * = based on Original Data
```

Initial Well 1 : TM Recharge
Initial Well 2 : ER-EC-14_m2
Final well : ER-18-2_m1

```
          Final    Initial 1   Initial 2
 C      14.1751      1.4314      2.6847
 S       0.5720      0.1426      0.4535
 CA      0.1375      0.2256      0.3250
 MG      0.0092      0.0822      0.0156
 NA     15.4843      1.1766      3.2809
 K       0.0898      0.1203      0.0527
 CL      0.3605      0.1938      0.5631
 SI      0.7087      0.8237      0.7123
 FE      0.0004      0.0006      0.0001
 AL      0.0004      0.0003      0.0002
 D    -110.0000   -103.7000   -115.1000

 CALCITE  CA   1.0000 C    1.0000 RS   4.0000 I1   0.0000 I2   0.0000
 DOLOMITE CA   1.0000 MG   1.0000 C    2.0000 RS   8.0000 I1   0.0000
          I2   0.0000
 GYPSUM   CA   1.0000 S    1.0000 RS   6.0000 I3  22.0000
 PYRITE   FE   1.0000 S    2.0000 RS   0.0000 I3 -60.0000
 NaCl     NA   1.0000 CL   1.0000
 SiO2     SI   1.0000
 EXCHANGE CA  -0.9372 NA   2.0000 MG  -0.0628
 TM-Glass K    0.3680 NA   0.3830 CA   0.0240 MG   0.0050 FE   0.0260
          AL   0.7890 SI   4.1730
 TM-Clay  K    0.0170 NA   0.1610 CA   0.1410 MG   0.1380 FE   0.0500
          AL   2.4380 SI   3.4620
 GOETHITE FE   1.0000 RS   3.0000
 CO2 GAS  C    1.0000 RS   4.0000 I1 -12.0000 I2 100.0000

            MODEL   1
  Init 1    + F        0.44737
  Init 2    + F        0.55263
  CALCITE              5.39615
  DOLOMITE             0.37806
  GYPSUM    +          0.25763
  NaCl      +         -0.03740      (Constraint ignored)
  SiO2                -0.11132
  EXCHANGE             6.58796
  TM-Glass  +          0.01888
  TM-Clay   -         -0.00603
  GOETHITE  -         -0.00013
  CO2 GAS              5.89884
                Computed    Observed
Carbon-13       -5.8973     -0.2117
C-14 (% mod)    46.7730*     1.0000
-------------------------------------------------------------------------
Adjusted C-14 age in years:  31788.*     * = based on Original Data

            MODEL   2
  Init 1    + F        0.44737
  Init 2    + F        0.55263
  CALCITE              5.65378
  DOLOMITE             0.37806
  PYRITE    +          0.12881
  NaCl      +         -0.03740      (Constraint ignored)
  SiO2                -0.11132
  EXCHANGE             6.58796
  TM-Glass  +          0.01888
  TM-Clay   -         -0.00603
  GOETHITE  -         -0.12894
  CO2 GAS              5.64121
                Computed    Observed
Carbon-13       -5.6792     -0.2117
C-14 (% mod)    44.9556*     1.0000
-------------------------------------------------------------------------
Adjusted C-14 age in years:  31460.*     * = based on Original Data
```

Initial Well 1 : TM Recharge
Initial Well 2 : UE-18r
Final well : ER-18-2_m1

```
          Final    Initial 1   Initial 2
 C      14.1751      1.4314      3.7792
 S       0.5720      0.1426      0.2391
 CA      0.1375      0.2256      0.4684
 MG      0.0092      0.0822      0.0263
 NA     15.4843      1.1766      3.3177
 K       0.0898      0.1203      0.1202
 CL      0.3605      0.1938      0.2337
 SI      0.7087      0.8237      0.7829
 FE      0.0004      0.0006      0.0008
 AL      0.0004      0.0003      0.0003
 D    -110.0000   -103.7000   -110.8890

 CALCITE  CA   1.0000 C    1.0000 RS   4.0000 I1   0.0000 I2   0.0000
 DOLOMITE CA   1.0000 MG   1.0000 C    2.0000 RS   8.0000 I1   0.0000
          I2   0.0000
 GYPSUM   CA   1.0000 S    1.0000 RS   6.0000 I3  22.0000
 PYRITE   FE   1.0000 S    2.0000 RS   0.0000 I3 -60.0000
 NaCl     NA   1.0000 CL   1.0000
 SiO2     SI   1.0000
 EXCHANGE CA  -0.9372 NA   2.0000 MG  -0.0628
 TM-Glass K    0.3680 NA   0.3830 CA   0.0240 MG   0.0050 FE   0.0260
          AL   0.7890 SI   4.1730
 TM-Clay  K    0.0170 NA   0.1610 CA   0.1410 MG   0.1380 FE   0.0500
          AL   2.4380 SI   3.4620
 GOETHITE FE   1.0000 RS   3.0000
 CO2 GAS  C    1.0000 RS   4.0000 I1 -12.0000 I2 100.0000

            MODEL   1
  Init 1    + F        0.12366
  Init 2    + F        0.87634
  CALCITE              4.77060
  DOLOMITE             0.35951
  GYPSUM    +          0.34405
  PYRITE    +          0.00041
  NaCl      +          0.13171
  SiO2                 0.17701
  EXCHANGE             6.16371
  TM-Glass  +         -0.08400      (Constraint ignored)
  TM-Clay   -          0.02724      (Constraint ignored)
  CO2 GAS              5.19663
                Computed    Observed
Carbon-13       -5.6353     -0.2117
C-14 (% mod)    39.7930*     1.0000
-------------------------------------------------------------------------
Adjusted C-14 age in years:  30452.*     * = based on Original Data
            MODEL   2
  Init 1    + F        0.12366
  Init 2    + F        0.87634
  CALCITE              5.11465
  DOLOMITE             0.35951
  PYRITE    +          0.17243
  NaCl      +          0.13171
  SiO2                 0.17701
  EXCHANGE             6.16371
  TM-Glass  +         -0.08400      (Constraint ignored)
  TM-Clay   -          0.02724      (Constraint ignored)
  GOETHITE  -         -0.17202
  CO2 GAS              4.85259
                Computed    Observed
Carbon-13       -5.3440     -0.2117
C-14 (% mod)    37.3658*     1.0000
-------------------------------------------------------------------------
Adjusted C-14 age in years:  29932.*     * = based on Original Data
```

Initial Well 1 : TM Recharge
Initial Well 2 : UE-18r
Final well : ER-18-2_m1

```
          Final    Initial 1   Initial 2
 C      14.1751      1.4314      3.7792
 S       0.5720      0.1426      0.2391
 CA      0.1375      0.2256      0.4684
 MG      0.0092      0.0822      0.0263
 NA     15.4843      1.1766      3.3177
 K       0.0898      0.1203      0.1202
 CL      0.3605      0.1938      0.2337
 SI      0.7087      0.8237      0.7829
 FE      0.0004      0.0006      0.0008
 AL      0.0004      0.0003      0.0003
 18    -14.6833    -13.9000    -14.8722

 CALCITE  CA   1.0000 C    1.0000 RS   4.0000 I1   0.0000 I2   0.0000
 DOLOMITE CA   1.0000 MG   1.0000 C    2.0000 RS   8.0000 I1   0.0000
          I2   0.0000
 GYPSUM   CA   1.0000 S    1.0000 RS   6.0000 I3  22.0000
 PYRITE   FE   1.0000 S    2.0000 RS   0.0000 I3 -60.0000
 NaCl     NA   1.0000 CL   1.0000
 SiO2     SI   1.0000
 EXCHANGE CA  -0.9372 NA   2.0000 MG  -0.0628
 TM-Glass K    0.3680 NA   0.3830 CA   0.0240 MG   0.0050 FE   0.0260
          AL   0.7890 SI   4.1730
 TM-Clay  K    0.0170 NA   0.1610 CA   0.1410 MG   0.1380 FE   0.0500
          AL   2.4380 SI   3.4620
 GOETHITE FE   1.0000 RS   3.0000
 CO2 GAS  C    1.0000 RS   4.0000 I1 -12.0000 I2 100.0000

            MODEL   1
  Init 1    + F        0.19430
  Init 2    + F        0.80570
  CALCITE              4.84981
  DOLOMITE             0.36023
  GYPSUM    +          0.35083
  PYRITE    +          0.00042
  NaCl      +          0.13453
  SiO2                 0.17416
  EXCHANGE             6.23793
  TM-Glass  +         -0.08401      (Constraint ignored)
  TM-Clay   -          0.02724      (Constraint ignored)
  CO2 GAS              5.28184
                Computed    Observed
 Carbon-13       -5.7225     -0.2117
 C-14 (% mod)    40.9348*     1.0000
 ------------------------------------------------------------------------
 Adjusted C-14 age in years:  30686.*     * = based on Original Data

            MODEL   2
  Init 1    + F        0.19430
  Init 2    + F        0.80570
  CALCITE              5.20064
  DOLOMITE             0.36023
  PYRITE    +          0.17584
  NaCl      +          0.13453
  SiO2                 0.17416
  EXCHANGE             6.23793
  TM-Glass  +         -0.08401      (Constraint ignored)
  TM-Clay   -          0.02724      (Constraint ignored)
  GOETHITE  -         -0.17542
  CO2 GAS              4.93101
                Computed    Observed
 Carbon-13       -5.4255     -0.2117
 C-14 (% mod)    38.4598*     1.0000
 ------------------------------------------------------------------------
 Adjusted C-14 age in years:  30170.*     * = based on Original Data
```

Initial Well : TM Recharge
Final Well : UE-18t 1988

	Final	Initial
C	5.4279	1.4314
S	0.1125	0.1426
CA	0.5542	0.2256
MG	0.0412	0.0822
NA	6.1368	1.1766
K	0.2088	0.1203
CL	1.8175	0.1938
SI	0.1166	0.8237
FE	0.0001	0.0006
AL	0.0002	0.0003

```
CALCITE  CA   1.0000 C    1.0000 RS   4.0000 I1   0.0000 I2   0.0000
DOLOMITE CA   1.0000 MG   1.0000 C    2.0000 RS   8.0000 I1   0.0000
         I2   0.0000
GYPSUM   CA   1.0000 S    1.0000 RS   6.0000 I3  22.0000
PYRITE   FE   1.0000 S    2.0000 RS   0.0000 I3 -60.0000
NaCl     NA   1.0000 CL   1.0000
SiO2     SI   1.0000
EXCHANGE CA  -0.9309 NA   2.0000 MG  -0.0691
TM-Glass K    0.3680 NA   0.3830 CA   0.0240 MG   0.0050 FE   0.0260
         AL   0.7890 SI   4.1730
TM-Clay  K    0.0170 NA   0.1610 CA   0.1410 MG   0.1380 FE   0.0500
         AL   2.4380 SI   3.4620
GOETHITE FE   1.0000 RS   3.0000
CO2 GAS  C    1.0000 RS   4.0000 I1 -12.0000 I2 100.0000
```

```
           MODEL   1
 CALCITE              3.83406
 DOLOMITE             0.08122
 GYPSUM    +         -2.06612      (Constraint ignored)
 PYRITE    +          1.01800
 NaCl      +          1.62373
 SiO2                -1.45252
 EXCHANGE             1.62779
 TM-Glass  +          0.24422
 TM-Clay   -         -0.07909
 GOETHITE  -         -1.02093
               Computed    Observed
Carbon-13       -3.7154   Undefined
C-14 (% mod)    25.6985   Undefined
```

```
           MODEL   2
 CALCITE              1.79805
 DOLOMITE             0.08122
 GYPSUM    +         -0.03012      (Constraint ignored)
 NaCl      +          1.62373
 SiO2                -1.45252
 EXCHANGE             1.62779
 TM-Glass  +          0.24422
 TM-Clay   -         -0.07909
 GOETHITE  -         -0.00293
 CO2 GAS              2.03600
               Computed    Observed
Carbon-13       -8.2166   Undefined
C-14 (% mod)    63.2086   Undefined
```

Initial Well 1 : TM Recharge
Initial Well 2 : ER-20-4_m1
Final well : UE-18r

	Final	Initial 1	Initial 2
C	3.7792	1.4314	1.7079
S	0.2391	0.1426	0.1760
CA	0.4684	0.2256	0.1051
MG	0.0263	0.0822	0.0019
NA	3.3177	1.1766	2.2610
K	0.1202	0.1203	0.0304
CL	0.2337	0.1938	0.1330
SI	0.7829	0.8237	0.8232
FE	0.0008	0.0006	0.0000
AL	0.0003	0.0003	0.0002
D	-110.8890	-103.7000	-115.0000

CALCITE	CA	1.0000	C	1.0000	RS	4.0000	I1	0.0000	I2	0.0000
DOLOMITE	CA	1.0000	MG	1.0000	C	2.0000	RS	8.0000	I1	0.0000
	I2	0.0000								
GYPSUM	CA	1.0000	S	1.0000	RS	6.0000	I3	22.0000		
PYRITE	FE	1.0000	S	2.0000	RS	0.0000	I3	-60.0000		
NaCl	NA	1.0000	CL	1.0000						
SiO2	SI	1.0000								
EXCHANGE	CA	-0.9468	NA	2.0000	MG	-0.0532				
TM-Glass	K	0.3680	NA	0.3830	CA	0.0240	MG	0.0050	FE	0.0260
	AL	0.7890	SI	4.1730						
TM-Clay	K	0.0170	NA	0.1610	CA	0.1410	MG	0.1380	FE	0.0500
	AL	2.4380	SI	3.4620						
GOETHITE	FE	1.0000	RS	3.0000						
CO2 GAS	C	1.0000	RS	4.0000	I1	-12.0000	I2	100.0000		

MODEL 1

Init 1	+	F 0.36381
Init 2	+	F 0.63619
CALCITE		0.83604
DOLOMITE		0.03665
GYPSUM	+	0.07526
NaCl	+	0.07858
SiO2		-0.52181
EXCHANGE		0.66026
TM-Glass	+	0.15765
TM-Clay	-	-0.05099
GOETHITE	-	-0.00094
CO2 GAS		1.26258

	Computed	Observed
Carbon-13	-6.9236	-4.5375
C-14 (% mod)	52.1843*	8.2000

Adjusted C-14 age in years: 15299.* * = based on Original Data

MODEL 2

Init 1	+	F 0.36381
Init 2	+	F 0.63619
CALCITE		0.91129
DOLOMITE		0.03665
PYRITE	+	0.03763
NaCl	+	0.07858
SiO2		-0.52181
EXCHANGE		0.66026
TM-Glass	+	0.15765
TM-Clay	-	-0.05099
GOETHITE	-	-0.03857
CO2 GAS		1.18732

	Computed	Observed
Carbon-13	-6.6846	-4.5375
C-14 (% mod)	50.1929*	8.2000

Adjusted C-14 age in years: 14977.* * = based on Original Data

Initial Well 1 : TM Recharge
Initial Well 2 : ER-20-4_m1
Final well : UE-18r

	Final	Initial 1	Initial 2
C	3.7792	1.4314	1.7079
S	0.2391	0.1426	0.1760
CA	0.4684	0.2256	0.1051
MG	0.0263	0.0822	0.0019
NA	3.3177	1.1766	2.2610
K	0.1202	0.1203	0.0304
CL	0.2337	0.1938	0.1330
SI	0.7829	0.8237	0.8232
FE	0.0008	0.0006	0.0000
AL	0.0003	0.0003	0.0002
18	-14.8722	-13.9000	-15.1000

CALCITE	CA	1.0000	C	1.0000	RS	4.0000	I1	0.0000	I2	0.0000
DOLOMITE	CA	1.0000	MG	1.0000	C	2.0000	RS	8.0000	I1	0.0000
	I2	0.0000								
GYPSUM	CA	1.0000	S	1.0000	RS	6.0000	I3	22.0000		
PYRITE	FE	1.0000	S	2.0000	RS	0.0000	I3	-60.0000		
NaCl	NA	1.0000	CL	1.0000						
SiO2	SI	1.0000								
EXCHANGE	CA	-0.9468	NA	2.0000	MG	-0.0532				
TM-Glass	K	0.3680	NA	0.3830	CA	0.0240	MG	0.0050	FE	0.0260
	AL	0.7890	SI	4.1730						
TM-Clay	K	0.0170	NA	0.1610	CA	0.1410	MG	0.1380	FE	0.0500
	AL	2.4380	SI	3.4620						
GOETHITE	FE	1.0000	RS	3.0000						
CO2 GAS	C	1.0000	RS	4.0000	I1	-12.0000	I2	100.0000		

MODEL 1

Init 1	+ F	0.18983
Init 2	+ F	0.81017
CALCITE		0.75267
DOLOMITE		0.04664
GYPSUM	+	0.06945
NaCl	+	0.08916
SiO2		-0.65348
EXCHANGE		0.55350
TM-Glass	+	0.20080
TM-Clay	-	-0.06495
GOETHITE	-	-0.00126
CO2 GAS		1.27786

	Computed	Observed
Carbon-13	-6.3099	-4.5375
C-14 (% mod)	47.6296*	8.2000

Adjusted C-14 age in years: 14544.* * = based on Original Data

MODEL 2

Init 1	+ F	0.18983
Init 2	+ F	0.81017
CALCITE		0.82212
DOLOMITE		0.04664
PYRITE	+	0.03473
NaCl	+	0.08916
SiO2		-0.65348
EXCHANGE		0.55350
TM-Glass	+	0.20080
TM-Clay	-	-0.06495
GOETHITE	-	-0.03599
CO2 GAS		1.20840

	Computed	Observed
Carbon-13	-6.0894	-4.5375
C-14 (% mod)	45.7919*	8.2000

Adjusted C-14 age in years: 14218.* * = based on Original Data

Initial Well 1 : TM Recharge
Initial Well 2 : ER-EC-12_m2
Final well : UE-18r

	Final	Initial 1	Initial 2
C	3.7792	1.4314	2.3671
S	0.2391	0.1426	0.3729
CA	0.4684	0.2256	0.0823
MG	0.0263	0.0822	0.0009
NA	3.3177	1.1766	3.4501
K	0.1202	0.1203	0.0126
CL	0.2337	0.1938	0.4510
SI	0.7829	0.8237	0.5332
FE	0.0008	0.0006	0.0037
AL	0.0003	0.0003	0.0007
D	-110.8890	-103.7000	-112.8500

CALCITE	CA	1.0000	C	1.0000	RS	4.0000	I1	0.0000	I2 0.0000
DOLOMITE	CA	1.0000	MG	1.0000	C	2.0000	RS	8.0000	I1 0.0000
	I2	0.0000							
GYPSUM	CA	1.0000	S	1.0000	RS	6.0000	I3	22.0000	
PYRITE	FE	1.0000	S	2.0000	RS	0.0000	I3	-60.0000	
NaCl	NA	1.0000	CL	1.0000					
SiO2	SI	1.0000							
EXCHANGE	CA	-0.9468	NA	2.0000	MG	-0.0532			
TM-Glass	K	0.3680	NA	0.3830	CA	0.0240	MG	0.0050	FE 0.0260
	AL	0.7890	SI	4.1730					
TM-Clay	K	0.0170	NA	0.1610	CA	0.1410	MG	0.1380	FE 0.0500
	AL	2.4380	SI	3.4620					
GOETHITE	FE	1.0000	RS	3.0000					
CO2 GAS	C	1.0000	RS	4.0000	I1	-12.0000	I2	100.0000	

MODEL 1

Init 1	+ F	0.21432
Init 2	+ F	0.78568
CALCITE		1.55460
DOLOMITE		0.02899
GYPSUM	+	-1.01494 (Constraint ignored)
PYRITE	+	0.46525
NaCl	+	-0.16217 (Constraint ignored)
SiO2		-0.52385
EXCHANGE		0.21997
TM-Glass	+	0.23316
TM-Clay	-	-0.07560
GOETHITE	-	-0.46974

	Computed	Observed
Carbon-13	-3.7685	-4.5375
C-14 (% mod)	15.7376*	8.2000

Adjusted C-14 age in years: 5389.* * = based on Original Data

MODEL 2

Init 1	+ F	0.21432
Init 2	+ F	0.78568
CALCITE		0.62410
DOLOMITE		0.02899
GYPSUM	+	-0.08444 (Constraint ignored)
NaCl	+	-0.16217 (Constraint ignored)
SiO2		-0.52385
EXCHANGE		0.21997
TM-Glass	+	0.23316
TM-Clay	-	-0.07560
GOETHITE	-	-0.00449
CO2 GAS		0.93050

	Computed	Observed
Carbon-13	-6.7231	-4.5375
C-14 (% mod)	40.3594*	8.2000

Adjusted C-14 age in years: 13174.* * = based on Original Data

Initial Well 1 : TM Recharge
Initial Well 2 : ER-EC-12_m2
Final well : UE-18r

	Final	Initial 1	Initial 2
C	3.7792	1.4314	2.3671
S	0.2391	0.1426	0.3729
CA	0.4684	0.2256	0.0823
MG	0.0263	0.0822	0.0009
NA	3.3177	1.1766	3.4501
K	0.1202	0.1203	0.0126
CL	0.2337	0.1938	0.4510
SI	0.7829	0.8237	0.5332
FE	0.0008	0.0006	0.0037
AL	0.0003	0.0003	0.0007
18	-14.8722	-13.9000	-15.0700

CALCITE	CA	1.0000	C	1.0000	RS	4.0000	I1	0.0000	I2	0.0000
DOLOMITE	CA	1.0000	MG	1.0000	C	2.0000	RS	8.0000	I1	0.0000
	I2	0.0000								
GYPSUM	CA	1.0000	S	1.0000	RS	6.0000	I3	22.0000		
PYRITE	FE	1.0000	S	2.0000	RS	0.0000	I3	-60.0000		
NaCl	NA	1.0000	CL	1.0000						
SiO2	SI	1.0000								
EXCHANGE	CA	-0.9468	NA	2.0000	MG	-0.0532				
TM-Glass	K	0.3680	NA	0.3830	CA	0.0240	MG	0.0050	FE	0.0260
	AL	0.7890	SI	4.1730						
TM-Clay	K	0.0170	NA	0.1610	CA	0.1410	MG	0.1380	FE	0.0500
	AL	2.4380	SI	3.4620						
GOETHITE	FE	1.0000	RS	3.0000						
CO2 GAS	C	1.0000	RS	4.0000	I1	-12.0000	I2	100.0000		

MODEL 1

Init 1	+ F	0.16906
Init 2	+ F	0.83094
CALCITE		1.50892
DOLOMITE		0.03066
GYPSUM	+	-1.00945 (Constraint ignored)
PYRITE	+	0.45730
NaCl	+	-0.17381 (Constraint ignored)
SiO2		-0.55170
EXCHANGE		0.17212
TM-Glass	+	0.24660
TM-Clay	-	-0.07996
GOETHITE	-	-0.46206

	Computed	Observed
Carbon-13	-3.6781	-4.5375
C-14 (% mod)	14.5180*	8.2000

Adjusted C-14 age in years: 4722.* * = based on Original Data

MODEL 2

Init 1	+ F	0.16906
Init 2	+ F	0.83094
CALCITE		0.59433
DOLOMITE		0.03066
GYPSUM	+	-0.09486 (Constraint ignored)
NaCl	+	-0.17381 (Constraint ignored)
SiO2		-0.55170
EXCHANGE		0.17212
TM-Glass	+	0.24660
TM-Clay	-	-0.07996
GOETHITE	-	-0.00476
CO2 GAS		0.91459

	Computed	Observed
Carbon-13	-6.5822	-4.5375
C-14 (% mod)	38.7188*	8.2000

Adjusted C-14 age in years: 12831.* * = based on Original Data

Initial Well 1 : TM Recharge
Initial Well 2 : ER-EC-14_m2
Final well : UE-18r

	Final	Initial 1	Initial 2
C	3.7792	1.4314	2.6847
S	0.2391	0.1426	0.4535
CA	0.4684	0.2256	0.3250
MG	0.0263	0.0822	0.0156
NA	3.3177	1.1766	3.2809
K	0.1202	0.1203	0.0527
CL	0.2337	0.1938	0.5631
SI	0.7829	0.8237	0.7123
FE	0.0008	0.0006	0.0001
AL	0.0003	0.0003	0.0002
D	-110.8890	-103.7000	-115.1000

CALCITE	CA	1.0000	C	1.0000	RS	4.0000	I1	0.0000	I2	0.0000
DOLOMITE	CA	1.0000	MG	1.0000	C	2.0000	RS	8.0000	I1	0.0000
	I2	0.0000								
GYPSUM	CA	1.0000	S	1.0000	RS	6.0000	I3	22.0000		
PYRITE	FE	1.0000	S	2.0000	RS	0.0000	I3	-60.0000		
NaCl	NA	1.0000	CL	1.0000						
SiO2	SI	1.0000								
EXCHANGE	CA	-0.9468	NA	2.0000	MG	-0.0532				
TM-Glass	K	0.3680	NA	0.3830	CA	0.0240	MG	0.0050	FE	0.0260
	AL	0.7890	SI	4.1730						
TM-Clay	K	0.0170	NA	0.1610	CA	0.1410	MG	0.1380	FE	0.0500
	AL	2.4380	SI	3.4620						
GOETHITE	FE	1.0000	RS	3.0000						
CO2 GAS	C	1.0000	RS	4.0000	I1	-12.0000	I2	100.0000		

MODEL 1

Init 1	+ F	0.36939
Init 2	+ F	0.63061
CALCITE		1.52434
DOLOMITE		0.01655
GYPSUM	+	-0.89991 (Constraint ignored)
PYRITE	+	0.40018
NaCl	+	-0.19297 (Constraint ignored)
SiO2		-0.32901
EXCHANGE		0.48412
TM-Glass	+	0.11740
TM-Clay	-	-0.03797
GOETHITE	-	-0.40079

	Computed	Observed
Carbon-13	-3.1147	-4.5375
C-14 (% mod)	16.8728*	8.2000

Adjusted C-14 age in years: 5965.* * = based on Original Data

MODEL 2

Init 1	+ F	0.36939
Init 2	+ F	0.63061
CALCITE		0.72397
DOLOMITE		0.01655
GYPSUM	+	-0.09954 (Constraint ignored)
NaCl	+	-0.19297 (Constraint ignored)
SiO2		-0.32901
EXCHANGE		0.48412
TM-Glass	+	0.11740
TM-Clay	-	-0.03797
GOETHITE	-	-0.00061
CO2 GAS		0.80037

	Computed	Observed
Carbon-13	-5.6561	-4.5375
C-14 (% mod)	38.0511*	8.2000

Adjusted C-14 age in years: 12688.* * = based on Original Data

Initial Well 1 : TM Recharge
Initial Well 2 : ER-20-4_m1
Final well : ER-EC-5_m1-3

```
          Final    Initial 1   Initial 2
 C       2.7469      1.4314      1.7079
 S       0.3724      0.1426      0.1760
 CA      0.5040      0.2256      0.1051
 MG      0.0208      0.0822      0.0019
 NA      3.2276      1.1766      2.2610
 K       0.0401      0.1203      0.0304
 CL      0.4481      0.1938      0.1330
 SI      0.6804      0.8237      0.8232
 FE      0.0001      0.0006      0.0000
 AL      0.0003      0.0003      0.0002
 D    -112.5000   -103.7000   -115.0000

 CALCITE  CA   1.0000 C    1.0000 RS   4.0000 I1   0.0000 I2   0.0000
 DOLOMITE CA   1.0000 MG   1.0000 C    2.0000 RS   8.0000 I1   0.0000
          I2   0.0000
 GYPSUM   CA   1.0000 S    1.0000 RS   6.0000 I3  22.0000
 PYRITE   FE   1.0000 S    2.0000 RS   0.0000 I3 -60.0000
 NaCl     NA   1.0000 CL   1.0000
 SiO2     SI   1.0000
 EXCHANGE CA  -0.9603 NA   2.0000 MG  -0.0397
 TM-Glass K    0.3680 NA   0.3830 CA   0.0240 MG   0.0050 FE   0.0260
          AL   0.7890 SI   4.1730
 TM-Clay  K    0.0170 NA   0.1610 CA   0.1410 MG   0.1380 FE   0.0500
          AL   2.4380 SI   3.4620
 GOETHITE FE   1.0000 RS   3.0000
 CO2 GAS  C    1.0000 RS   4.0000 I1 -12.0000 I2 100.0000

            MODEL   1
  Init 1    + F        0.22124
  Init 2    + F        0.77876
  CALCITE              0.58888
  DOLOMITE             0.01821
  GYPSUM    +          0.20344
  PYRITE    +          0.00020
  NaCl      +          0.30162
  SiO2                -0.05764
  EXCHANGE             0.45708
  TM-Glass  +         -0.02796      (Constraint ignored)
  TM-Clay   -          0.00908      (Constraint ignored)
  CO2 GAS              0.47496
                Computed    Observed
 Carbon-13       -5.3380     -2.7750
 C-14 (% mod)    37.5306*     6.9000
-------------------------------------------------------------------------
 Adjusted C-14 age in years:  14001.*     * = based on Original Data

            MODEL   2
  Init 1    + F        0.22124
  Init 2    + F        0.77876
  CALCITE              0.79232
  DOLOMITE             0.01821
  PYRITE    +          0.10192
  NaCl      +          0.30162
  SiO2                -0.05764
  EXCHANGE             0.45708
  TM-Glass  +         -0.02796      (Constraint ignored)
  TM-Clay   -          0.00908      (Constraint ignored)
  GOETHITE  -         -0.10172
  CO2 GAS              0.27152
                Computed    Observed
 Carbon-13       -4.4493     -2.7750
 C-14 (% mod)    30.1245*     6.9000
-------------------------------------------------------------------------
 Adjusted C-14 age in years:  12184.*     * = based on Original Data
```

Initial Well 1 : TM Recharge
Initial Well 2 : ER-20-4_m1
Final well : ER-EC-5_m1-3

	Final	Initial 1	Initial 2
C	2.7469	1.4314	1.7079
S	0.3724	0.1426	0.1760
CA	0.5040	0.2256	0.1051
MG	0.0208	0.0822	0.0019
NA	3.2276	1.1766	2.2610
K	0.0401	0.1203	0.0304
CL	0.4481	0.1938	0.1330
SI	0.6804	0.8237	0.8232
FE	0.0001	0.0006	0.0000
AL	0.0003	0.0003	0.0002
18	-15.0000	-13.9000	-15.1000

CALCITE	CA	1.0000	C	1.0000	RS	4.0000	I1	0.0000	I2	0.0000
DOLOMITE	CA	1.0000	MG	1.0000	C	2.0000	RS	8.0000	I1	0.0000
	I2	0.0000								
GYPSUM	CA	1.0000	S	1.0000	RS	6.0000	I3	22.0000		
PYRITE	FE	1.0000	S	2.0000	RS	0.0000	I3	-60.0000		
NaCl	NA	1.0000	CL	1.0000						
SiO2	SI	1.0000								
EXCHANGE	CA	-0.9603	NA	2.0000	MG	-0.0397				
TM-Glass	K	0.3680	NA	0.3830	CA	0.0240	MG	0.0050	FE	0.0260
	AL	0.7890	SI	4.1730						
TM-Clay	K	0.0170	NA	0.1610	CA	0.1410	MG	0.1380	FE	0.0500
	AL	2.4380	SI	3.4620						
GOETHITE	FE	1.0000	RS	3.0000						
CO2 GAS	C	1.0000	RS	4.0000	I1	-12.0000	I2	100.0000		

MODEL 1

Init 1	+ F	0.08333
Init 2	+ F	0.91667
CALCITE		0.52011
DOLOMITE		0.02727
GYPSUM	+	0.19923
NaCl	+	0.31001
SiO2		-0.16201
EXCHANGE		0.37245
TM-Glass	+	0.00625
TM-Clay	-	-0.00198
GOETHITE	-	-0.00006
CO2 GAS		0.48746

	Computed	Observed
Carbon-13	-4.6704	-2.7750
C-14 (% mod)	32.5777*	6.9000

Adjusted C-14 age in years: 12831.* * = based on Original Data

MODEL 2

Init 1	+ F	0.08333
Init 2	+ F	0.91667
CALCITE		0.71934
DOLOMITE		0.02727
PYRITE	+	0.09961
NaCl	+	0.31001
SiO2		-0.16201
EXCHANGE		0.37245
TM-Glass	+	0.00625
TM-Clay	-	-0.00198
GOETHITE	-	-0.09967
CO2 GAS		0.28823

	Computed	Observed
Carbon-13	-3.8001	-2.7750
C-14 (% mod)	25.3249*	6.9000

Adjusted C-14 age in years: 10749.* * = based on Original Data

Initial Well 1 : TM Recharge
Initial Well 2 : ER-EC-12_m2
Final well : ER-EC-5_m1-3

	Final	Initial 1	Initial 2
C	2.7469	1.4314	2.3671
S	0.3724	0.1426	0.3729
CA	0.5040	0.2256	0.0823
MG	0.0208	0.0822	0.0009
NA	3.2276	1.1766	3.4501
K	0.0401	0.1203	0.0126
CL	0.4481	0.1938	0.4510
SI	0.6804	0.8237	0.5332
FE	0.0001	0.0006	0.0037
AL	0.0003	0.0003	0.0007
D	-112.5000	-103.7000	-112.8500

CALCITE	CA	1.0000	C	1.0000	RS	4.0000	I1	0.0000	I2 0.0000
DOLOMITE	CA	1.0000	MG	1.0000	C	2.0000	RS	8.0000	I1 0.0000
	I2	0.0000							
GYPSUM	CA	1.0000	S	1.0000	RS	6.0000	I3	22.0000	
PYRITE	FE	1.0000	S	2.0000	RS	0.0000	I3	-60.0000	
NaCl	NA	1.0000	CL	1.0000					
SiO2	SI	1.0000							
EXCHANGE	CA	-0.9603	NA	2.0000	MG	-0.0397			
TM-Glass	K	0.3680	NA	0.3830	CA	0.0240	MG	0.0050	FE 0.0260
	AL	0.7890	SI	4.1730					
TM-Clay	K	0.0170	NA	0.1610	CA	0.1410	MG	0.1380	FE 0.0500
	AL	2.4380	SI	3.4620					
GOETHITE	FE	1.0000	RS	3.0000					
CO2 GAS	C	1.0000	RS	4.0000	I1	-12.0000	I2	100.0000	

MODEL 1

Init 1	+ F	0.03825
Init 2	+ F	0.96175
CALCITE		0.31445
DOLOMITE		0.01614
GYPSUM	+	0.00835
NaCl	+	0.00693
SiO2		-0.06013
EXCHANGE		-0.08188
TM-Glass	+	0.06448
TM-Clay	-	-0.02104
GOETHITE	-	-0.00415
CO2 GAS		0.06886

	Computed	Observed
Carbon-13	-5.0020	-2.7750
C-14 (% mod)	17.6307*	6.9000

Adjusted C-14 age in years: 7755.* * = based on Original Data

MODEL 2

Init 1	+ F	0.03825
Init 2	+ F	0.96175
CALCITE		0.32280
DOLOMITE		0.01614
PYRITE	+	0.00417
NaCl	+	0.00693
SiO2		-0.06013
EXCHANGE		-0.08188
TM-Glass	+	0.06448
TM-Clay	-	-0.02104
GOETHITE	-	-0.00832
CO2 GAS		0.06051

	Computed	Observed
Carbon-13	-4.9655	-2.7750
C-14 (% mod)	17.3268*	6.9000

Adjusted C-14 age in years: 7611.* * = based on Original Data

Initial Well 1 : TM Recharge
Initial Well 2 : ER-EC-12_m2
Final well : ER-EC-5_m1-3

```
          Final    Initial 1   Initial 2
 C       2.7469      1.4314      2.3671
 S       0.3724      0.1426      0.3729
 CA      0.5040      0.2256      0.0823
 MG      0.0208      0.0822      0.0009
 NA      3.2276      1.1766      3.4501
 K       0.0401      0.1203      0.0126
 CL      0.4481      0.1938      0.4510
 SI      0.6804      0.8237      0.5332
 FE      0.0001      0.0006      0.0037
 AL      0.0003      0.0003      0.0007
 18    -15.0000    -13.9000    -15.0700

 CALCITE  CA   1.0000 C    1.0000 RS   4.0000 I1   0.0000 I2   0.0000
 DOLOMITE CA   1.0000 MG   1.0000 C    2.0000 RS   8.0000 I1   0.0000
          I2   0.0000
 GYPSUM   CA   1.0000 S    1.0000 RS   6.0000 I3  22.0000
 PYRITE   FE   1.0000 S    2.0000 RS   0.0000 I3 -60.0000
 NaCl     NA   1.0000 CL   1.0000
 SiO2     SI   1.0000
 EXCHANGE CA  -0.9603 NA   2.0000 MG  -0.0397
 TM-Glass K    0.3680 NA   0.3830 CA   0.0240 MG   0.0050 FE   0.0260
          AL   0.7890 SI   4.1730
 TM-Clay  K    0.0170 NA   0.1610 CA   0.1410 MG   0.1380 FE   0.0500
          AL   2.4380 SI   3.4620
 GOETHITE FE   1.0000 RS   3.0000
 CO2 GAS  C    1.0000 RS   4.0000 I1 -12.0000 I2 100.0000

            MODEL   1
  Init 1    + F        0.05983
  Init 2    + F        0.94017
  CALCITE              0.32926
  DOLOMITE             0.01504
  GYPSUM    +          0.01332
  NaCl      +          0.01248
  SiO2                -0.04686
  EXCHANGE            -0.05906
  TM-Glass  +          0.05808
  TM-Clay   -         -0.01896
  GOETHITE  -         -0.00402
  CO2 GAS              0.07644
                Computed    Observed
 Carbon-13       -5.0944     -2.7750
 C-14 (% mod)    18.7068*     6.9000
-------------------------------------------------------------------------
 Adjusted C-14 age in years:   8245.*     * = based on Original Data

            MODEL   2
  Init 1    + F        0.05983
  Init 2    + F        0.94017
  CALCITE              0.34258
  DOLOMITE             0.01504
  PYRITE    +          0.00666
  NaCl      +          0.01248
  SiO2                -0.04686
  EXCHANGE            -0.05906
  TM-Glass  +          0.05808
  TM-Clay   -         -0.01896
  GOETHITE  -         -0.01068
  CO2 GAS              0.06313
                Computed    Observed
 Carbon-13       -5.0362     -2.7750
 C-14 (% mod)    18.2220*     6.9000
-------------------------------------------------------------------------
 Adjusted C-14 age in years:   8028.*     * = based on Original Data
```

Initial Well 1 : TM Recharge
Initial Well 2 : ER-EC-14_m2
Final well : ER-EC-5_m1-3

	Final	Initial 1	Initial 2
C	2.7469	1.4314	2.6847
S	0.3724	0.1426	0.4535
CA	0.5040	0.2256	0.3250
MG	0.0208	0.0822	0.0156
NA	3.2276	1.1766	3.2809
K	0.0401	0.1203	0.0527
CL	0.4481	0.1938	0.5631
SI	0.6804	0.8237	0.7123
FE	0.0001	0.0006	0.0001
AL	0.0003	0.0003	0.0002
D	-112.5000	-103.7000	-115.1000

CALCITE	CA	1.0000	C	1.0000	RS	4.0000	I1	0.0000	I2	0.0000
DOLOMITE	CA	1.0000	MG	1.0000	C	2.0000	RS	8.0000	I1	0.0000
	I2	0.0000								
GYPSUM	CA	1.0000	S	1.0000	RS	6.0000	I3	22.0000		
PYRITE	FE	1.0000	S	2.0000	RS	0.0000	I3	-60.0000		
NaCl	NA	1.0000	CL	1.0000						
SiO2	SI	1.0000								
EXCHANGE	CA	-0.9603	NA	2.0000	MG	-0.0397				
TM-Glass	K	0.3680	NA	0.3830	CA	0.0240	MG	0.0050	FE	0.0260
	AL	0.7890	SI	4.1730						
TM-Clay	K	0.0170	NA	0.1610	CA	0.1410	MG	0.1380	FE	0.0500
	AL	2.4380	SI	3.4620						
GOETHITE	FE	1.0000	RS	3.0000						
CO2 GAS	C	1.0000	RS	4.0000	I1	-12.0000	I2	100.0000		

	MODEL 1		
Init 1	+ F	0.22807	
Init 2	+ F	0.77193	
CALCITE		0.44668	
DOLOMITE		-0.00347	
GYPSUM	+	-0.01135	(Constraint ignored)
PYRITE	+	0.00061	
NaCl	+	-0.03078	(Constraint ignored)
SiO2		0.17836	
EXCHANGE		0.24147	
TM-Glass	+	-0.07722	(Constraint ignored)
TM-Clay	-	0.02502	(Constraint ignored)
CO2 GAS		-0.09165	

	Computed	Observed
Carbon-13	-3.2310	-2.7750
C-14 (% mod)	16.4028*	6.9000

Adjusted C-14 age in years: 7158.* * = based on Original Data

Initial Well 1 : TM Recharge
Initial Well 2 : ER-20-4_m1
Final well : ER-OV-3c_p1

```
          Final    Initial 1   Initial 2
 C       2.7926      1.4314      1.7079
 S       0.4626      0.1426      0.1760
 CA      0.3860      0.2256      0.1051
 MG      0.0151      0.0822      0.0019
 NA      3.4242      1.1766      2.2610
 K       0.0314      0.1203      0.0304
 CL      0.4698      0.1938      0.1330
 SI      0.6790      0.8237      0.8232
 FE      0.0000      0.0006      0.0000
 AL      0.0003      0.0003      0.0002
 D    -109.0000   -103.7000   -115.0000

 CALCITE  CA   1.0000 C    1.0000 RS   4.0000 I1   0.0000 I2   0.0000
 DOLOMITE CA   1.0000 MG   1.0000 C    2.0000 RS   8.0000 I1   0.0000
          I2   0.0000
 GYPSUM   CA   1.0000 S    1.0000 RS   6.0000 I3  22.0000
 PYRITE   FE   1.0000 S    2.0000 RS   0.0000 I3 -60.0000
 NaCl     NA   1.0000 CL   1.0000
 SiO2     SI   1.0000
 EXCHANGE CA  -0.9624 NA   2.0000 MG  -0.0376
 TM-Glass K    0.3680 NA   0.3830 CA   0.0240 MG   0.0050 FE   0.0260
          AL   0.7890 SI   4.1730
 TM-Clay  K    0.0170 NA   0.1610 CA   0.1410 MG   0.1380 FE   0.0500
          AL   2.4380 SI   3.4620
 GOETHITE FE   1.0000 RS   3.0000
 CO2 GAS  C    1.0000 RS   4.0000 I1 -12.0000 I2 100.0000

            MODEL   1
  Init 1    + F        0.53097
  Init 2    + F        0.46903
  CALCITE              0.62940
  DOLOMITE            -0.00684
  GYPSUM    +          0.30234
  PYRITE    +          0.00098
  NaCl      +          0.30453
  SiO2                 0.24895
  EXCHANGE             0.73855
  TM-Glass  +         -0.12890      (Constraint ignored)
  TM-Clay   -          0.04172      (Constraint ignored)
  CO2 GAS              0.61582
                Computed    Observed
 Carbon-13       -7.4176     -3.1500
 C-14 (% mod)    53.6389*     6.8000
 ------------------------------------------------------------------------
 Adjusted C-14 age in years:  17074.*     * = based on Original Data

            MODEL   2
  Init 1    + F        0.53097
  Init 2    + F        0.46903
  CALCITE              0.93174
  DOLOMITE            -0.00684
  PYRITE    +          0.15215
  NaCl      +          0.30453
  SiO2                 0.24895
  EXCHANGE             0.73855
  TM-Glass  +         -0.12890      (Constraint ignored)
  TM-Clay   -          0.04172      (Constraint ignored)
  GOETHITE  -         -0.15117
  CO2 GAS              0.31347
                Computed    Observed
 Carbon-13       -6.1222     -3.1500
 C-14 (% mod)    42.8439*     6.8000
------------------------------------------------------------------------
 Adjusted C-14 age in years:  15216.*     * = based on Original Data
```

Initial Well 1 : TM Recharge
Initial Well 2 : ER-20-4_m1
Final well : ER-OV-3c_p1

```
          Final    Initial 1   Initial 2
C       2.7926      1.4314      1.7079
S       0.4626      0.1426      0.1760
CA      0.3860      0.2256      0.1051
MG      0.0151      0.0822      0.0019
NA      3.4242      1.1766      2.2610
K       0.0314      0.1203      0.0304
CL      0.4698      0.1938      0.1330
SI      0.6790      0.8237      0.8232
FE      0.0000      0.0006      0.0000
AL      0.0003      0.0003      0.0002
18    -14.7000    -13.9000    -15.1000

CALCITE  CA   1.0000 C    1.0000 RS   4.0000 I1   0.0000 I2   0.0000
DOLOMITE CA   1.0000 MG   1.0000 C    2.0000 RS   8.0000 I1   0.0000
         I2   0.0000
GYPSUM   CA   1.0000 S    1.0000 RS   6.0000 I3  22.0000
PYRITE   FE   1.0000 S    2.0000 RS   0.0000 I3 -60.0000
NaCl     NA   1.0000 CL   1.0000
SiO2     SI   1.0000
EXCHANGE CA  -0.9624 NA   2.0000 MG  -0.0376
TM-Glass K    0.3680 NA   0.3830 CA   0.0240 MG   0.0050 FE   0.0260
         AL   0.7890 SI   4.1730
TM-Clay  K    0.0170 NA   0.1610 CA   0.1410 MG   0.1380 FE   0.0500
         AL   2.4380 SI   3.4620
GOETHITE FE   1.0000 RS   3.0000
CO2 GAS  C    1.0000 RS   4.0000 I1 -12.0000 I2 100.0000

           MODEL   1
 Init 1    + F        0.33333
 Init 2    + F        0.66667
 CALCITE              0.53017
 DOLOMITE             0.00642
 GYPSUM    +          0.29647
 PYRITE    +          0.00062
 NaCl      +          0.31655
 SiO2                 0.09937
 EXCHANGE             0.61727
 TM-Glass  +         -0.07987      (Constraint ignored)
 TM-Clay   -          0.02587      (Constraint ignored)
 CO2 GAS              0.63389
              Computed    Observed
Carbon-13      -6.5111     -3.1500
C-14 (% mod)    46.9321*     6.8000
 ------------------------------------------------------------------------ Adjusted C-14 age
in years:  15969.*     * = based on Original Data

           MODEL   2
 Init 1    + F        0.33333
 Init 2    + F        0.66667
 CALCITE              0.82664
 DOLOMITE             0.00642
 PYRITE    +          0.14885
 NaCl      +          0.31655
 SiO2                 0.09937
 EXCHANGE             0.61727
 TM-Glass  +         -0.07987      (Constraint ignored)
 TM-Clay   -          0.02587      (Constraint ignored)
 GOETHITE  -         -0.14823
 CO2 GAS              0.33742
              Computed    Observed
Carbon-13      -5.2372     -3.1500
C-14 (% mod)    36.3159*     6.8000
-------------------------------------------------------------------------
 Adjusted C-14 age in years:  13849.*     * = based on Original Data
```

Initial Well 1 : TM Recharge
Initial Well 2 : ER-EC-12_m2
Final well : ER-OV-3c_p1

```
          Final    Initial 1   Initial 2
C        2.7926      1.4314      2.3671
S        0.4626      0.1426      0.3729
CA       0.3860      0.2256      0.0823
MG       0.0151      0.0822      0.0009
NA       3.4242      1.1766      3.4501
K        0.0314      0.1203      0.0126
CL       0.4698      0.1938      0.4510
SI       0.6790      0.8237      0.5332
FE       0.0000      0.0006      0.0037
AL       0.0003      0.0003      0.0007
D     -109.0000   -103.7000   -112.8500

CALCITE  CA   1.0000 C    1.0000 RS   4.0000 I1   0.0000 I2   0.0000
DOLOMITE CA   1.0000 MG   1.0000 C    2.0000 RS   8.0000 I1   0.0000
         I2   0.0000
GYPSUM   CA   1.0000 S    1.0000 RS   6.0000 I3  22.0000
PYRITE   FE   1.0000 S    2.0000 RS   0.0000 I3 -60.0000
NaCl     NA   1.0000 CL   1.0000
SiO2     SI   1.0000
EXCHANGE CA  -0.9624 NA   2.0000 MG  -0.0376
TM-Glass K    0.3680 NA   0.3830 CA   0.0240 MG   0.0050 FE   0.0260
         AL   0.7890 SI   4.1730
TM-Clay  K    0.0170 NA   0.1610 CA   0.1410 MG   0.1380 FE   0.0500
         AL   2.4380 SI   3.4620
GOETHITE FE   1.0000 RS   3.0000
CO2 GAS  C    1.0000 RS   4.0000 I1 -12.0000 I2 100.0000

           MODEL   1
 Init 1    + F        0.42077
 Init 2    + F        0.57923
 CALCITE              0.46101
 DOLOMITE            -0.00738
 GYPSUM    +          0.18656
 NaCl      +          0.12704
 SiO2                 0.24745
 EXCHANGE             0.41395
 TM-Glass  +         -0.07322      (Constraint ignored)
 TM-Clay   -          0.02358      (Constraint ignored)
 GOETHITE  -         -0.00164
 CO2 GAS              0.37295
              Computed    Observed
Carbon-13      -7.2249     -3.1500
C-14 (% mod)    41.9613*     6.8000
------------------------------------------------------------------------
Adjusted C-14 age in years:  15044.*     * = based on Original Data

           MODEL   2
 Init 1    + F        0.42077
 Init 2    + F        0.57923
 CALCITE              0.64757
 DOLOMITE            -0.00738
 PYRITE    +          0.09328
 NaCl      +          0.12704
 SiO2                 0.24745
 EXCHANGE             0.41395
 TM-Glass  +         -0.07322      (Constraint ignored)
 TM-Clay   -          0.02358      (Constraint ignored)
 GOETHITE  -         -0.09492
 CO2 GAS              0.18639
              Computed    Observed
Carbon-13      -6.4256     -3.1500
C-14 (% mod)    35.3005*     6.8000
------------------------------------------------------------------------
Adjusted C-14 age in years:  13615.*     * = based on Original Data
```

Initial Well 1 : TM Recharge
Initial Well 2 : ER-EC-12_m2
Final well : ER-OV-3c_p1

```
          Final    Initial 1   Initial 2
C       2.7926      1.4314      2.3671
S       0.4626      0.1426      0.3729
CA      0.3860      0.2256      0.0823
MG      0.0151      0.0822      0.0009
NA      3.4242      1.1766      3.4501
K       0.0314      0.1203      0.0126
CL      0.4698      0.1938      0.4510
SI      0.6790      0.8237      0.5332
FE      0.0000      0.0006      0.0037
AL      0.0003      0.0003      0.0007
18    -14.7000    -13.9000    -15.0700

CALCITE  CA   1.0000 C    1.0000 RS   4.0000 I1   0.0000 I2   0.0000
DOLOMITE CA   1.0000 MG   1.0000 C    2.0000 RS   8.0000 I1   0.0000
         I2   0.0000
GYPSUM   CA   1.0000 S    1.0000 RS   6.0000 I3  22.0000
PYRITE   FE   1.0000 S    2.0000 RS   0.0000 I3 -60.0000
NaCl     NA   1.0000 CL   1.0000
SiO2     SI   1.0000
EXCHANGE CA  -0.9624 NA   2.0000 MG  -0.0376
TM-Glass K    0.3680 NA   0.3830 CA   0.0240 MG   0.0050 FE   0.0260
         AL   0.7890 SI   4.1730
TM-Clay  K    0.0170 NA   0.1610 CA   0.1410 MG   0.1380 FE   0.0500
         AL   2.4380 SI   3.4620
GOETHITE FE   1.0000 RS   3.0000
CO2 GAS  C    1.0000 RS   4.0000 I1 -12.0000 I2 100.0000

           MODEL   1
 Init 1    + F        0.31624
 Init 2    + F        0.68376
 CALCITE              0.38879
 DOLOMITE            -0.00181
 GYPSUM    +          0.16249
 NaCl      +          0.10016
 SiO2                 0.18312
 EXCHANGE             0.30344
 TM-Glass  +         -0.04218      (Constraint ignored)
 TM-Clay   -          0.01351      (Constraint ignored)
 GOETHITE  -         -0.00226
 CO2 GAS              0.33620
              Computed    Observed
Carbon-13      -6.8119     -3.1500
C-14 (% mod)   37.0072*     6.8000
------------------------------------------------------------------------
Adjusted C-14 age in years:  14005.*     * = based on Original Data

           MODEL   2
 Init 1    + F        0.31624
 Init 2    + F        0.68376
 CALCITE              0.55128
 DOLOMITE            -0.00181
 PYRITE    +          0.08125
 NaCl      +          0.10016
 SiO2                 0.18312
 EXCHANGE             0.30344
 TM-Glass  +         -0.04218      (Constraint ignored)
 TM-Clay   -          0.01351      (Constraint ignored)
 GOETHITE  -         -0.08351
 CO2 GAS              0.17371
              Computed    Observed
Carbon-13      -6.1141     -3.1500
C-14 (% mod)   31.1928*     6.8000
------------------------------------------------------------------------
Adjusted C-14 age in years:  12592.*     * = based on Original Data
```

Initial Well 1 : TM Recharge
Initial Well 2 : ER-EC-14_m2
Final well : ER-OV-3c_p1

```
          Final    Initial 1   Initial 2
 C       2.7926      1.4314      2.6847
 S       0.4626      0.1426      0.4535
 CA      0.3860      0.2256      0.3250
 MG      0.0151      0.0822      0.0156
 NA      3.4242      1.1766      3.2809
 K       0.0314      0.1203      0.0527
 CL      0.4698      0.1938      0.5631
 SI      0.6790      0.8237      0.7123
 FE      0.0000      0.0006      0.0001
 AL      0.0003      0.0003      0.0002
 D    -109.0000   -103.7000   -115.1000

 CALCITE  CA   1.0000 C    1.0000 RS   4.0000 I1   0.0000 I2   0.0000
 DOLOMITE CA   1.0000 MG   1.0000 C    2.0000 RS   8.0000 I1   0.0000
          I2   0.0000
 GYPSUM   CA   1.0000 S    1.0000 RS   6.0000 I3  22.0000
 PYRITE   FE   1.0000 S    2.0000 RS   0.0000 I3 -60.0000
 NaCl     NA   1.0000 CL   1.0000
 SiO2     SI   1.0000
 EXCHANGE CA  -0.9624 NA   2.0000 MG  -0.0376
 TM-Glass K    0.3680 NA   0.3830 CA   0.0240 MG   0.0050 FE   0.0260
          AL   0.7890 SI   4.1730
 TM-Clay  K    0.0170 NA   0.1610 CA   0.1410 MG   0.1380 FE   0.0500
          AL   2.4380 SI   3.4620
 GOETHITE FE   1.0000 RS   3.0000
 CO2 GAS  C    1.0000 RS   4.0000 I1 -12.0000 I2 100.0000

            MODEL   1
  Init 1    + F        0.53509
  Init 2    + F        0.46491
  CALCITE              0.54320
  DOLOMITE            -0.01961
  GYPSUM    +          0.17298
  PYRITE    +          0.00122
  NaCl      +          0.10433
  SiO2                 0.39109
  EXCHANGE             0.60869
  TM-Glass  +         -0.15857      (Constraint ignored)
  TM-Clay   -          0.05132      (Constraint ignored)
  CO2 GAS              0.27456
                Computed    Observed
 Carbon-13       -6.1074     -3.1500
 C-14 (% mod)    39.2239*     6.8000
 ------------------------------------------------------------------------
 Adjusted C-14 age in years:  14486.*     * = based on Original Data
            MODEL   2
  Init 1    + F        0.53509
  Init 2    + F        0.46491
  CALCITE              0.71618
  DOLOMITE            -0.01961
  PYRITE    +          0.08771
  NaCl      +          0.10433
  SiO2                 0.39109
  EXCHANGE             0.60869
  TM-Glass  +         -0.15857      (Constraint ignored)
  TM-Clay   -          0.05132      (Constraint ignored)
  GOETHITE  -         -0.08649
  CO2 GAS              0.10158
                Computed    Observed
 Carbon-13       -5.3698     -3.1500
 C-14 (% mod)    33.0777*     6.8000
 ------------------------------------------------------------------------
 Adjusted C-14 age in years:  13077.*     * = based on Original Data
```

Initial Well 1 : TM Recharge
Initial Well 2 : ER-EC-5_m1-3
Final well : ER-OV-3c_p1

```
          Final    Initial 1   Initial 2
C        2.7926      1.4314      2.7469
S        0.4626      0.1426      0.3724
CA       0.3860      0.2256      0.5040
MG       0.0151      0.0822      0.0208
NA       3.4242      1.1766      3.2276
K        0.0314      0.1203      0.0401
CL       0.4698      0.1938      0.4481
SI       0.6790      0.8237      0.6804
FE       0.0000      0.0006      0.0001
AL       0.0003      0.0003      0.0003
D     -109.0000   -103.7000   -112.5000

CALCITE  CA   1.0000 C    1.0000 RS   4.0000 I1   0.0000 I2   0.0000
DOLOMITE CA   1.0000 MG   1.0000 C    2.0000 RS   8.0000 I1   0.0000
         I2   0.0000
GYPSUM   CA   1.0000 S    1.0000 RS   6.0000 I3  22.0000
PYRITE   FE   1.0000 S    2.0000 RS   0.0000 I3 -60.0000
NaCl     NA   1.0000 CL   1.0000
SiO2     SI   1.0000
EXCHANGE CA  -0.9624 NA   2.0000 MG  -0.0376
TM-Glass K    0.3680 NA   0.3830 CA   0.0240 MG   0.0050 FE   0.0260
         AL   0.7890 SI   4.1730
TM-Clay  K    0.0170 NA   0.1610 CA   0.1410 MG   0.1380 FE   0.0500
         AL   2.4380 SI   3.4620
GOETHITE FE   1.0000 RS   3.0000
CO2 GAS  C    1.0000 RS   4.0000 I1 -12.0000 I2 100.0000

           MODEL   1
 Init 1    + F        0.39773
 Init 2    + F        0.60227
 CALCITE              0.27356
 DOLOMITE            -0.01721
 GYPSUM    +          0.17982
 PYRITE    +          0.00086
 NaCl      +          0.12287
 SiO2                 0.28367
 EXCHANGE             0.46326
 TM-Glass  +         -0.11206      (Constraint ignored)
 TM-Clay   -          0.03625      (Constraint ignored)
 CO2 GAS              0.32976
              Computed    Observed
Carbon-13      -5.8738     -3.1500
C-14 (% mod)   35.3556*     6.8000
------------------------------------------------------------------------
Adjusted C-14 age in years:  13628.*     * = based on Original Data

           MODEL   2
 Init 1    + F        0.39773
 Init 2    + F        0.60227
 CALCITE              0.45337
 DOLOMITE            -0.01721
 PYRITE    +          0.09077
 NaCl      +          0.12287
 SiO2                 0.28367
 EXCHANGE             0.46326
 TM-Glass  +         -0.11206      (Constraint ignored)
 TM-Clay   -          0.03625      (Constraint ignored)
 GOETHITE  -         -0.08991
 CO2 GAS              0.14995
              Computed    Observed
Carbon-13      -5.1062     -3.1500
C-14 (% mod)   28.9592*     6.8000
------------------------------------------------------------------------
Adjusted C-14 age in years:  11978.*     * = based on Original Data
```

Initial Well 1 : TM Recharge
Initial Well 2 : ER-EC-5_m1-3
Final well : ER-OV-3c_p1

```
          Final    Initial 1   Initial 2
 C       2.7926      1.4314      2.7469
 S       0.4626      0.1426      0.3724
 CA      0.3860      0.2256      0.5040
 MG      0.0151      0.0822      0.0208
 NA      3.4242      1.1766      3.2276
 K       0.0314      0.1203      0.0401
 CL      0.4698      0.1938      0.4481
 SI      0.6790      0.8237      0.6804
 FE      0.0000      0.0006      0.0001
 AL      0.0003      0.0003      0.0003
 18    -14.7000    -13.9000    -15.0000

 CALCITE  CA   1.0000 C    1.0000 RS   4.0000 I1   0.0000 I2   0.0000
 DOLOMITE CA   1.0000 MG   1.0000 C    2.0000 RS   8.0000 I1   0.0000
          I2   0.0000
 GYPSUM   CA   1.0000 S    1.0000 RS   6.0000 I3  22.0000
 PYRITE   FE   1.0000 S    2.0000 RS   0.0000 I3 -60.0000
 NaCl     NA   1.0000 CL   1.0000
 SiO2     SI   1.0000
 EXCHANGE CA  -0.9624 NA   2.0000 MG  -0.0376
 TM-Glass K    0.3680 NA   0.3830 CA   0.0240 MG   0.0050 FE   0.0260
          AL   0.7890 SI   4.1730
 TM-Clay  K    0.0170 NA   0.1610 CA   0.1410 MG   0.1380 FE   0.0500
          AL   2.4380 SI   3.4620
 GOETHITE FE   1.0000 RS   3.0000
 CO2 GAS  C    1.0000 RS   4.0000 I1 -12.0000 I2 100.0000

            MODEL   1
  Init 1    + F        0.27273
  Init 2    + F        0.72727
  CALCITE              0.15083
  DOLOMITE            -0.01284
  GYPSUM    +          0.15149
  PYRITE    +          0.00066
  NaCl      +          0.09109
  SiO2                 0.21720
  EXCHANGE             0.34639
  TM-Glass  +         -0.08442      (Constraint ignored)
  TM-Clay   -          0.02731      (Constraint ignored)
  CO2 GAS              0.27929
                Computed    Observed
 Carbon-13       -5.1188     -3.1500
 C-14 (% mod)    28.3278*     6.8000
 ------------------------------------------------------------------------
 Adjusted C-14 age in years:  11796.*     * = based on Original Data

            MODEL   2
  Init 1    + F        0.27273
  Init 2    + F        0.72727
  CALCITE              0.30232
  DOLOMITE            -0.01284
  PYRITE    +          0.07640
  NaCl      +          0.09109
  SiO2                 0.21720
  EXCHANGE             0.34639
  TM-Glass  +         -0.08442      (Constraint ignored)
  TM-Clay   -          0.02731      (Constraint ignored)
  GOETHITE  -         -0.07575
  CO2 GAS              0.12780
                Computed    Observed
 Carbon-13       -4.4709     -3.1500
 C-14 (% mod)    22.9292*     6.8000
------------------------------------------------------------------------
 Adjusted C-14 age in years:  10048.*     * = based on Original Data
```

STANDING DISTRIBUTION LIST

John Myers
UGTA Activity Lead
U.S. Department of Energy
Environmental Management Nevada Program
100 N. City Parkway, Suite 1750
Las Vegas, NV 89106
John.Myers@emcbc.doe.gov

Wilhelm Wilborn
Deputy Program Manager, Operations
U.S. Department of Energy
Environmental Management Nevada Program
100 N. City Parkway, Suite 1750
Las Vegas, NV 89106
Bill.Wilborn@emcbc.doe.gov

Ken Rehfeldt
Navarro
100 N. City Parkway, Suite 1750
Las Vegas, NV 89106
Ken.Rehfeldt@emnv.doe.gov

Jeff Berger
Nevada Field Office
National Nuclear Security Administration
U.S. Department of Energy
P.O. Box 98518
Las Vegas, NV 89193-8518
Jeff.Berger@nnsa.doe.gov

Ed Kwicklis
Los Alamos National Laboratory
P.O. Box 1663
Los Alamos, NM 87544
kwicklis@lanl.gov

Paul K. Ortego
Mission Support and Test Services, LLC
P.O. Box 98521
M/S NLV082
Las Vegas, NV 89193-8521
ortegopk@nv.doe.gov

Jeffrey Sanders
U.S. Geological Survey
Nevada Water Science Center
160 N. Stephanie St.
Henderson, NV 89074-8829
jvsanders@usgs.gov

Andy Tompson
Lawrence Livermore National Laboratory
P.O. Box 808, L-231
Livermore, CA 94551-0808
Tompson1@llnl.gov

Brian Haight
Navarro
100 N. City Parkway, Suite 1750
Las Vegas, NV 89106
Brian.Haight@emnv.doe.gov

Chuck Russell
Division of Hydrologic Sciences
Desert Research Institute
755 E. Flamingo Road
Las Vegas, NV 89119-7363
Chuck.Russell@dri.edu

Patrick Sawyer
DOE Program Manager
Division of Hydrologic Sciences
Desert Research Institute
755 E. Flamingo Road
Las Vegas, NV 89119-7363
Patrick.Sawyer@dri.edu

Nevada State Library and Archives
State Publications
100 North Stewart Street
Carson City, NV 89701-4285
NSLstatepubs@admin.nv.gov

Archives Getchell Library
University of Nevada, Reno
1664 N. Virginia St.
Reno, NV 89557
tradniecki@unr.edu

DeLaMare Library/262
University of Nevada, Reno
1664 N. Virginia St.
Reno, NV 89557
tradniecki@unr.edu

Document Section, Library
University of Nevada, Las Vegas
4505 Maryland Parkway
Las Vegas, NV 89154
sue.wainscott@unlv.edu

†Library Southern Nevada Science Center
Desert Research Institute
755 E. Flamingo Road
Las Vegas, NV 89119-7363

‡Martha DeMarre
Nuclear Testing Archive
Mission Support and Test Services (MSTS)
Contractor for the Nevada National Security Site
Mail Stop 400
PO Box 98521
Las Vegas, NV 89193-8521
demarrme@nv.doe.gov
(2 CDs)

§Office of Scientific and Technical Information
U.S. Department of Energy
P.O. Box 62
Oak Ridge, TN 37831-9939

All on distribution list receive one electronic PDF copy, unless otherwise noted.

_____

† 2 paper copies; CD with pdf (from which to print)
‡ compact disc only
§ electronic copy (pdf) only